Habilitation à diriger des recherches

Noise, chirality, and chaos in the dynamics of magnons and magnetic solitons

Joo-Von Kim
Centre de Nanosciences et de Nanotechnologies
CNRS, Université Paris-Sud, Université Paris-Saclay
Orsay, France

Document Version: 22 December 2019 at 17:03

Changes since version of 23 April 2018 at 10:04:
– Pagination corrected from Page 62 onwards
– Some spelling and formatting errors fixed
– Updated arXiv references

Colophon
This manuscript is typeset using Sabon LT Std (body text), Trade Gothic LT Std (headings, captions, and boxed text), and Andale Mono (this text).

Abstract

This dissertation provides an overview of the research activities I have undertaken in theoretical magnetism since taking up my CNRS position in 2004. It covers work on the stochastic theory of spin-torque nano-oscillators, nanocontact vortex oscillators including chaotic phases, channelling and nonreciprocal spin wave propagation in chiral systems, thermally-driven domain wall processes, and skyrmion dynamics. I conclude with some perspectives that follow from this research, namely chaos-based information processing, time-delay phenomena in micromagnetism, and stochastic processes in chiral magnets.

Résumé

Ce mémoire présente un résumé des activités de recherche théorique en magnétisme que j'ai menées depuis mon recrutement au CNRS en 2004. Il traite la théorie stochastique des nano-oscillateurs à transfert de spin, les oscillateurs à vortex dans les nanocontacts (y compris leurs phases chaotiques), la canalisation et la propagation non réciproque des ondes de spin dans les systèmes chiraux, les processus thermiquement activés des parois de domaine et la dynamique des skyrmions. Je conclus en détaillant quelques perspectives issues de ces travaux, notamment le traitement de l'information par le chaos, les phénomènes de rétroaction dans le micro-magnétisme et les processus stochastiques dans les aimants chiraux.

It's chaos, but it works.

Four Cypresses – Grizzly Bear

Table of contents

1. Overview

1.1. Preface

This dissertation provides an overview of my research activities since taking up my CNRS position in October 2004. They have been carried at the *Institut d'Electronique Fondamentale* (IEF) in Orsay, which since 1 June 2016 has become the *Centre de Nanosciences et de Nanotechnologies* (C2N) through a merger with the *Laboratoire de Photonique et de Nanostructures* (LPN).

The work covers diverse aspects of magnetisation dynamics which are tied together by an underlying thread involving excitations such as spin waves and magnetic solitons (domain walls, vortices, and skyrmions), with particular attention given to the role of noise, chirality, and nonlinear phenomena such as chaos. While my research is exclusively theoretical, it has been carried out within an experimental group with expertise on microwave electronics, broadband ferromagnetic resonance, magnetotransport measurements, Kerr microscopy, and nano-fabrication. As such, my work has invariably been informed by experimental considerations, and vice versa, which has led to a fruitful synergy between theory and experiment over the past decade and a half.

The start of my tenure at IEF coincided with the advent of spin-transfer torques in magnetic devices, notably with the first observations of spin-torque—induced precessions in spin valve nanopillars (Kiselev 2003) and nanocontacts (Rippard 2004). My activities have tracked the evolution in magnetics research from applications related to hard disk drives toward spin-torque random access memories, spin-torque nano-oscillators, domain wall racetrack devices, magnonics, and more recently skyrmionic systems. During this period, I have also had the opportunity to co-supervise a number of Masters students, PhD students, and postdoctoral researchers, both on the theoretical and experimental aspects of the work conducted in our group. I have shared their enthusiasm at solving the new problems at every turn; their valued contributions have underpinned much of the work discussed here.

After a brief overview of the main theoretical methods used in the remainder of this chapter, I give a summary of key scientific results obtained in the chapters that follow. In Chapter 2, I describe a stochastic theory of spin-torque nano-oscillators that provides a description of the spectral line shape and linewidth. In Chapter 3, I discuss our work on nanocontact vortex oscillators by detailing their discovery, the occurrence of modulated and chaotic phases, and ballistic vortex transport in multi-nanocontact systems. Chapter 4 is dedicated to spin wave propagation in chiral magnetic systems, where nonreciprocal propagation and caustics appear. In Chapter 5, I describe studies on thermally-driven processes in domain wall motion, notably depinning transitions from defects. Various aspects of skyrmion dynamics are presented in Chapter 6. In Chapter 7, I conclude by offering some perspectives for the research I intend to undertake in the short- and medium-term future.

1.2. Theoretical background and methods

Landau-Lifshitz equation

The vast majority of my research in theoretical magnetism has been dedicated to the study of the magnetisation dynamics in thin films and nanostructured materials. In strong ferromagnets, such as the transition metals iron, cobalt, nickel, and their alloys, the magnetisation dynamics in the low-energy limit is well described by the Landau-Lifshitz equation,

$$\frac{d\mathbf{m}}{dt} = -|\gamma|\mu_0 \mathbf{m} \times \mathbf{H}_{\text{eff}} + \alpha\, \mathbf{m} \times \frac{d\mathbf{m}}{dt} + \mathbf{\Gamma}, \tag{1.1}$$

where $\mathbf{m}(\mathbf{r}, t)$ is a unit vector that describes the time-dependent magnetisation configuration, γ is the gyromagnetic constant, and μ_0 is the permeability of free space. The effective field, $\mathbf{H}_{\text{eff}}$, is given by the variational derivative of the total energy of the system, U, with respect to the magnetisation field,

$$\mathbf{H}_{\text{eff}} = -\frac{1}{\mu_0 M_s} \frac{\delta U}{\delta \mathbf{m}}. \tag{1.2}$$

Here, M_s is the saturation magnetisation. The effective field takes both short-range (e.g., anisotropies, exchange interactions) and long-range interactions (i.e., dipole-dipole) into account and depends on the instantaneous configuration of the system. The first term on the right-hand side of Eq. (1.1) represents the precession of the magnetisation about this effective field. Dissipation is taken into account phenomenologically with the second term on the right-hand side of Eq. (1.1), which represents a viscous damping as proposed by Gilbert (2004) with α being the damping constant. Finally, $\mathbf{\Gamma}$ is taken to represent other external conservative and dissipative torques, such as current-induced effects. Despite its simplicity, the equation of motion (1.1) can provide a variety of rich phenomena as a result of the strong nonlinearities inherent to (1.1) and (1.2). It is quite remarkable that a host of physical processes can be described accurately with these equations alone.

Current-driven phenomena have remained a central focus of my work. These can be categorised into two broad classes. The first involves spin-transfer torques resulting from currents flowing perpendicular to the film plane (CPP). One example occurs in magnetoresistive multilayers such as spin valves or magnetic tunnel junctions, where the torques are exerted on the free layer magnetisation by an electrical current that becomes spin-polarised through its passage through the reference layer. Berger (1996) and Slonczewski (1996) proposed a torque of the form,

$$\mathbf{\Gamma}_{\text{STT}} = \sigma I \mathbf{m} \times \big(\mathbf{m} \times \mathbf{p}\big), \tag{1.3}$$

where $\mathbf{p}$ is the effective spin polarisation of the spin current, σ is an efficiency parameter, and I is the current density. This form is also applicable to torques due to the spin Hall effect, although there are indications that an additional field-like term $\big(\mathbf{m} \times \mathbf{p}\big)$ should also be included in that case. The second case involves torques that are generated when spin-polarised currents flow through regions in which magnetisation gradients are present. Zhang and Li (2004) proposed the form,

$$\boldsymbol{\Gamma}_{\mathrm{CIP}} = -(\mathbf{u}\cdot\nabla\mathbf{m}) + \beta\,\mathbf{m}\times(\mathbf{u}\cdot\nabla\mathbf{m}), \tag{1.4}$$

which is parametrised by an effective spin drift velocity (Thiaville 2005),

$$\mathbf{u} = \mathbf{J}\frac{Pg\mu_B}{2eM_s}, \tag{1.5}$$

where P is the spin polarisation, μ_B is the Bohr magneton, and e is the electron charge. These torques allow a wide variety of current-driven phenomena to be described, such as the spin-wave Doppler effect, spin-torque oscillations, domain wall motion, vortex gyration, and skyrmion dynamics.

Lagrangian Methods

While Eq. (1.1) may be amenable to solution under certain circumstances, such as linearisation to compute spin wave excitations or directly using numerical methods, there are instances in which other formulations are more useful. For example, reduced-variable models are more convenient to describe the motion of magnetic solitons such as domain walls, vortices, and skyrmions, where the salient features can be captured in the dynamics of the wall or core position (and other relevant internal modes).

One approach that allows equations of motion to be derived readily for such problems is the Lagrangian formalism. By parametrising the magnetisation field $\mathbf{m}$ using spherical coordinates, $\mathbf{m} = \left(\cos\phi\,\sin\theta, \sin\phi\,\sin\theta, \cos\theta\right)$, we can write the spin Lagrangian density as

$$\mathscr{L} = \frac{M_s}{\gamma}\dot{\phi}\,(1-\cos\theta) - \mathscr{U}(\theta,\phi), \tag{1.6}$$

where the first term is the Berry-phase term (Braun 1996, 2012) and $\mathscr{U}$ is the magnetic energy density Eq. (1.6) accounts for conservative processes. Non-conservative processes can be taken into account through a dissipation function, $\mathscr{W}$. Equations of motion for the reduced variables are derived by elevating these to dynamical variables in the collective coordinate approach. As an example, let us consider the case in which the position of a magnetic texture, $\mathbf{q}(t)$, plays the role of the collective coordinate. We can then write $\theta = \theta(\mathbf{r}-\mathbf{q}(t))$, etc., and integrate $\mathscr{L}$ and $\mathscr{W}$ over all space to obtain the Lagrangian and dissipation function, L and W, respectively. The equations of motion for the collective variables $q_i(t)$ are then obtained in the usual way,

$$\frac{d}{dt}\frac{\partial L}{\partial \dot{q}_i} - \frac{\partial L}{\partial q_i} + \frac{\partial W}{\partial \dot{q}_i} = 0, \tag{1.7}$$

where $\dot{q} \equiv \partial_t q$.

This approach can be applied to derive the one-dimensional model for domain wall dynamics and the Thiele equation for vortex and skyrmion dynamics. It also provides a prescription for obtaining equations of motion for other internal modes and describing scattering between the collective variables and normal modes. We will discuss several examples of this in this dissertation.

Numerical methods

Many problems in thin film magnetism and nanostructured materials are difficult to solve with analytical or semi-analytical means. In such cases, it is necessary to perform the time-integration in Eq. (1.1) numerically by discretising the system studied using either finite-difference or finite-element methods. This is the micromagnetics approach. Since 2011, I have incorporated significant use of micromagnetics simulations in my research. This date corresponds to the advent of codes that exploit graphics processing units (GPUs), which allow massively parallel computations to be performed for certain tasks, such as matrix algebra and fast Fourier transforms. In particular, I have been an early adopter of the MuMax code developed at Ghent University (Vansteenkiste 2011, 2014). Notably, my postdoc Felipe Garcia-Sanchez has made contributions to the implementation of the Dzyaloshinskii-Moriya interaction in versions 2 and 3 of the code.

These simulation tools have often been completed by other analytical and numerical tools such as COMSOL for finite element electromagnetics and MATHEMATICA for symbolic computation. Extensive use of the latter is made in reduced-variable problems such as Thiele models, eigenvalue problems, and more recently for classification of dynamical behaviour using algorithms based on machine learning.

2. Stochastic theory of spin-torque nano-oscillators

2.1. Background

Spin-transfer torques represent dissipative processes that cannot be described by or derived from a magnetic potential. The essential feature involves the transfer of spin angular momentum from a spin-polarised current to the local magnetisation. Depending on the physical geometry and micromagnetic state, spin torques can either contribute to magnetic relaxation processes that are inherent in magnetisation dynamics, leading to stronger damping, or compensate for these processes such that the overall damping is reduced.

One of the first experimental demonstrations of spin-transfer torques involved the amplification of thermal spin waves in multilayer structures under dc currents (Tsoi 1998, Slonczewski 1999, Tsoi 2002). Under sufficiently high currents, magnetic damping can become entirely compensated by spin torques, leading to either instabilities in the magnetic state or *self-sustained oscillations of the magnetisation*. In spin valves and magnetic tunnel junctions, the time-varying magnetisation (of the free magnetic layer, for example) translates into a high-frequency electrical signal by virtue of the giant- or tunnel-magnetoresistance effects. Because the underlying dynamics is driven by dc currents only, current-driven magnetisation oscillations have inspired many proposals for microwave frequency electrical oscillators based on such magnetoresistive devices. These systems are referred to as *spin-torque nano-oscillators* (STNOs). Since the first observations in nanopillars (Kiselev 2003, 2004) and nanocontacts (Rippard 2003, 2004, 2004b), spin-torque–induced oscillations involving vortex gyration in nanopillars (Pribiag 2007, Dussaux 2010, Locatelli 2011) and nanocontacts (Pufall 2007, Mistral 2008), perpendicular polarisers (Houssameddine 2007), spin wave bullets (Slavin 2005, Consolo 2007), droplet solitons (Mohseni 2013), skyrmion gyration (Garcia-Sanchez 2016), have also been observed experimentally or predicted theoretically.

From a fundamental point of view, these systems are interesting because the oscillatory behaviour is a result of the interplay between nonlinear magnetisation processes and spin-dependent transport through magnetic heterostructures, where the strong nonlinearity can lead to large variations in the oscillation frequency with applied currents. From a technological perspective, they are enticing because they may allow for frequency-tuneable oscillators on the nanoscale (Villard 2010), with potential applications in mobile telecommunications, for example, where several frequency bands could be handled by a single device. Recent work shows that output powers of 10 μW may be achieved (Tsunegi 2016b), which make them relevant for such applications. STNOs have also been proposed for field sensing (Braganca 2010), spin wave generation for magnonics (Madami 2011), and memory and computation (Macia 2011, Csaba 2012, Vodenicarevic 2016).

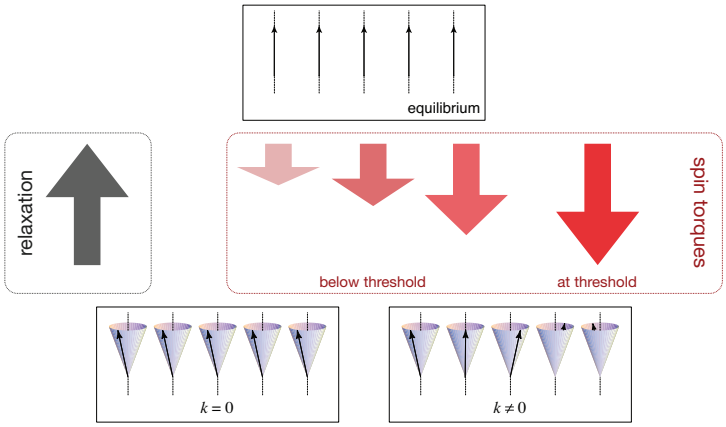

Fig. 2.1. Illustration of spin-torque driven excitations of spin waves. Below threshold, spin torques partially compensate the damping rate of spin waves. Self-oscillations emerge when the relaxation rate is compensated by the spin-torques.

Since 2005, I have been involved in a number of theoretical and experimental studies at IEF/C2N on STNOs. In this chapter, I give an overview of my research activities on the stochastic properties of STNOs. I outline the stochastic model based on a spin wave theory that is extended to include spin transfer torques and describe how this model can predict the spectral properties in the subcritical and supercritical limits. I also illustrate how the spectral line shape can be distorted near the threshold for self-oscillation. Aspects of this theory have been confirmed in experiments conducted by Quentin Mistral and Laurence Bianchini, as part of their PhD research that I supervised.

2.2. Stochastic oscillator model

Shortly after the discovery of self-sustained oscillations in nanopillar (Kiselev 2003) and nanocontact devices (Rippard (2004b), an important open question concerned the origin of the narrow spectral lines observed. For example, quality factors close to 1000 were observed for current-driven oscillations in magnetic nanocontacts (Rippard 2004b), which is an order of magnitude larger than what might be expected from the damping constant (~0.01) in these materials. Indeed, early theoretical attempts to describe these features in terms of *resonances* were ultimately fruitless, since the underlying physics involves self-sustained oscillations rather than driven (resonant) oscillations.

The onset of self-sustained oscillations and their stability were first examined in the context of nonlinear dynamical system and bifurcation theory (Bertotti 2005). The connection to generic oscillator models was made independently by Rezende *et al.* (2005) and Slavin and Kabos (Slavin 2005b) by using spin wave theory. This was achieved by expanding Eq. (1.1) with Eq. (1.3) in terms of spin wave eigenmodes c_k through the usual series of Holstein-Primakoff (Holstein 1940) and Bogoliubov (1947) transformations, which results in the equation of motion

$$\frac{dc_k}{dt} = -i\left(\omega_k + N_k|c_k|^2\right)c_k - \left(\Gamma_k - \sigma I + \sigma I|c_k|^2\right)c_k, \qquad (2.1)$$

where ω_k is the mode frequency, N_k is the nonlinear frequency shift parameter,

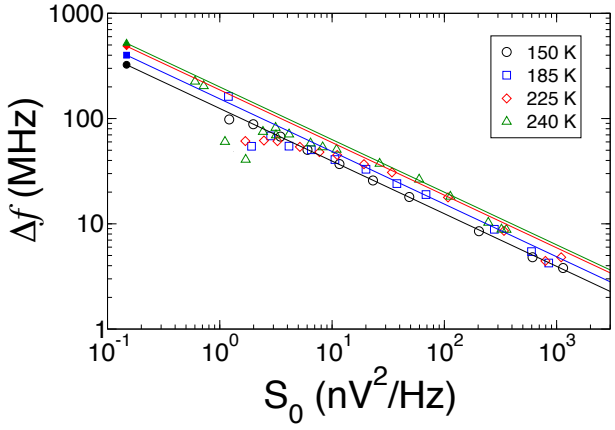

Fig. 2.2. Comparison between Eq. (2.6) (lines) with the experimental data from Mistral (2006). The only fitting parameter is the scale factor relating the measured mode intensity S_0 to the pumped magnon population n_p, which is obtained from one data point from the 150 K series. After Figure 5 of Kim (2006).

Γ_k is the damping rate, σ is the spin torque efficiency, and I is the applied current. For positive currents, the spin torque opposes Γ_k and therefore can be interpreted as negative damping. Self-oscillations occur when the rate of spin angular moment transferred exceeds the damping, $\sigma I > \Gamma_k$. Eq. (2.1) represents a dynamical system in which a limit cycle appears through a supercritical Hopf bifurcation (Strogatz 1994). Note that this approach assumes that the excited mode is inherently stable; loss of stability can occur at stronger drive and more sophisticated approaches are required in such cases (Bonin 2012).

I recognised that the spectral properties of spin-torque nano-oscillators can be described in terms of thermal noise acting on a free-running oscillator, rather than dissipation in a resonant system. I developed the stochastic model by solving Eq. (2.2) with an additional stochastic term $f_k(t)$,

$$\frac{dc_k}{dt} = -i\left(\omega_k + N_k|c_k|^2\right)c_k - \left(\Gamma_k - \sigma I + \sigma I\,|c_k|^2\right)c_k + f_k. \tag{2.2}$$

This stochastic term represents Gaussian white noise, which satisfies the spectral properties,

$$\langle f_k(t)\rangle = 0 \quad \langle f_k^*(t) f_{k'}(t')\rangle = 2q\delta_{k,k'}\delta(t-t'). \tag{2.3}$$

q is the noise amplitude and is related to the thermal magnon population and the dissipation rate (Kim 2006). Indeed, it can be shown that in the absence of spin torque Eq. (2.2) describes how fluctuations in the spin wave mode population $n_k = \langle c_k^* c_k\rangle$ returns back to its equilibrium value,

$$\frac{dn_k}{dt} = -2\Gamma_k\,(n_k - n_{k,0}). \tag{2.4}$$

In 2006, I first considered the linear limit of Eq. (2.2) in which the frequency shift term N_k was neglected (Kim 2006). With this approximation, it is possi-

ble to obtain the power spectral density $\mathcal{S}_k(\omega)$ for the self-sustained oscillation of mode k from the Fourier transform of the two-time correlation function,

$$\mathcal{S}_k(\omega) = \int_{-\infty}^{\infty} dt\ e^{-i\omega t} \langle c_k^*(t) c_k(0), \tag{2.5}$$

which is a Lorentzian function with a (full width at half maximum) linewidth of

$$\Delta\omega_k = 2\gamma^2 D_r + \Gamma_k \frac{k_B T}{n_p}. \tag{2.6}$$

D_r is a diffusion constant related to random field fluctuations parallel to the static magnetisation configuration, which results in fluctuations in the mode frequency and is usually negligible for stable oscillations*. The key result here is the second term on the right hand side, which shows that the linewidth is inversely proportional to the pumped magnon population, n_p. In other words, the further the system is driven from equilibrium, the narrower the spectral line should be because the amplitude of the thermal noise becomes comparatively smaller.

The behaviour in Eq. (2.6) can be tested against experimental data by assuming that the pumped magnon population is proportional to the amplitude of the measured spectral lines. In Fig. 2.2, we present a comparison with data obtained for current-driven excitations in spin valve nanopillars (Kim 2006, Mistral 2006). The data are taken from a low-current regime in which only one oscillation mode is observed and no evidence of mode instability is detected. The solid lines are based on the theoretical prediction of Eq. (2.6), where the smallest linewidth value from the 150 K data was used to obtain a correspondence between the measured spectral line intensity S_0 and the parametric magnon population n_p; this is the only fitting parameter. While deviations from theory can be seen at higher temperatures, the theory gives a good account of the trends seen experimentally.

2.3. Nonlinear model

This initial model spurred a new collaboration with Vasil Tiberkevich and Andrei Slavin at Oakland University (Michigan, USA), with whom I continued to extend the stochastic model to account for the nonlinear frequency shift. It was recognised that this nonlinear term could provide an important contribution to the linewidth, since fluctuations in the oscillator amplitude would also translate into phase noise.

We revisited the problem in Eq. (2.1) by considering explicitly the amplitude and phase fluctuations. By writing

$$c_k(t) = r(t) e^{-i\varphi(t)} = \left(r_0 + \delta r\right) e^{-i\varphi(t)}, \tag{2.7}$$

* The contrary is also true. Time-resolved experiments have shown that extinction events or situations in which large fluctuations in the mode frequency are present lead to additional contributions to the spectral linewidth (Houssameddine 2009).

where r_0 is the steady state oscillation amplitude and $r_0 \gg \delta r$, we can linearise (2.1) about the steady state to obtain

$$\frac{d\delta r(t)}{dt} + 2\left(\sigma I - \Gamma_k\right)\delta r(t) = \mathrm{Re}\left[\tilde{f}_k(t)\right], \tag{2.8a}$$

$$\frac{d\varphi(t)}{dt} + \omega(r_0^2) = -2N_k r_0\,\delta r(t) + \frac{1}{r_0}\mathrm{Im}\left[\tilde{f}_k(t)\right], \tag{2.8b}$$

which describe the amplitude and phase fluctuations, respectively. We can immediately recognise that two distinct stochastic processes are at play. First, the amplitude fluctuations in (2.8a) are described by an Ornstein-Uhlenbeck process (Risken 1989) and are damped out at a rate $\Gamma_a = \sigma I - \Gamma_k$. In other words, the further away the system is from threshold, the stronger the damping is in the amplitude fluctuations. These fluctuations have zero mean and possess the spectral properties

$$\langle \delta r(t)\delta r(t')\rangle = \frac{q}{2\Gamma_a} e^{-2\Gamma_a|t-t'|}. \tag{2.9}$$

While $\delta r(t)$ is a Gaussian process by virtue of $\tilde{f}_k$ being a Gaussian process, the finite relaxation time Γ_a means that these fluctuations have a memory on the order of time scales of Γ_a^{-1}. As such, the amplitude fluctuations have the characteristics of a *coloured* noise source. The oscillator phase is therefore governed by a stochastic process in which *both* coloured and white noise sources drive the dynamics, as described by the first and second terms on the right hand side of Eq. (2.8b), respectively. By integrating this first-order differential equation, the phase variance is found to be

$$\Delta\varphi^2(t) = \frac{q}{r_0^2}\left[\left(1+\nu^2\right)|t| - \frac{\nu^2}{2\Gamma_a}\left(1 - e^{-2\Gamma_a|t|}\right)\right], \tag{2.9}$$

where

$$\nu = \frac{N_k}{\sigma I} \tag{2.10}$$

is the dimensionless nonlinear frequency shift parameter. The spectral linewidth can be obtained directly from the phase variance. Eq. (2.9) constitutes the key result of this work (Kim 2008, Tiberkevich 2008).

While a general expression for the linewidth described by (2.9) is not possible, there are two limits in which analytical expressions can be found. At sufficiently low temperatures where the coherence time of the oscillations, τ_c, is much longer than the damping rate of the amplitude fluctuations, $\tau_c \gg \Gamma_a^{-1}$, the coloured properties of the amplitude fluctuations are unimportant for the phase oscillations and they can be taken to be a white noise source. In this limit, the long-time approximation can be applied to neglect the exponential term in (2.9), which leads to

$$\Delta\varphi^2(t) \approx \frac{q}{r_0^2}\left(1+\nu^2\right)|t|. \tag{2.11}$$

A linear time dependence of the phase variance is recovered, but the frequency nonlinearity leads to a renormalisation of the linear oscillator linewidth by

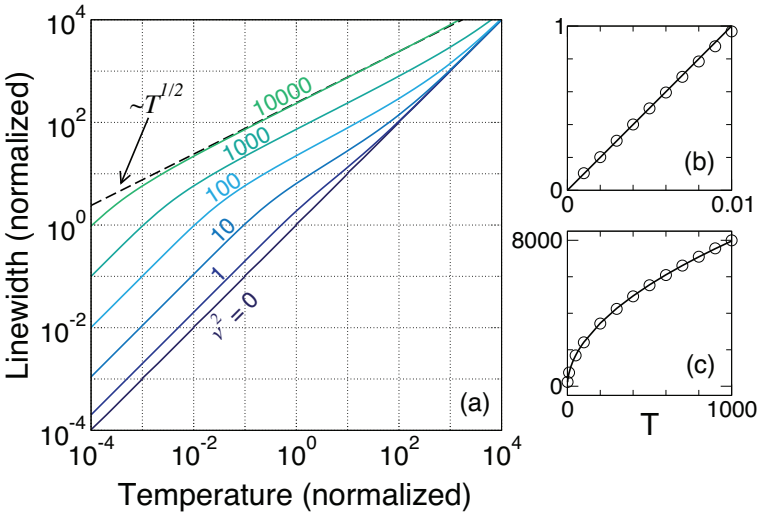

Fig. 2.3. (a) Temperature dependence of the oscillator linewidth for different values of the frequency nonlinearity. (b) Example of the linear temperature dependence at weak nonlinearity ($\nu^2 = 1$). (c) Example of a square root temperature dependence at strong nonlinearity ($\nu^2 = 10\,000$). After Figure 1 of Tiberkevich (2008).

a factor of $(1 + \nu^2)$,

$$\Delta\omega_{\mathrm{LT}} = \frac{q}{r_0^2}\left(1 + \nu^2\right). \tag{2.12}$$

The spectral line shape is therefore *Lorentzian* at low temperatures with a linewidth that increases linearly as a function of the temperature. At sufficiently high temperatures at which the coherence time of the oscillations is much shorter than the decay rate of amplitude fluctuations, $\tau_c \ll \Gamma_a^{-1}$, the finite lifetime or "memory" of these fluctuations must be accounted for. A short-time approximation can be used in this limit to expand the exponential in (2.9) in a power series, giving

$$\Delta\varphi^2(t) \approx \frac{q}{r_0^2}\left(|t| + \nu^2\Gamma_a t^2\right). \tag{2.13}$$

For sufficiently large frequency nonlinearities, $\nu^2 \gg 1$, the linear term can be neglected and only the quadratic term in t can be retained. In contrast to the linear and low-temperature cases, the spectral function corresponding to a correlation function with a quadratic time dependence is a *Gaussian*, with a full width at half maximum of

$$\Delta\omega_{\mathrm{HT}} = 2\sqrt{2\ln 2}\,\frac{|\nu|}{r_0}\sqrt{q\Gamma_a}. \tag{2.14}$$

It is interesting to note that the linewidth in the high temperature limit varies like $\sqrt{T}$, in contrast to the linear time dependence observed in the linear or low-temperature cases. This behaviour is characteristic of *inhomogeneous broadening* (Kubo 1962), where in the present case the amplitude fluctuations lead to fluctuations in the oscillator frequency as a result of the frequency nonlinearity. This temperature dependence has also been reported in macrospin simulations of spin torque oscillators (Sankey 2005). The transition between the low and high temperature regimes can be seen in Fig. 2.3,

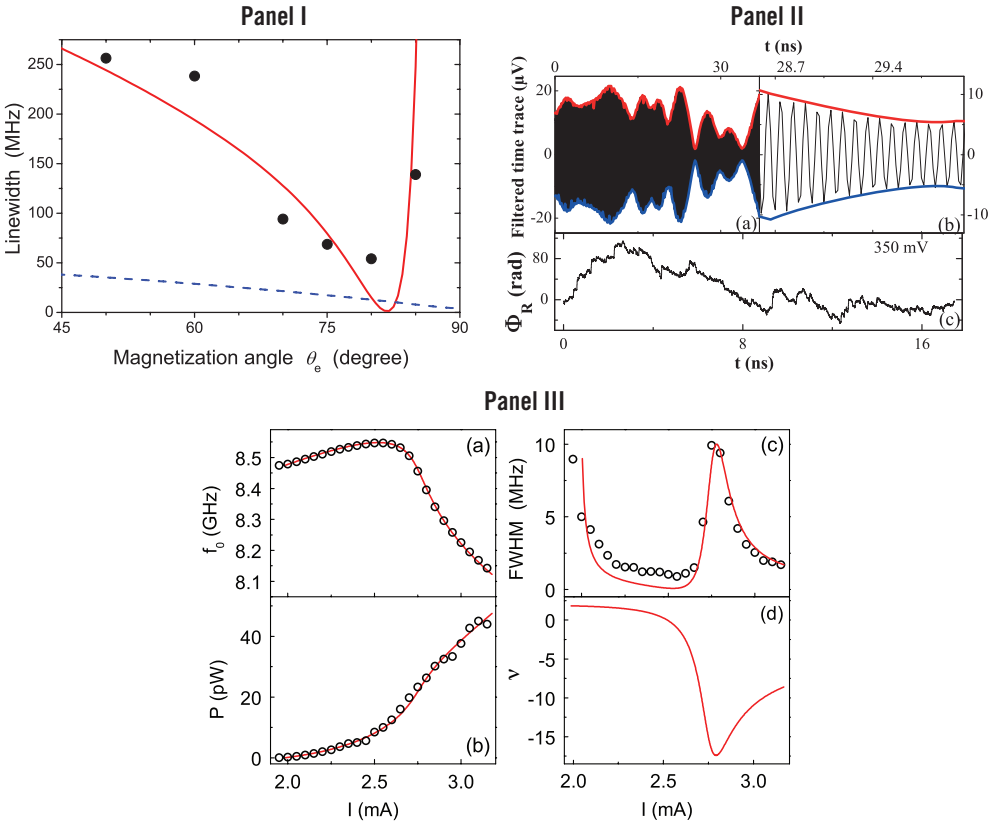

Fig. 2.4. Comparison of the nonlinear stochastic model with experiment. Panel I shows the linewidth variation with magnetisation angle, measured relative to the film plane, for nanocontact oscillations. The dots indicate experimental data, the solid line represents the nonlinear theory, and the dashed line represents the linear theory (Kim 2008). Panel II illustrates time-resolved electrical measurements of magnetisation oscillations in magnetic tunnel junctions. From this, the phase variance was measured and a direct proof of phase-amplitude coupling was found (Bianchini 2010). Panel III shows experimental data from Urazhdin et al. (2010), which can be fitted accurately with the nonlinear theory (solid lines).

where the linewidths were obtained numerically for different values of the frequency nonlinearity.

Aspects of this theory have been tested with experimental data in different ways. First, we showed that the linewidth variation with perpendicular magnetic fields in magnetic nanocontacts can be explained with our theory, where the field dependence can be accounted by changes in ν that results from in-plane to out-of-plane precession (Fig. 2.4, Panel I; Kim 2008). Second, we conducted experiments at IEF to determine the phase-amplitude coupling in STNOs based on magnetic tunnel junctions. Some representative data are shown in Panel II of Fig. 2.4, where time-resolved measurements of the amplitude and phase of the oscillations were extracted from Hilbert transform of the measured voltage signals (Bianchini 2010), from which we were able to reconstruct the phase variance as described in Eq. (2.9). This formed part of the PhD work of Laurence Bianchini. Phase-amplitude coupling has also been examined in detail by other groups, notably in magnetic tunnel junctions (Quinsat 2010, Sierra 2012) and vortex oscillators (Grimaldi 2014). Finally, experiments on nanocontacts conducted by Urazhdin (2010) showed

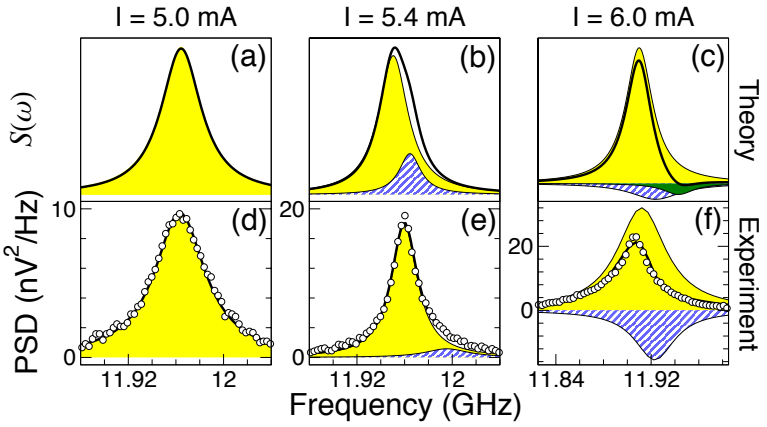

Fig. 2.5. (a) Comparison of theoretical and experimental spectral lines near threshold (5.2 mA) for a spin valve nanopillar oscillator. Thick solid lines in (a)-(c) represent spectral lines as predicted by Eq. (2.19), with the first dominant modes shown as shaded curves. Circles in (d)-(f) are experimental data at $T =$ 225 K taken from Mistral (2006), with thick solid lines representing a double Lorentzian fit. Shaded curves are individual Lorentzian profiles used in the fits. After Figure 2 of Kim (2008b).

that the nonlinear model can describe the spectral properties over a wide range of applied currents, as shown in Panel III of Fig. 2.4.

2.4. Line shape distortion at threshold

As discussed in the previous section, an expression for the spectral line shape can only be obtained in certain limits as a result of the strong phase-amplitude coupling in STNOs. This is also true close to the threshold for self-oscillation, where the amplitude fluctuations δr can be as large as r_0 itself. As such, it is not possible to apply the same linearisation methods that were used to obtain Eq. (2.8).

I developed a more general approach that allows the power spectrum to be described at all levels of supercriticality (Kim 2008b). The method relies on solving the Fokker-Planck equation associated with the nonlinear Langevin equation in (2.2). The Fokker-Planck equation governs the time evolution of the probability density function $\mathscr{P}(c_k, t)$, which describes the probability of finding the stochastic oscillator in the state c_k at time t. Because the Fokker-Planck problem involves solving a deterministic linear differential equation, its solution is usually more tractable than the stochastic nonlinear differential equation in (2.2). The Fokker-Planck equation is given by

$$\frac{\partial \mathscr{P}(r,\varphi,t)}{\partial t} = \hat{L}_{\mathrm{FP}}\, \mathscr{P}(r,\varphi,t). \tag{2.15}$$

With the supercriticality parameter defined as $\zeta = \sigma I/\Gamma_k$, the Fokker-Planck operator corresponding to (2.2) can be expressed in reduced units as

$$\hat{L}_{\mathrm{FP}} = \frac{\partial}{\partial r}\left[\zeta r^3 - (\zeta - 1)r - \frac{q}{r}\right] + \left(\omega_k + N_k r^2\right)\frac{\partial}{\partial \varphi} + q\left(\frac{\partial^2}{\partial r^2} + \frac{1}{r^2}\frac{\partial^2}{\partial \varphi^2}\right). \tag{2.16}$$

By performing an appropriate transformation, we can solve the Fokker-

Planck equation for $\mathscr{P}$ as an eigenvalue problem, where the eigenfunctions $\psi_{m,n}(r)$ satisfy the one-dimensional Schrödinger equation

$$q\frac{\partial^2\psi_{m,n}}{\partial r^2} - [V_n(r) - \lambda_{m,n}]\,\psi_{m,n} = 0, \tag{2.17}$$

where the effective potential can be expressed as a simple polynomial function of the oscillator amplitude,

$$V_n(r) = \frac{a_{-2}}{r^2} + a_0 + a_2 r^2 + a_4 r^4 + a_6 r^6. \tag{2.18}$$

Thus, the problem of the nonlinear Langevin equation in (2.2) can be transformed to the more tractable problem of (2.17), for which many approaches exist. The key point here is that the power spectrum can ultimately be obtained from the eigenvalues $\lambda_{m,n}$ and eigenfunctions of (2.17), namely

$$\mathscr{S}(\omega) = \sum_m \frac{F_{m,1}}{\left[\Omega - \omega_k - \Gamma_k \mathrm{Im}\left(\lambda_{m,1}\right)\right]^2 + \left[\Gamma_k \mathrm{Re}\left(\lambda_{m,1}\right)\right]^2}, \tag{2.19}$$

where the weighting factors $F_{m,1}$ are given by vector products of the eigenfunctions.

The result Eq. (2.19) shows that the power spectrum can be described by a sum of partial Lorentzians, where each contribution possesses a slightly different central frequency and linewidth. As such, the spectral line shape is predicted to be asymmetric in general. However, in practice the asymmetry is only expected to be important near threshold. To test this prediction, we analysed experimental data of current-driven oscillations near threshold in spin valve nanopillars (Mistral 2006). An example of the comparison between theory and experiment is shown in Fig. 2.5. The threshold current is estimated to be 5.2 mA. Below this threshold current, the line shape is Lorentzian, where only the lowest order term in the expansion (2.19) contributes to the power spectrum. For applied currents slightly above the threshold, non-negligible contributions from the higher-order terms are observed, which lead to a measurable distortion in the spectral line profile.

Related Publications

Stochastic theory of spin-transfer oscillator linewidths
J.-V. Kim
Physical Review B **73**, 174412 (2006).

Generation Linewidth of an Auto-Oscillator with a Nonlinear Frequency Shift: Spin-Torque Nano-Oscillator
J.-V. Kim, V. S. Tiberkevich, and A. N. Slavin
Physical Review Letters **100**, 017207 (2008).

Line Shape Distortion in a Nonlinear Auto-Oscillator Near Generation Threshold: Application to Spin-Torque Nano-Oscillators
J.-V. Kim, Q. Mistral, C. Chappert, V. S. Tiberkevich, and A. N. Slavin
Physical Review Letters **100**, 167201 (2008).

Temperature dependence of nonlinear auto-oscillator linewidths: Application to spin-torque nano-oscillators
V. S. Tiberkevich, A. N. Slavin, and J.-V. Kim
Physical Review B **78**, 092401 (2008).

Direct experimental measurement of phase-amplitude coupling in spin torque oscillators
L. Bianchini, S. Cornelissen, J.-V. Kim, T. Devolder, W. Van Roy, L. Lagae, and C. Chappert
Applied Physics Letters **97**, 032502 (2010).

Spin-torque oscillators
J.-V. Kim
In volume 63 of *Solid State Physics*, R. E. Stamps & R. E. Camley, eds. (Academic Press, 2012), pp. 217–294.

3. Nanocontact vortex oscillators

3.1. Background

The discussion in the last chapter was centred on the self-oscillatory dynamics of linear and nonlinear spin wave modes. In the linear limit, these modes represent the normal modes of an equilibrium micromagnetic state, which may be spatially nonuniform depending on the oscillator geometry. At large driving currents, nonlinearities arise but can be described as extensions of these linear spin wave modes. In this chapter, a different kind of self-sustained dynamics is discussed in which the oscillation involves the spatial translation of a well-defined micromagnetic state.

We focus here on the magnetic vortex, which represents a micromagnetic configuration in which the moments curl in the film plane and culminate out of the film plane in a compact region termed the vortex core. The configuration results from a competition between the exchange and dipolar energies of the interacting magnetic moments. Magnetic vortices are ground states in confined geometries such as thin film discs, where for certain disc aspect ratios they become more favourable energetically than the uniform state (Metlov 2002). This stability is maintained under spin transfer torques, which can lead to self-sustained gyration of the vortex core in the sub-GHz frequency range (Pribiag 2007).

Since 2007, we have studied intensively a different physical system, the magnetic nanocontact (Fig. 3.1), in which vortex oscillations can also be induced by spin transfer torques. In contrast to discs in which the minimisation of surface charges at the edges lead to the vortex state, it is the Zeeman potential due to the Oersted-Ampère fields, generated by the perpendicular current

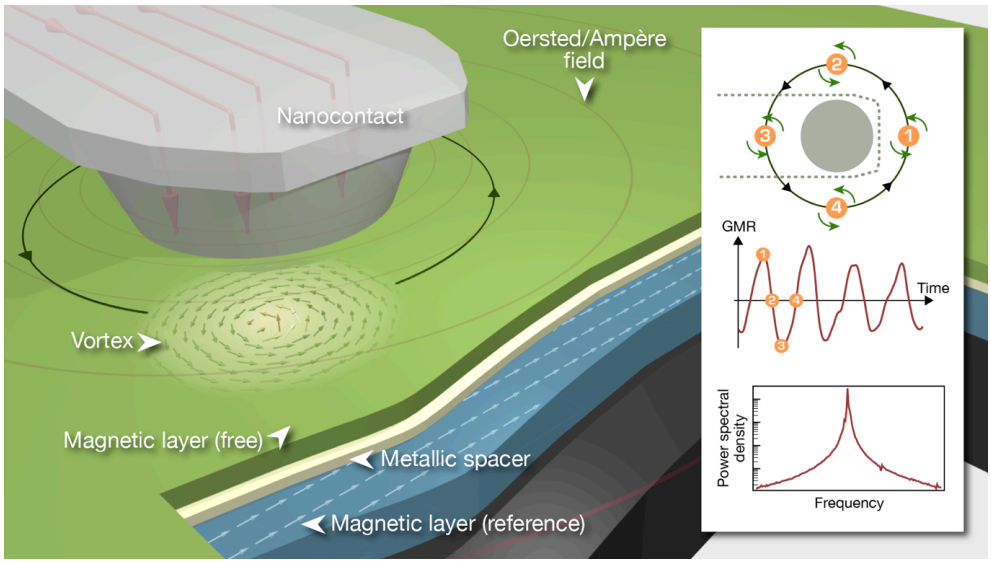

Fig. 3.1. Schematic illustration of a nanocontact vortex oscillator. The Zeeman potential associated with the Oersted-Ampère field acts as a confining potential for the magnetic vortex, while spin torques drive it to steady-state gyration. Changes in the giant magnetoresistance (GMR) allow its dynamics to be probed electrically.

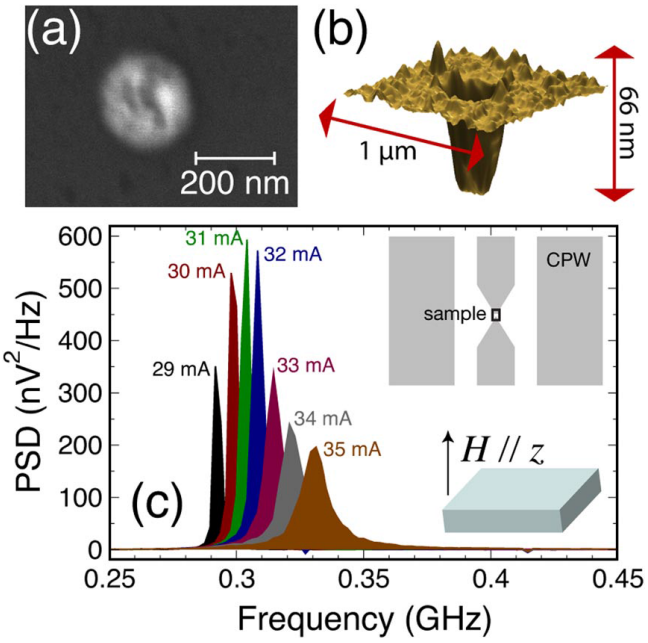

Fig. 3.2. Nanocontact and power spectral density of vortex oscillations. (a) Scanning electron microscopy and (b) and atomic force microscopy images of the nanocontact. (c) Low-frequency power spectral density measured under a perpendicular applied field of 210 mT for several applied currents. The coplanar waveguide (CPW) and applied field geometry are illustrated in the inset of (c). After Figure 1 of Mistral (2008).

flow, that acts to stabilise the vortex. As a result of the large in-plane component of the applied current, the Zhang-Li spin torques (1.4) drive the vortex into steady state gyration around the nanocontact, which can be detected through changes in the giant magnetoresistance of the multilayer. While such oscillations share some similarities with their counterparts in nanopillars, we will show below that a number of other phenomena are also possible, namely periodic reversals of the vortex core and ballistic transport between several nanocontacts.

The work presented below represents one of my key activities of research of the past decade and has involved a number of collaborators at IEF/C2N and abroad.

3.2. Discovery of nanocontact vortex oscillations

The magnetic nanocontact oscillator was one of the key experimental systems developed and studied in the TUNAMOS project (2005-2008), which was funded by the 5th Framework Programme of the European Commission. The devices were fabricated at IMEC (Leuven, Belgium) and the high-frequency electrical measurements were performed at IEF, primarily as part of the PhD work of Quentin Mistral that I supervised. Along with Gino Hrkac at the University of Sheffield (UK), we made the discovery of vortex oscillations in this system.

The nanocontact device we studied comprises a 4-nm-thick NiFe free layer, with a 3.5 nm-thick $Co_{90}Fe_{10}$ reference layer that is exchange biased by 7 nm

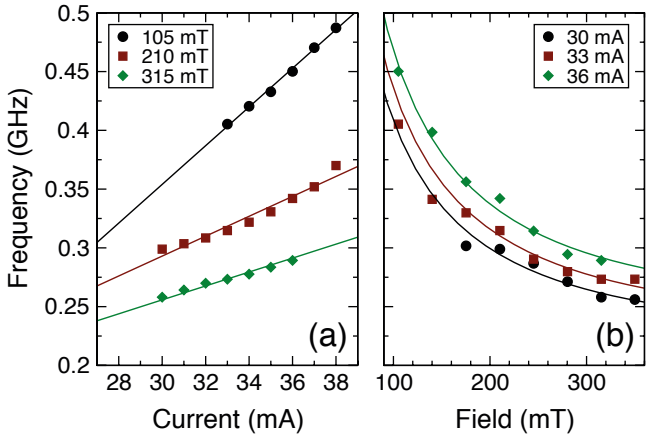

Fig. 3.3. Nanocontact vortex oscillation frequency as a function of (a) applied current and (b) applied perpendicular field. Dots are experimental data and solid lines are fits based on Eq. (3.2). After Figure 3 of Mistral (2008).

of IrMn. An example of the low-frequency power spectra that we observed is presented in Fig. 3.2. The peaks shown represent the fundamental mode for several applied currents under a perpendicular field of 210 mT. Harmonics to fourth order are also observed, but these are several orders of magnitude smaller than the fundamental. The oscillations have quality factors up to 250, which corresponds to the narrowest linewidth of 1.2 MHz observed at a frequency of 299 MHz. These sub-GHz modes are consistent with vortex motion rather than uniform precession. Indeed, the Smit-Beljers equation for uniform magnetisation precession predicts a precession frequency of 1.08 GHz with our experimental parameters, which is clearly 4–5 times higher than what we observe. In contrast to earlier experiments in which nominally smaller diameter contacts were studied (Rippard 2004b), the Oersted fields in our samples are significantly larger (at equivalent current densities) at the contact edges and therefore favour vortex formation. For example, a 30 mA current generates an Oersted-Ampère field of 60 mT at the contact edge, which is a significant fraction of the perpendicular applied fields that we considered. We studied the power spectra over an applied current range of 0-40 mA.

To better understand the nature of the low-frequency oscillations, full micromagnetic simulations were performed by Gino Hrkac at the University of Sheffield. These simulations reveal that the oscillations observed are related to the large-amplitude translational motion of a magnetic vortex. In contrast to the nanopillar geometry in which the vortex core precesses within the confining part of the Oersted field, the dynamics here correspond to an orbital motion *outside* the contact region. This behaviour can be likened to planetary orbital motion under the influence of a gravitational field; the spin-transfer torque leads to a centripetal motion of the vortex core, which is counter-balanced by the attractive potential provided by the Oersted field. Good quantitative agreement between the simulation and experimental frequencies is achieved (Mistral 2008).

To complement this work, I developed a Thiele model for the nanocontact vortex oscillations. At this time (2007-2008), micromagnetics simulations were computationally-intensive and time-consuming, so it was all the more important to have an analytical model with which certain trends could be confirmed (parameter scans using simulations were not feasible). I used the Lagrangian method discussed in the Chapter 1 to account for spin-transfer torques in the nanocontact geometry, along with a linear approximation for the confining potential due to the Oersted fields. By assuming that the vortex core dynamics can be described entirely by the core position, $\mathbf{X}_0(t)$, we can derive the Thiele equation

$$\mathbf{G} \times \dot{\mathbf{X}}_0 + \alpha D \dot{\mathbf{X}}_0 = -\frac{\partial U}{\partial \mathbf{X}_0} + \mathbf{F}_{\mathrm{STT}}, \tag{3.1}$$

where $\mathbf{G} = G\hat{\mathbf{z}}$ is the gyrovector, D is a damping structure factor, U is the vortex energy, and $\mathbf{F}_{\mathrm{STT}}$ represent the nonconservative forces due to spin-transfer torques. With justifiable assumptions (Mistral 2008), we can derive an expression for the steady-state gyration,

$$\omega = \frac{\kappa I}{G R_0}, \tag{3.2}$$

where κ is a prefactor, G is the magnitude of the gyrovector, I is the applied current, and R_0 is the radius of gyration measured from the nanocontact centre. The key prediction here is that the frequency varies linearly with current and that the radius of gyration is essentially current-independent. In stark contrast to the oscillator model presented in Chapter 2, the theory here does not predict a threshold current for self-oscillation, but rather it is contained in the parameter κ that determines whether the overall spin-torques can overcome the viscous damping for the given material system; in fact, the presence of a finite positive steady-state solution for the radius R_0 is a manifestation of this property.

A comparison between the Thiele model prediction (3.2) and experiments is shown in Fig. 3.3. We observe a quasi-linear variation of the oscillation frequency with current in experiment, which is consistent with theory and is due to the linear dependence of the Oersted field energy on current. To produce the theoretical curves in Fig. 3.3(a), we first fit the 105 mT series using Eq. (3.2) and then use the theoretical field dependence of the gyration radius (not shown) to compute the slopes for the other applied fields, which are in good quantitative agreement with the experimental data. The theory also accounts for the frequency variation with applied field, as shown in Fig. 3.3(b). As before, we fit (3.2) to one data set (36 mA) and used the predicted current variation for the other sets. Overall, good agreement is found between theory and experiment.

Since the steady state radius is independent of current (3.2), any instantaneous changes to the applied current will result in an immediate change in the gyration frequency. This behaviour leads to the prospect of fast frequency modulation using such vortex nanocontact oscillators. In collaboration with

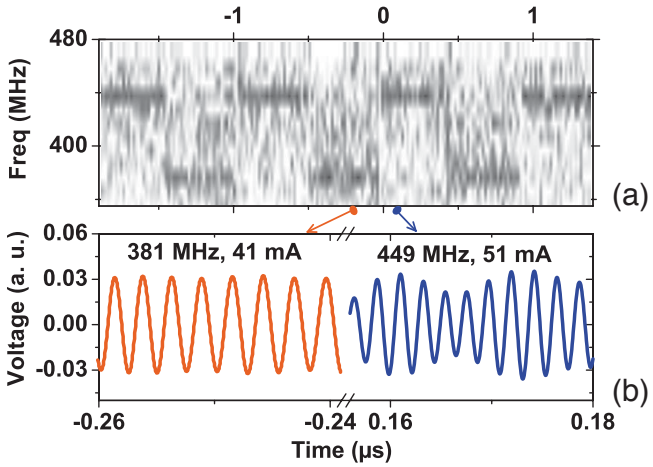

Fig. 3.4. Frequency agility of a nanocontact vortex oscillator. (a) Time-dependent power spectra in response to a square wave current signal. (b) Time-resolved voltage signals before and after the current step. After Figure 3 of Manfrini (2009).

Mauricio Manfrini (PhD student at IMEC at the time), we verified this aspect experimentally at IEF with Thibaut Devolder. In Fig. 3.4, we show experimental data of the change in oscillation frequency when a square-wave function in current is applied to the nanocontact. Within the limit of the time-resolution of the experiment (20 ns), we observe that the gyration frequency switches in response to the current steps on a scale below this resolution, which is consistent with the model. This behaviour might be useful fort frequency-modulation techniques for communications applications (Manfrini 2011, Ruiz-Calaforra 2017).

3.3. Periodic core reversal and self—phase-locking

Despite the success of the Thiele model (3.2), we have also studied other nanocontact systems in which the simple gyration picture breaks down. A particular example is the geometry shown in Fig. 3.5(a), where the nanocontact is fabricated using a nano-indentation technique (Bouzehouane 2003) that result in diameters as small as 20 nm at the free layer surface, which is an order of magnitude smaller than the nanocontacts discussed in the previous section. These samples were developed at *Unité Mixte de Physique CNRS/Thales* (UMPhy) and studied in the context of the Initial Training Network "SPINSWITCH", funded by the 6th Framework Programme of the European Commission. Measurements were conducted by Antonio Ruotolo at UMPhy and at IEF. The novel feature of this system is the occurrence of periodic core reversal, which is accompanied by a change in the sense of gyration [Fig. 3.5(c)]. This leads to a second free-running oscillator within the system, which competes with and modulates the gyration [Fig. 3.5(d)].

An example of the self-modulation observed is given in Figs. 3.5(e) and (f). Below a threshold current, the oscillator behaves in the "normal" state, where sub-GHz gyration frequencies are observed with a rich harmonic content [Fig. 3.5(e)], which suggests an elliptical trajectory of the vortex core around

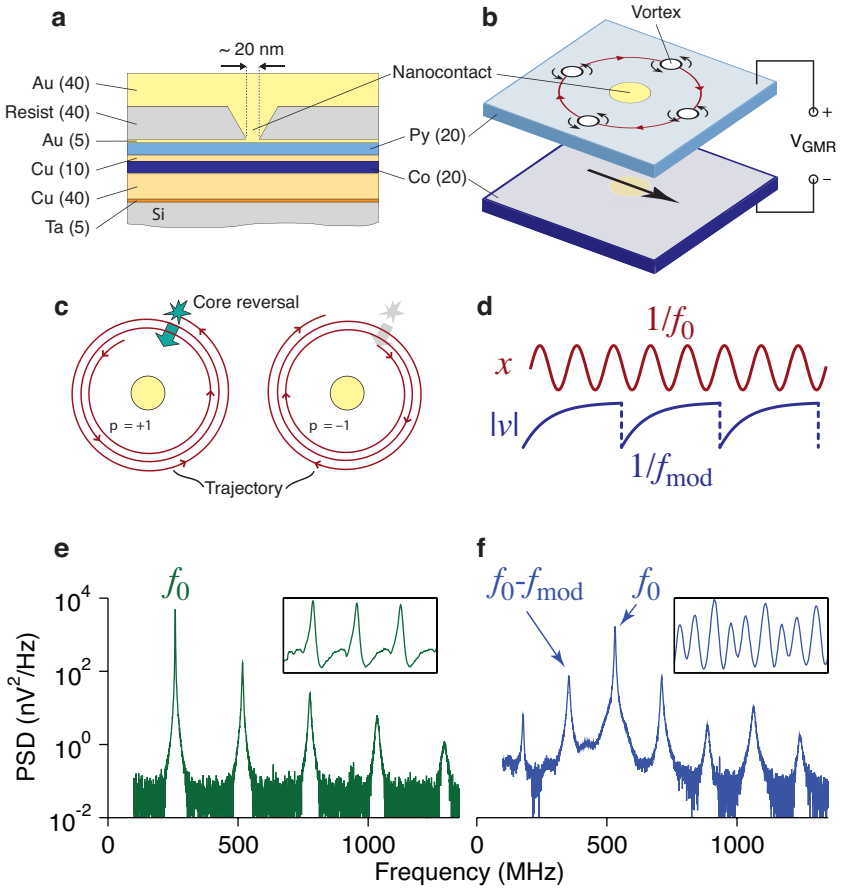

Fig. 3.5. Periodic core reversal in 20-nm diameter nanocontacts. (a) Multilayer and nanocontact geometry. (b) Schematic illustration of vortex gyration and the resultant magnetoresistance signal. (c) Core reversal leading to change in radius and sense of gyration. (d) Comparison between oscillations in position (gyration) and core velocity (periodic core reversal). (e) Experimental power spectra showing high harmonic content, suggesting elliptical orbits. (f) Self-modulations indicating periodic core reversal. After Figure 1 of Petit-Watelot (2012).

the nanocontact. Above the threshold, modulation sidebands appear in the power spectra [Fig. 3.5(f)]. The variation of the power spectra as a function of applied current is shown in Fig. 3.6(a). Here, the threshold current of around 10.2 mA can clearly be identified. Above this, we observe that the behaviour of the modulation sidebands is nontrivial, where the number of visible branches change as the applied current is increased. Interestingly, the ratio between the modulation and gyration frequencies is found to lock into different integer ratios as the current is varied, as shown in Fig. 3.6(b). We observe plateaus corresponding to ratios such as 1/8, 1/5, 1/4, 1/3, and 1/2. Such phenomena are suggestive of a phase-locking phenomenon. Indeed, the coherence time of the oscillations, as determined from time-resolved measurements, is found to decrease as one moves away from these plateaus, as shown in Fig. 3.6(c) for the 1/2 plateau.

To gain deeper insight, we used micromagnetics simulations combined with finite-element electromagnetics modelling to compute the magnetisation dynamics in the free layer of the nanocontact device. The COMSOL software was used to compute the spatial profiles of the current flow and its associated

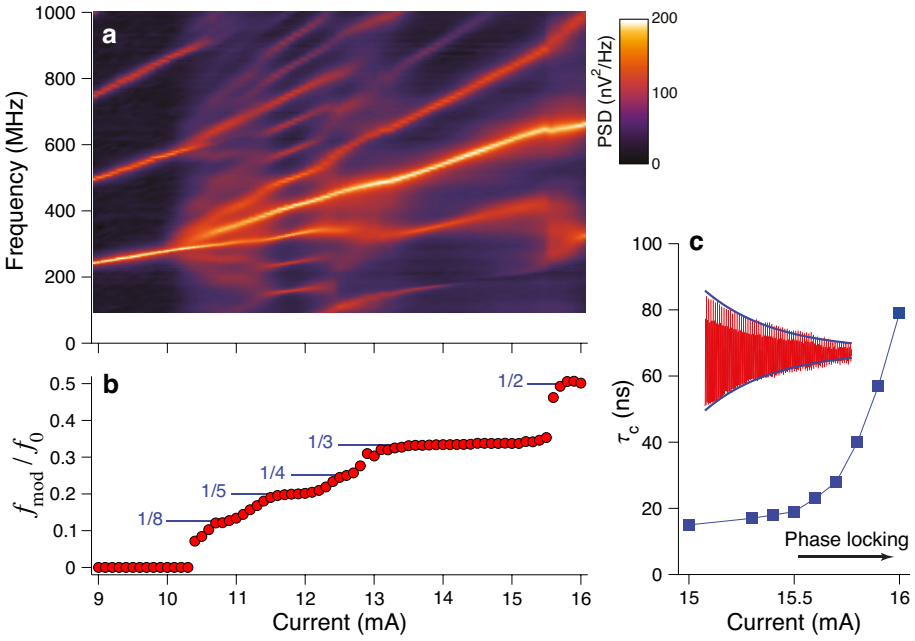

Fig. 3.6. Experimental power spectrum of the nanocontact vortex oscillator. (a) Colour map of the power spectral density (PSD) as a function of current, where modulation of the main frequency branch is visible with different modulation rates. (b) Variation of the ratio between the modulation and central frequencies as a function of applied current, where plateaus indicate phase-locking between the gyration and modulation. (c) Signal coherence time as a function of applied current around the f_{mod} / f_0 = 1/2 plateau, showing a strong improvement in coherence as the system is driven toward a phase-locked state. After Figure 2 of Petit-Watelot (2012).

Oersted-Ampère field (Petit-Watelot 2012b), which were then used as inputs into the open source MuMax code for micromagnetics simulations. These developments were led by Sébastien Petit-Watelot, a postdoc in the group at the time.

The results of the micromagnetics simulations are shown in Fig. 3.7. From the colour map of the current-dependence of the power spectrum [Fig. 3.7(a)], we can see that the micromagnetics simulations give a good quantitative account of the gyration and modulation frequencies. The simulations confirmed that the modulation is due to a periodic reversal of the vortex core, where each reversal event results in a change in the sense of gyration. As such, a modulation ratio of 1/5 corresponds to one reversal event after every five revolutions of the vortex core around the nanocontact, 1/4 means a reversal after every four revolutions, and so on. We observe similar modulation ratios and plateaus as the experimental data in Fig. 3.7(b) (1/8, 1/5, 1/4, 1/3, 1/2), but also additional ratios such as 1/9 and 2/7. The calculated trajectories of the vortex core, as shown in Fig. 3.7(c), indicate that the reversal events always occur in similar regions around the nanocontact, where presumably the criterion for core reversal (critical deformation in the spin structure) is met. The simulations also show that other irrational modulation ratios are also possible when the perpendicular fields are varied, which are indicative of *chaotic* states of the oscillator. These are discussed in more detail in Chapter 7.

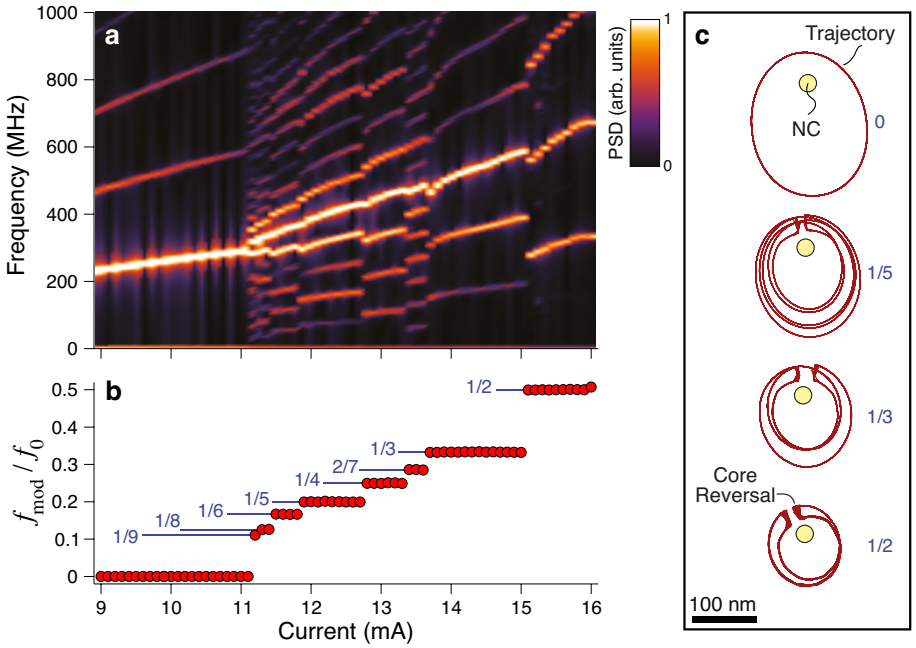

Fig. 3.7. Nanocontact vortex dynamics computed with micromagnetics simulations. (a) Colour map of the power spectral density (PSD) as a function of current, showing the same features as the experimental data. (b) Variation of the ratio between the modulation and central frequencies as a function of applied current, where distinct phase-locking plateaus with integer ratios are observed. (c) Core trajectories illustrating different phase-locking regimes. After Figure 3 of Petit-Watelot (2012).

3.4. Ballistic transport in multiple nanocontact systems

Armed with the theoretical and experimental expertise developed on nanocontact vortex oscillators, the IEF and IMEC groups continued to explore richer dynamics in multiple nanocontact systems. A number of different geometries were fabricated at IMEC for this (as part of the PhD research of Mauricio Manfrini), where pair and quadruple nanocontact arrays were produced. In the latter lines, 'Y' branches, and diamond arrangements were considered with centre-to-centre NC separations ranging from 300 nm to 1 500 nm. The electrode geometry was designed and fabricated such that each nanocontact has an independent electrical access, in contrast to previous work on multiple nanocontact systems (Ruotolo 2009).

Two competing phenomena can be envisaged in a system with several NCs. First, the combination of the Oersted-Ampère fields across several NCs might lead to an array of vortices and antivortices, which reflect the arrangement of the NCs (Ruotolo 2009). On the other hand, the competition between the spin-torques and Oersted fields might result in a change in the overall trajectory of a single vortex core. To investigate this question in greater depth, experiments were performed on double-nanocontact systems [Fig. 3.8(a)]. In one experiment where the separation is 500 nm, a vortex nucleated at the "East" NC could be transported toward the "West" NC by keeping constant the total current applied to both NCs. This process was also found in micromagnetics simulations, where realistic current and Oersted-Ampère field profiles for the double nanocontact where included. Some examples of the trajec-

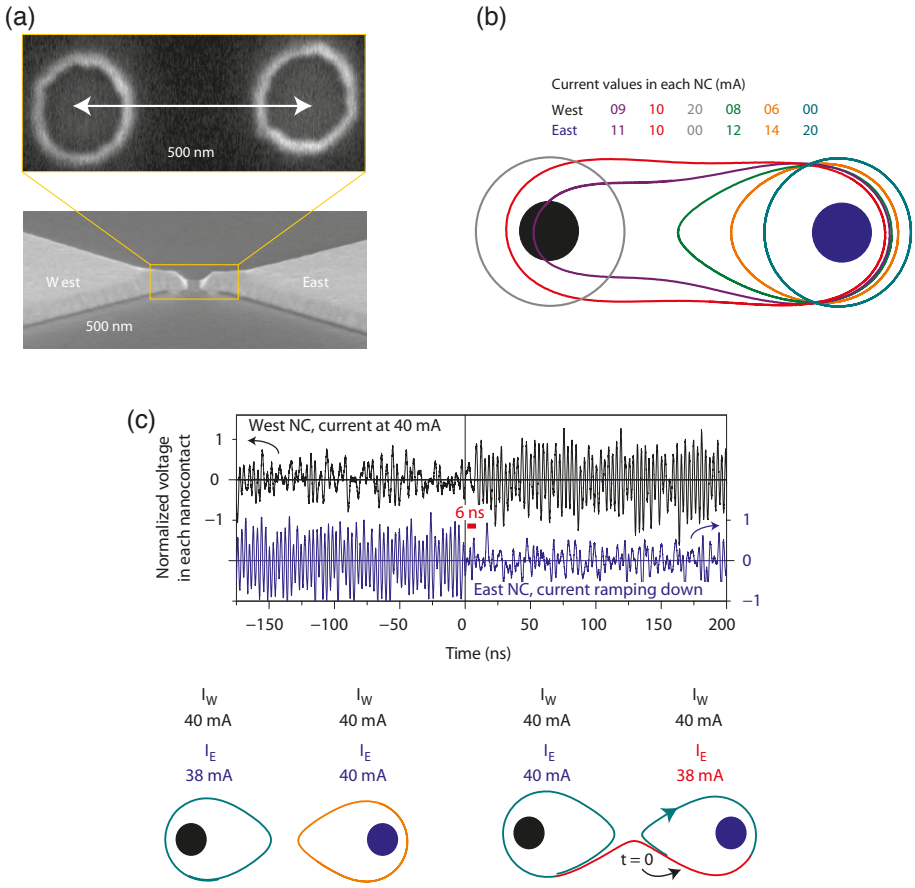

Fig. 3.8 Ballistic vortex motion in multiple nanocontact devices. (a) Scanning electron microscopy images of the two NCs during (top) and after (bottom) microfabrication. (b) Micromagnetic simulation of the vortex trajectories for the current partitioning scheme used in experiment. (c) Release and capture of a vortex in NCs separated by 680 nm. The top panel shows experimental (single-shot) time traces that show an abrupt transition between the oscillations around the West and East nanocontacts, respectively. The bottom panel illustrates the simulated steady-state orbits for asymmetric and symmetric current conditions, where an abrupt change between the two can lead to vortex gyration between transferred from one NC to the other. After Manfrini (2014).

tories are shown in Fig. 3.8(b), where it can be seen that the initial orbit around the "East" nanocontact can be gradually shifted to encompass both nanocontacts as the current is gradually decreased in one NC and increased in the other. This shows the strength of the attractive Zeeman potential can be tuned directly by the relative strength of the currents applied through both NCs and allows the vortex core to be transported from one NC to the other.

For larger nanocontact separations (e.g., 680 nm), the trajectories do not encompass both nanocontacts, as shown in Fig. 3.8(c), where two distinct orbits around the nanocontacts can be seen. Nevertheless, the abrupt change in the current balance can lead to a transfer of the vortex core from one orbit to another, which is akin to a hopping process rather than the continuous transfer shown in Fig. 3.8(b). This hopping was observed experimentally in time-resolved measurements of the magnetoresistance signal from each nanocontact, where the change in current resulted in oscillations disappearing from one NC and appearing in the other. The transit time [6 ns in Fig. 3.8(c)] was

observed to fluctuate between measurements, which suggests this process is partially driven by thermal fluctuations. Nevertheless, the experimental observations confirm the picture obtained from micromagnetics simulations.

Related Publications

Current-driven vortex oscillations in metallic nanocontacts
Q. Mistral, M. van Kampen, G. Hrkac, J.-V. Kim, T. Devolder, P. Crozat, C. Chappert, L. Lagae, and T. Schrefl
Physical Review Letters **100**, 257201 (2008).

Agility of vortex-based nanocontact spin torque oscillators
M. Manfrini, T. Devolder, J.-V. Kim, P. Crozat, N. Zerounian, C. Chappert, W. Van Roy, L. Lagae, G. Hrkac, and T. Schrefl
Applied Physics Letters **95**, 192507 (2009).

Commensurability and chaos in magnetic vortex oscillations
S. Petit-Watelot, J.-V. Kim, A. Ruotolo, R. M. Otxoa, K. Bouzehouane, J. Grollier, A. Vansteenkiste, B. Van de Wiele, V. Cros, and T. Devolder
Nature Physics **8**, 682 (2012).

Propagation of magnetic vortices using nanocontacts as tunable attractors
M. Manfrini, J.-V. Kim, S. Petit-Watelot, W. Van Roy, L. Lagae, C. Chappert, and T. Devolder
Nature Nanotechnology **9**, 121 (2014).

Spin-torque oscillators
J.-V. Kim
In volume 63 of *Solid State Physics*, R. E. Stamps and R. E. Camley, eds. (Academic Press, 2012), pp. 217–294.

4. Spin wave channelling in chiral spin systems

4.1. Background

An alternative mechanism for transporting information through the spin variable is available and in fact has been studied for over 80 years. Spin waves and their particle-like counterpart, *magnons*, are the low-lying energy states of spin systems and were first predicted by Bloch (1930). Not only do spin wave excitations exhibit a wide variety of linear and nonlinear properties, they also exist in the GHz to THz region of the frequency spectrum, which is appropriate for telecommunications and information technologies. New technologies that allow the fabrication of devices in the nanoscale together have led to the discovery of phenomena such as spin pumping (Tserkovnyak 2002), spin transfer torque (Berger 1996, Slonczewski 1996), and spin Hall effects (Dyakonov 1971, Hirsch 1999). The field now called "magnonics" is concerned with consequences of the fact that the transport and processing of information can be achieved without physical charge transport.

Challenges addressed in this field pertain to issues related with spin wave dissipation, device miniaturisation, and fabrication of artificial magnonic crystals. Recently, consequences of the Dzyaloshinskii-Moriya interaction (DMI) on spin wave properties has been studied extensively, especially in regards to interface-induced DMI. The DMI arises in low-symmetry materials with a strong spin orbit coupling and is modelled as an antisymmetric form of the exchange interaction. Dzyaloshinskii first postulated this interaction in order to explain weak ferromagnetism in antiferromagnets (Dzyaloshinsky 1958). A few years later Moriya (1960, 1960b) calculated the second order energy terms associated with spin orbit couplings for the exchange interaction, thereby establishing a mechanism for the interaction.

Interfacial DMI is of particular interest for magnonics. Udvardi and Szunyogh in 2009 suggested the possibility that the spin wave chiral degeneracy (resulting from the isotropic part of the exchange) could be lifted in the presence of DMI. From a first-principles calculation they found an asymmetric magnon dispersion for an iron monolayer on tungsten for a certain direction of propagation that was explained by the presence of the DMI. Shortly thereafter, Zakeri *et al.* (2010) demonstrated a DMI driven asymmetry in the spin wave dispersion using spin-polarised electron energy loss spectroscopy on an iron double-layer grown on tungsten. Theoretical studies suggested that DMI induced non-reciprocity should exist (Costa 2010, Cortes-Ortuno 2013, Moon 2013) and inelastic light scattering studies provided evidence for non-reciprocal dispersion phenomenon and has been used to obtain measures of its strength (Di 2015, Di 2015b, Belmeguenai 2015, Nembach 2015, Cho 2015, Soucaille 2016). Localised spin wave modes have been studied for many years and are particularly important for thin film geometries and in-

homogeneous magnetic configurations. In particular, Winter calculated spin wave properties for propagation along a Bloch domain wall in the context of nuclear magnetic resonances in 1961 and outlined the properties of a wall localised mode that appears in the modified spin wave dispersion. An unpinned wall supports a mode with zero energy for propagation perpendicular to the plane of the wall and a quadratic gapless dispersion for propagation parallel to the plane of the wall in which there is no spatial variation of the static magnetisation.

In this chapter, I present theoretical studies of spin wave channelling in ultrathin films, in particular, along domain walls and as a result of the Dzyaloshinskii-Moriya interaction and dipolar effects. I describe how the DMI affects the gap between the energies of freely propagating spin waves and the spin waves channelled along walls, as well as consequent non-reciprocities. These features provide the essential ingredients for a new type of application whereby domain walls are used to guide and control the flow of spin wave information. Much of this work was carried out with Felipe Garcia-Sanchez (postdoc) at IEF, along with Pablo Borys (PhD) and Robert Stamps at the University of Glasgow, and Robert Camley at the University of Colorado at Colorado Springs.

4.2. Spin wave focusing and caustics

To understand how the nonreciprocal behaviour comes about, it is useful to consider the magnetisation dynamics in the micromagnetics approximation. By linearising the Landau-Lifshitz equation (1.1), we can compute the dispersion relation for spin waves in an ultrathin film with DMI in the Damon-Eshbach geometry, where the magnetisation is saturated along the y direction by a magnetic field and spin waves are assumed to propagate in the film plane (Kim 2016),

$$\omega(\mathbf{k}) = \sqrt{\omega_{||}(\mathbf{k})\omega_{\perp}(\mathbf{k})} - \frac{2\gamma D k_x}{M_s}. \tag{4.1}$$

Here, D is the DMI constant, M_s is the saturation magnetisation, k_x is the wave vector component along x, and γ is the gyromagnetic constant. The square root term indicates a geometric average over two frequencies (energies),

$$\omega_{||}(\mathbf{k}) = \omega_0 + \omega_{\mathrm{ex}}(k) + \frac{1}{2}\gamma\mu_0 M_s d\,\frac{k_x^2}{k}, \tag{4.2}$$

$$\omega_{\perp}(\mathbf{k}) = \omega_0 + \omega_{\mathrm{ex}}(k) - \omega_K - \frac{1}{2}\gamma\mu_0 M_s d k, \tag{4.3}$$

which expresses the fact that the precession is elliptical. ω_{ex} is the exchange contribution, ω_K is the anisotropy contribution, d is the film thickness, and the dipolar interaction is captured by the terms containing M_s. From Eq. (4.1), one can immediately deduce the nonreciprocal propagation introduced by the linear term in k_x. Note that propagation is reciprocal along the y direction, parallel to the magnetisation.

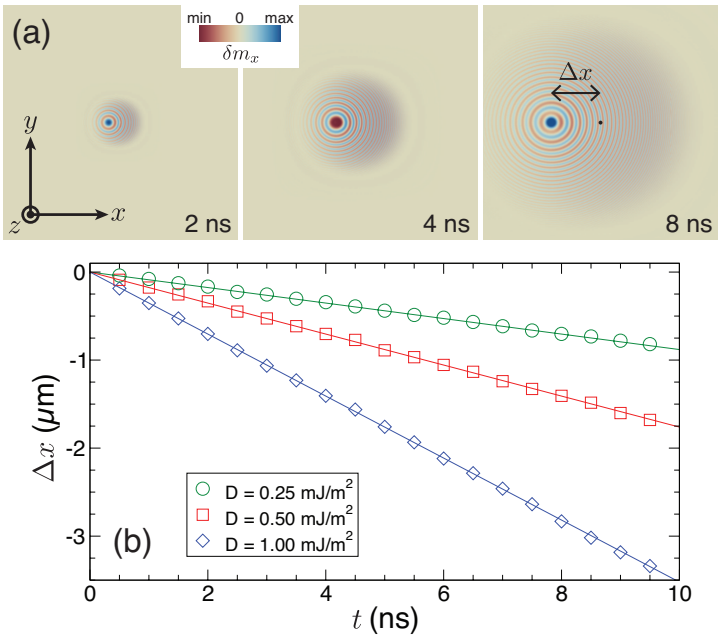

Fig. 4.1 DMI-induced drift of a spin wave ripple. (a) Time evolution of a spin wave ripple at three instants (2, 4, and 8 ns) after the application of a sinusoidal field pulse at the centre of the image, with $D = 1$ mJ/m^2. The image dimensions are 10 μm × 10 μm. Δx denotes the displacement of the ripple centre. (b) Ripple displacement as a function of time for three different values of D. Symbols correspond to simulation data while solid lines are based on theory. After Figure 2 of Kim (2016).

Another interesting consequence of the shifted dispersion relation can be seen in Figure 4.1, where results of micromagnetics simulations of the transient response of the dynamical magnetisation to a pulsed field excitation are shown. After the application of the field pulse, we observe a ripple structure that represents spin waves radiating outward from the excitation source, a common feature of wave phenomena like the water ripples observed after a pebble is thrown into a pond. An important feature for the DMI case is that the centre of the ripple is observed to drift along the $-x$ direction as its size grows, which can be seen from the snapshots in Fig. 4.1(a) taken at different instants after the field pulse. In Fig. 4.1(b), the displacement of this ripple is shown as a function of time after the application of the field pulse for different values of the DMI constant. The drift velocity of the ripple depends on D, where the lines indicate the expected displacement given by the drift part of the dispersion relation, which represents the component for which the phase and group velocities are identical. The simulated displacement of the ripple agrees very well with this interpretation, indicating that the DMI leads to an underlying drift in the spin wave propagation in the Damon-Eshbach geometry. This is consistent with a recent idea that the DMI can be interpreted in terms of a Doppler shift by an intrinsic spin current (Kikuchi 2016).

The DMI-induced drift in the spin waves has interesting consequences for power flow. With interfacial DMI and for propagation in the Damon-Eshbach geometry, the dispersion curve is approximately parabolic but with the

minimum shifted away from the origin along the wave vector axis. This results in the group velocity being opposite to the phase velocity in some regions. However, this simple analysis is not sufficient to capture all the important features of the anisotropic power flow created by the DMI. The study of focusing patterns for bulk (Taylor 1969) and surface phonons (Camley 1983) in crystals is well known. The corresponding investigations in thick film magnetic systems have begun only recently with both experimental (Demidov 2007, Demidov 2009, Schneider 2010, Sebastian 2013) and theoretical results (Veerakumar 2006). The focusing results have already shown remarkable behaviours, including focusing effects of energy well below the expected diffraction limit and an interesting reflection behaviour for energy where the angle of incidence is not equal to the angle of reflection. In many respects the magnetic system offers richer phenomena because the external magnetic field offers the opportunity to tune the dispersion relations and alter the focusing patterns, something that is not available in phonon focusing.

In general, the far-field radiation pattern of waves excited by a point source can be predicted from the slowness surface, i.e., a constant frequency curve in $k-$space. The radiation or focusing pattern can then be determined from the power flow, directed along the normal to the slowness surface, and with an amplitude which is inversely proportional to the square root of the curvature of the slowness surface (Veerakumar 2006). *Caustics* appear at points along the slowness surface at which its curvature goes to zero, resulting in a divergence in the power flow. To understand how caustics appear for spin waves in ultrathin films with interfacial DMI, let us return to the dispersion relation in Eq. (4.1) from which the slowness surfaces can be computed. There are three main contributions to the spin wave energy that are wave vector-dependent. First, the exchange term, $\omega_{\text{ex}} \sim k^2$, gives a circular component to the slowness surface that results in a finite and positive curvature for all propagation directions in the film plane. As such, radiation of spin wave power from an excitation point source is isotropic with only the exchange term. Second, the DMI results in simple displacement of the slowness surface in wave vector space, but does not influence the curvature in any way. This results in the overall drift of excitation patterns, as discussed above. Third, the dipole-dipole interaction not only leads to elliptical precession but also *anisotropic* propagation in the film plane with respect to the magnetisation orientation.

The combination of these three terms leads to nontrivial spin wave flow. Some examples are shown in Figure 4.2, where the slowness surface and focusing patterns are presented at five different frequencies for a 2-nm-thick film. In Fig. 4.2(a), the slowness surface for each frequency is shown, where elements of the three interaction terms can be seen. The group velocity vectors are also indicated along each slowness surface. The expected focusing patterns are shown in Fig. 4.2(b), computed from the curvature of the slowness surface in Fig. 4.2(a). For the lowest frequency considered (4.2 GHz), a caustic can be seen for spin wave propagation in the $-x$ direction, which is a consequence of the flattening on the left part of the slowness surface. As the

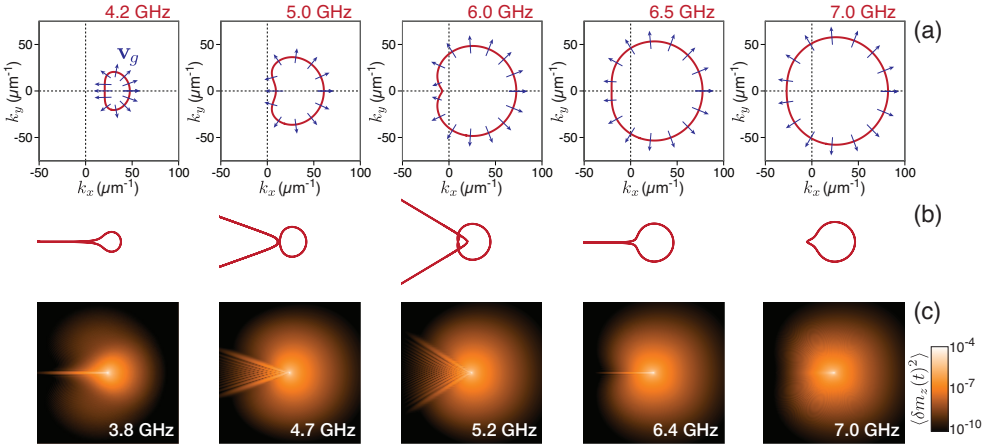

Fig. 4.2 Spin wave power flow and caustics. (a) Slowness surfaces for different frequencies determined from Eq. (4.1). $\mathbf{v}_g$ denotes the group velocity vector. (b) Predicted focusing patterns based on the slowness surfaces in (a). (c) Simulated focusing patterns due to a sinusoidal point source excitation at different frequencies. Each image represents an area of 20 μm × 20 μm and the point source is located at the centre. The frequencies are chosen to match the focusing patterns in (b). After Figure 4 of Kim (2016).

frequency is increased to 5 and 6 GHz, a 'dent' develops in the slowness surface, leading to two caustics propagating outward in the $-x$ direction. The presence of the dent leads to the curvature vanishing at two points along the slowness surface, resulting in the two focused beams predicted. As the frequency is further increased, the dent vanishes and a single caustic is recovered at 6.5 GHz. For higher frequencies, the exchange terms become dominant in the dispersion relation and the slowness surfaces recover a more circular shape, resulting in smaller focusing effects as seen for 7.0 GHz.

The predicted focusing patterns can be compared with results from micromagnetics simulations, with which the spin wave power flow from a point source excitation can be computed. The same geometry as for Fig. 4.1 is considered, but instead the response to a continuous sinusoidal point source field excitation is computed. In Fig. 4.2(c), the spin wave power is presented for five difference excitation frequencies, which is computed by time averaging the m_z component of the dynamic magnetisation, following the application of the field excitation. The excitation frequencies used in the simulations were chosen to match as closely as possible the focusing patterns predicted from the dispersion relation [Fig. 4.2(b)]. While the agreement in the frequencies is only semi-quantitative, the simulations reproduce well the different focusing patterns predicted, namely the orientation and trends in the different caustics as the excitation frequency is increased. The discrepancy is likely due to the local approximation used for the dipolar interaction in Eq. (4.1). Nevertheless, relatively good agreement between the simple analytical theory and full micromagnetics can be achieved.

Another remarkable feature of Eq. (4.1) is the possibility of generating interference patterns from a single point source. Some evidence of interference can already by seen in Fig. 4.2(c) for the excitation frequencies of 4.7 and 5.2

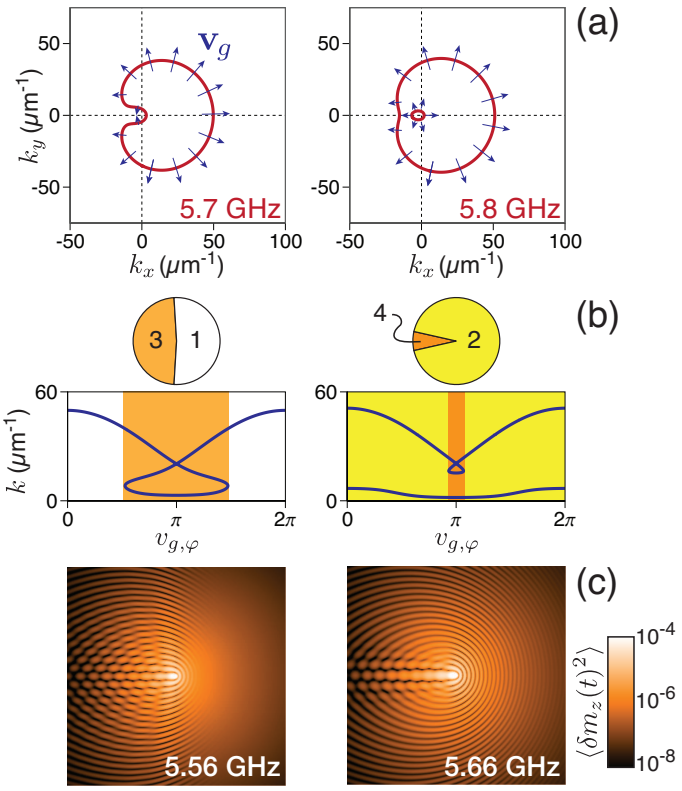

Fig. 4.3 Interference patterns. (a) Slowness surfaces for two frequencies determined from Eq. (4.1). $\mathbf{v}_g$ denotes the group velocity vector. (b) Wave vector k as a function of the direction of $\mathbf{v}_g$ for the slowness surfaces in (a). The shaded regions denote propagation directions for which several k are possible. In the top inset, a schematic real space representation of propagation directions along which interference is expected, where the numbers indicate the number of allowed k. (c) Simulated interference patterns due to a point source excitation at different frequencies. Each image represents an area of 5 μm × 5 μm with the point source located at the centre. The frequencies are chosen to match the interference patterns expected from (b). After Figure 5 of Kim (2016).

GHz in the region bounded by the two focused beams. To illustrate how such effects arise, we consider an example in which the dent in the slowness surface evolves into two distinct surfaces between 5.7 and 5.8 GHz, as shown in Figure 4.3(a). Consider first the response to the excitation at 5.7 GHz, which results in a *C*-shaped slowness surface. By looking at how the group velocity vector evolves around this surface, we notice that certain orientations of $\mathbf{v}_g$ appear at multiple points along this surface, which indicates that propagation along these directions can involve partial waves with different wave vectors. To see this more clearly, we plot in Fig 4.3(b) the magnitude of the wave vector k as a function of the propagation direction in the film plane, $v_{g,\phi}$, for the two excitation frequencies considered. For 5.7 GHz, a range of propagation angles can be identified in which three values of the wave vector are allowed, while only a single k is allowed outside this range. This is illustrated schematically above the graph in Fig. 4.3(b), which suggests that three-wave interference should only be seen for propagation near the $-x$ direction, while no interference is expected for propagation along $+x$. This picture is verified in

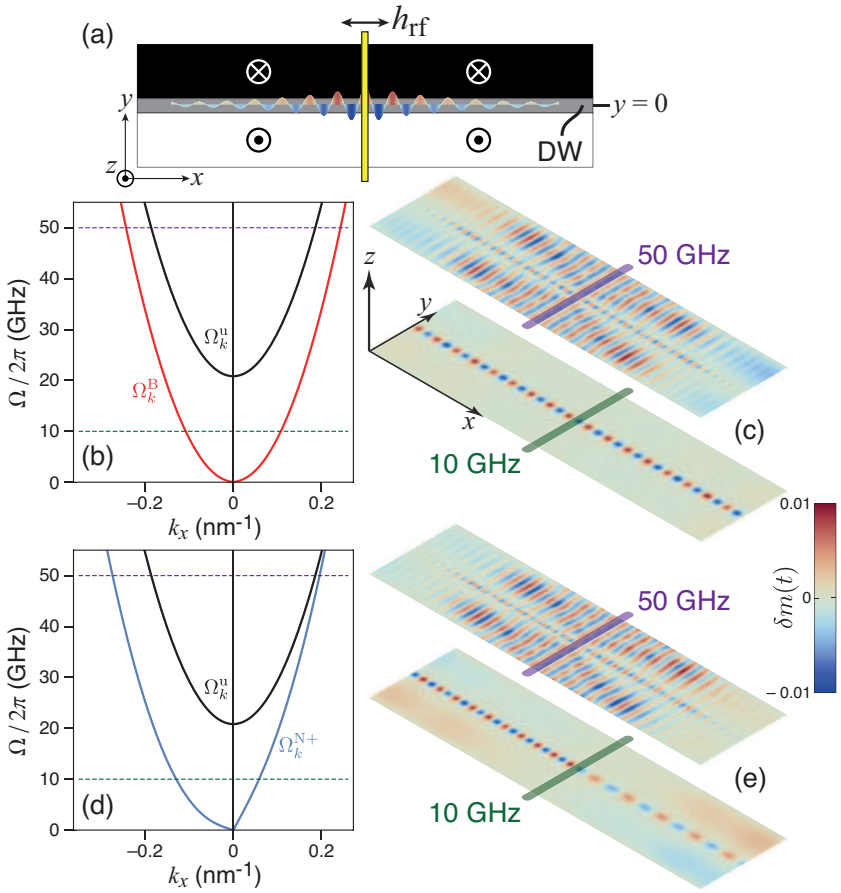

Fig. 4.4 A magnonic waveguide based on a domain wall (DW). (a) Geometry for spin wave propagation along the centre of the wall, where an radio-frequency antenna generating an alternating field h_{rf} excites spin waves that propagate along x. (b, d) Dispersion relation for channelled Bloch (b, red curve) and Néel (d, blue curve), domain wall spin wave modes in comparison with bulk spin waves (black curve). For the Néel wall, $D = 1.5$ mJ/m^2. (c, e) Simulation results of propagating modes for excitation field frequencies in the bulk (50 GHz) and in the gap (10 GHz) for Bloch (c) and Néel (e) walls. These driving frequencies are shown as dashed lines in (b, d). After Figure 1 of Garcia-Sanchez (2015).

micromagnetics simulations at a similar excitation frequency of 5.56 GHz, where interference is mostly localised to the $x < 0$ region.

4.3. Spin wave channelling in domain walls

Surfaces and boundaries are natural elements along which propagating waves can become localised. A well known example concerns whispering gallery modes, which represent a class of eigenmodes in which multiple reflections along a concave boundary leads to localised waves that propagate freely along curved surfaces. Such channeled modes appear in a wide variety of contexts, ranging from the original observation by Lord Rayleigh of whispering gallery sound waves in the rotunda of St. Paul's Cathedral (Rayleigh 1910) to guided light in nanometer scale dielectric resonators based on zinc oxide needles (Nobis 2004). In ferromagnetic systems, spin waves can be localised along film surfaces due to the dipolar interaction. Such excitations are known as Damon-Eshbach modes and represent long wavelength spin waves in the magnetostatic limit. We show here that spin wave excitations localised

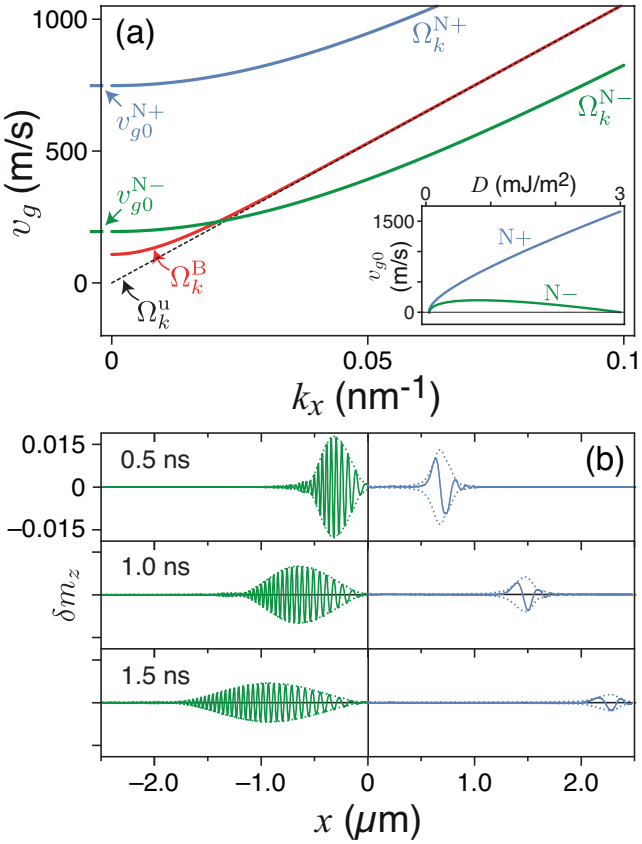

Fig. 4.5 (a) Group velocity for domain wall channelled and bulk spin waves. The branches are indicated in Fig. 4.4(a) and the sign denote the direction of propagation. The inset shows the $k \to 0$ limit of the group velocity for the two Néel wall modes as a function of the Dzyaloshinskii-Moriya constant, D. (b) Wave packets in a Néel wall channel at three instants after generation by a sinusoidal pulse with a frequency of 7.5 GHz. After Figure 4 of Garcia-Sanchez (2015).

to a domain wall can have unexpected and previously unrecognised features. One consequence is that we can view these as an unusual analogy to whispering gallery modes with features not found in other systems due to a breaking of chiral symmetry.

We have investigated a paradigm for spin wave propagation that relies on magnetic domain walls as natural waveguides. It is well known that spin waves propagating across a domain wall experience a scattering potential, which for static Bloch-type walls is reflection-less (Winter 1961, Braun 1994) and only leads to phase shifts (Hertel 2004, Bayer 2005) but can result in momentum transfer for dynamic walls (Zvezdin 1984, Bouzidi 1990, LeMaho 2009). Phenomena related to the latter have motivated studies examining how domain wall motion can be effected by spin waves alone (Mikhailov 1984, Hinzke 2011, Tveten 2014). Instead, we focus on a class of eigenmodes localised to the domain wall centre but which propagate freely in the direction parallel to the wall as a result of a confining potential. We show theoretically and through micromagnetics simulations that such modes can be channeled in curved geometries with no additional scattering, particularly for excitation frequencies in the gap of bulk spin wave modes. These modes are distinct from other known examples of whispering gallery modes because

they are one dimensional. Moreover, chiral symmetry breaking due to a Dzyaloshinskii-Moriya interaction (DMI) leads to nonreciprocal propagation along Néel walls, a feature unknown for whispering gallery modes.

The basic principle of the domain wall magnonic waveguide is illustrated in Fig. 4.4. A domain wall separates two uniformly magnetised "up" and "down" states with the wall axis along y, which is perpendicular to the wire axis x. The spin waves considered are associated with localised domain wall eigenmodes that propagate along the x direction, parallel to the domain wall. In the micromagnetics simulations used (Vansteenkiste 2014), these modes are driven by a microwave antenna that is modelled as a line source of a sinusoidal excitation field h_{rf}. For a microwave field excitation in the frequency gap of the bulk modes, one observes that only the localised Winter modes are excited and are effectively channelled along the domain wall centre [Fig. 4.4(c), excitation at 10 GHz], which acts as a local potential well for the spin waves. The wavelength at 10 GHz is approximately 60 nm, which means there is sub-wavelength confinement in both the film thickness (1 nm) and across the width of the domain wall (~18 nm); such localised modes therefore represent true one-dimensional propagation of spin waves. When the microwave field is applied in the frequency band of the bulk modes, the channelling phenomenon is preserved whereby the localised modes can be seen to propagate with a higher wave vector than the bulk modes [Fig. 4.4(c), excitation at 50 GHz].

For Néel walls, the behaviour is similar except that a strong nonreciprocity can be seen in the channelled modes. Néel walls can be stabilised in ultrathin films with the DMI, which results in a hybridisation of the Winter modes. Nevertheless, it is possible to obtain an expression for the dispersion relation by using perturbation theory, where the usual Winter modes are used as the scattering basis. We find

$$\Omega_k^{\mathrm{N}\pm} = \sqrt{\omega_k \left(\omega_k - \omega_\perp + \frac{\pi \omega_{D,k}}{k\Delta} \right)} \pm \pi \omega_{D,k}, \tag{4.4}$$

which possess a similar structure to the propagation modes in the uniform state [Eq. (4.1)]. ω_k is the exchange term and $\omega_\perp$ represents a transverse anisotropy, which essentially models the dipolar energy that separates the Bloch and Néel states. $\omega_{D,k}$ represents the DMI and is identical to contribution in Eq. (4.1). A notable difference is the presence of the domain wall parameter, Δ, which sets a length scale for the Winter modes. There is also another importance difference: the linear k_x dependence does not lead to a shift in the quadratic dispersion as a result of the ellipticity. Instead, the dispersion relation becomes markedly asymmetric with respect to $k_x = 0$ [Fig. 4.4(d)], where a quasi-linear variation is seen for $k_x > 0$ while a strongly quadratic variation is preserved for $k_x < 0$. This asymmetry leads to pronounced differences in the left- and right-propagating wave vectors, which can be seen for microwave field excitations in the frequency gap and in the frequency band of

the bulk spin wave modes [Fig. 4.4(e)]. The channelling properties of the Néel-type wall are preserved even in cases where the localised and propagating mode frequencies are closely spaced, which can be seen for the $k_x > 0$ propagation at around 50 GHz. It is interesting to note that the energies of the channelled and bulk mode become degenerate for a certain value of k_x for finite D, where an inversion of the gap separating the localised from the bulk states occurs.

Because of its strong asymmetry, the dispersion relation in Eq. (4.4) for Néel wall modes has interesting consequences for wave packet propagation. In Fig. 4.5(a), the group velocity of the Bloch and Néel modes are shown as a function of wave vector. The dispersion for Bloch modes are dominated by the exchange, leading to strong dispersion that is similar to the bulk modes. For the Néel modes, on the other hand, we observe a weaker dispersion with a large group velocity in the zero wave vector limit, which has a strong dependence on the DMI [Fig. 4.5(a), inset)]. The consequences on wave packet propagation are illustrated in Fig. 4.5(b), where the response to a sinusoidal field pulse is shown at three instants in time. We observe a noticeable dispersion in the '–' branch for the leftward propagating wave packet, while its rightward counterpart ('+') largely retains its shape after distances of a few microns. Moreover, the group velocity here is found to be 1550 m/s from simulation, which is close to the theoretical value of 1700 m/s predicted by the analytical model. Such features may be promising for magnonic circuits.

4.4. Edge (partial wall) channelling

Another important consequence of the Dzyaloshinskii-Moriya interaction in finite-sized nanostructures is the appearance of twisted spin states at boundary edges. This can be accounted for in the micromagnetics description from the usual variational procedure of the energy functional (Rohart 2013, Garcia-Sanchez 2014). With only energy terms due to the exchange interaction and perpendicular anisotropy, one obtains the usual free boundary conditions in the absence of any surface pinning. Crucially, the inclusion of the Dzyaloshinskii-Moriya interaction requires satisfaction of twisted boundary conditions. For example, the boundary surface normal to the y direction has the conditions,

$$D m_z + 2A\, \partial_y m_y = 0; \;\; - D m_y + 2A\, \partial_y m_z = 0, \qquad (4.5)$$

which couples the perpendicular magnetisation $m_z$with gradients in the transverse components $m_{x,y}$, and vice versa. Such conditions lead to tilts in the magnetisation at the edges even if the system is uniformly magnetised in the bulk, where the magnitude of the tilt is governed by the ratio between the exchange (A) and DMI (D) constants.

Interestingly, these tilts can be described by a partial domain wall, which is pinned at the boundary and centred *outside* the system (Garcia-Sanchez 2014). This behaviour is reminiscent of the partial twists encountered in exchange spring systems and ferromagnet/antiferromagnet bilayers where the

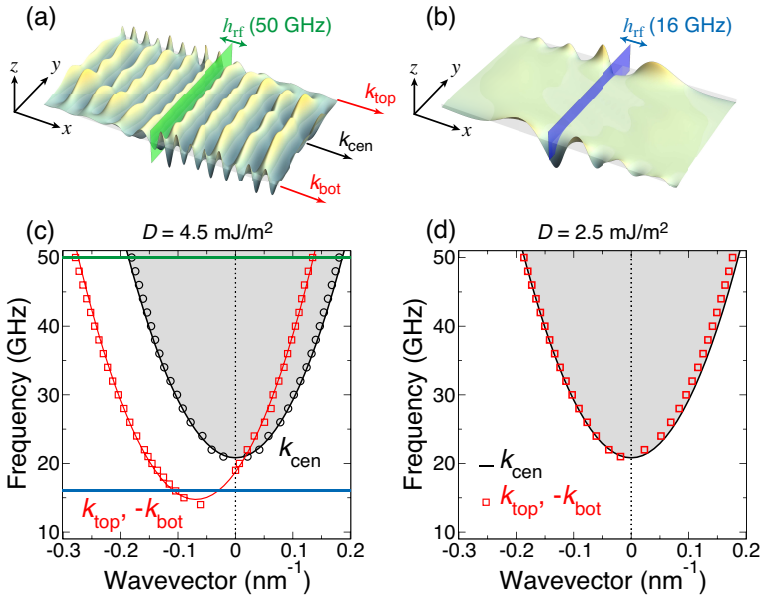

Fig. 4.6 Nonreciprocal propagation in a thin rectangular wire. (a,b) Spatial profiles of m_x resulting from an rf field excitation of 5 mT at (a) 50 GHz and (b) 16 GHz. The different wave vector components considered are illustrated. In (a), the frequency is in the spin wave band and nonreciprocal propagation occurs at the top and bottom edge, while propagation is symmetric along the centre. In (b), the frequency is in the gap of the bulk modes and only edge modes are excited. (c, d) Dispersion relations computed from simulations for two DMI constants. Dots represent simulation results. The solid black curve (and grey shaded area) represents the theoretical dispersion relation for exchange modes. The solid red curve represents a fit given by a shifted quadratic function. After Figure 3 of Garcia-Sanchez (2014).

gradual rotation of the uniformly magnetised hard (ferromagnetic) layer creates torques at the interface that are compensated by formation of a partial wall structure in the soft (antiferromagnetic) layer (Suess 2005, Mauri 1987, Kim 2005). Here, the DMI pins a partial wall at the edges through Eq. (4.5), and its strength governs the extent to which the partial wall enters the film.

The consequences for propagation along the edges of the spin texture induced by the DMI follow from the preceding discussion on Néel wall channelling. Since the edge tilts are partial Néel walls, the tails that extend into the system possess a specific chirality determined by the DMI and, as a result, the energies of spin-wave states propagating along a given edge will depend on their propagation direction relative to the (partial) domain wall orientation. The lowest-energy spin waves propagate only along one direction when localised on one side of the wire and flow in the opposite direction when localised on the other side (Fig. 4.6). For excitation frequencies in the spin-wave band, three distinct wave vectors can be identified for propagation along one direction, which correspond to the top, centre, and bottom of the wire. For rightward propagation, we note that $|k_{top}| < |k_{cen}| < |k_{bot}|$, while for leftward propagation, the opposite inequality applies. Moreover, $k_{top} = -k_{bot}$, which is a clear signature of nonreciprocal propagation. We observe a shifted dispersion relation for the edge modes, while the central modes remain symmetric about zero wave vector. For the central modes, the

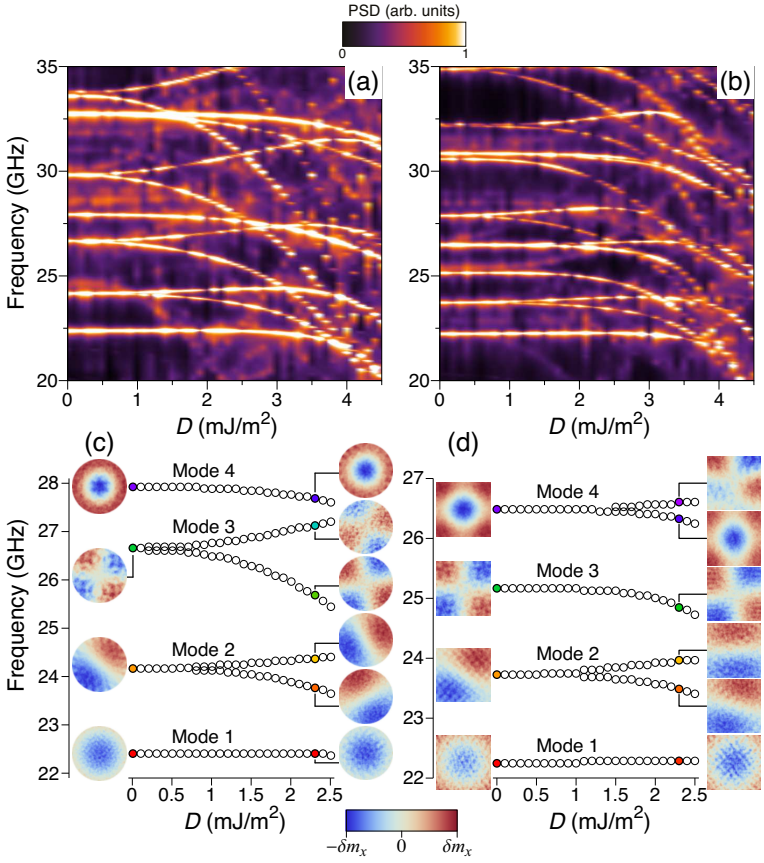

Fig. 4.7 (a) Map of the eigenmode power spectral density (PSD) as a function of D for (a) 100 nm diameter circular dots and (b) 100 nm wide square dots. Selected profiles of the four lowest modes for different strengths of the DMI for the (c) circular and (d) square dots. After Figure 4 of Garcia-Sanchez (2014).

dispersion relation is well described by exchange-dominated spin waves, where the theoretical curve agrees well with simulation. For the edge modes, the shifted dispersion relation is well described by a reduction in the spin-wave gap due to the reduced anisotropy field at the edge in addition to a linear wave vector term that describes the nonreciprocity. The centre of the partial wall is located farther outside the wire for smaller values of the DMI, which results in a weaker nonreciprocal channeling effect. This can be seen in the dispersion relation of the edge modes in Fig. 4.6(d), where the shifts become less pronounced as D decreases. This phenomenon is reminiscent of edge modes in topological insulators.

Finally, we describe the consequences of edge tilts for finite-sized nanostructures. In a circular dot, clockwise (CW) and counterclockwise (CCW) propagating azimuthal spin waves are degenerate in frequency. The DMI, however, lifts this degeneracy by favouring one handedness over the other. One can imagine the edge modes in a circular dot constructed by deforming a rectangular wire bent into a ring-shaped structure. The lowest-frequency spin waves travelling along outer circumference can propagate with only one handedness. Spin waves travelling along the inner circumference travel with the opposite handedness at the same frequency.

Fig. 4.7 illustrates the spin-wave spectra for a circular dot and a square dot. A key feature is the frequency splitting of certain modes as the DMI strength is increased. For a similar dot size, the magnitude of the splitting appears to be larger for the circular dots, which suggests that the azimuthal component of the eigenmodes plays an important role. For the circular dots, the frequency splitting with increasing DMI is associated with lifting in the degeneracy of eigenmodes with a strong azimuthal character, such as Modes 2 and 3 in Fig. 4.7(c). While there is no obvious change in the spatial profile, a frequency splitting of around 1 GHz appears at $D = 2.5$ mJ/m^2. Modes with a strong radial character, such as Modes 1 and 4 in Fig. 4.7(c), experience only a slight decrease in their frequency with increasing D and little change in their spatial profile. These differences can be understood in terms of the nonreciprocal wall channelling described above, where radial modes are similar modes that traverse a domain wall, while azimuthal modes are similar to modes that are channelled by the domain wall, which are strongly nonreciprocal. Similar features are also seen in the square dots, but the distinction between "radial" and "azimuthal" modes is not as sharp. One difference can be seen in Mode 4 in Fig. 4.7(d), which represents a mixed radial-azimuthal excitation for which splitting due to the DMI results in an asymmetric profile at higher frequencies.

Related Publications

Nonreciprocal spin-wave channeling along textures driven by the Dzyaloshinskii-Moriya interaction
F. Garcia-Sanchez, P. Borys, A. Vansteenkiste, J.-V. Kim, and R. L. Stamps
Physical Review B **89**, 224408 (2014).

Narrow Magnonic Waveguides Based on Domain Walls
F. Garcia-Sanchez, P. Borys, R. Soucaille, J.-P. Adam, R. L. Stamps, and J.-V. Kim
Physical Review Letters **114**, 247206 (2015).

Spin Wave Eigenmodes of Dzyaloshinskii Domain Walls
P. Borys, F. Garcia-Sanchez, J.-V. Kim, and R. L. Stamps
Advanced Electronic Materials **2**, 1500202 (2016).

Spin Wave Power Flow and Caustics in Ultrathin Ferromagnets with the Dzyaloshinskii-Moriya Interaction
J.-V. Kim, R. L. Stamps, and R. E. Camley
Physical Review Letters **117**, 197204 (2016).

Spin Waves on Spin Structures: Topology, Localization, and Nonreciprocity
R. L. Stamps, J.-V. Kim, F. Garcia-Sanchez, P. Borys, G. Gubbiotti, Y. Li, and R. E. Camley
In *Spin Wave Confinement II: Propagating Waves*, S. O. Demokritov, ed. (Pan Stanford Publishing, 2017), pp. 219-260.

5. Thermal processes in domain wall motion

5.1. Background

Much of the research over the past decade on magnetic domain wall dynamics has been (directly or indirectly) motivated by the *racetrack memory*, a serial magnetic shift register proposed by Stuart Parkin (2008). From a fundamental point of view, the problem has attracted much interest because it associates a complex spin-dependent transport problem with nonlinear magnetisation dynamics. This is equally true for ferromagnets based on $3d$ transition metals, such as iron, nickel, cobalt, and associated alloys, as for dilute magnetic semiconductors such as (Ga,Mn)As. On the transport side, the problem involves computing the correct torques exerted on the magnetisation by the conduction electron spins. On the magnetism side, issues involve understand how these torques drive the motion of the domain wall, particularly when defects and thermal effects are present.

It is possible to gain good insight into the physics of current-driven motion through the one-dimensional model (ODM) for domain-wall dynamics. This model was much studied in the 1970s (Schryer 1974, Malozemoff 1979) and later adapted to the case of exchange torques due to coupling to conduction electrons by Berger (Berger 1984, Freitas 1985, Berger 1992) and Tatara and Kohno (Tatara 2004). The one-dimensional model can be derived using the Lagrangian formulation. By assuming the usual Bloch wall profile as a solution and elevating the wall position, $q(t)$, and the internal angle, $\varphi(t)$, to collective coordinates, we can derive the equations of motion

$$\dot{\varphi} + \alpha \frac{\dot{q}}{\Delta} = -\left(\frac{\gamma}{2M_s}\right)\frac{\partial U}{\partial q} + \frac{\beta u}{\Delta}, \tag{5.1a}$$

$$\frac{\dot{q}}{\Delta} - \alpha\dot{\varphi} = \left(\frac{\gamma}{2M_s\Delta}\right)\frac{\partial U}{\partial \varphi} + \frac{u}{\Delta}. \tag{5.1b}$$

Here, Δ is the domain wall width parameter, α is the Gilbert damping constant, β is the nonadiabatic spin torque parameter, and U is the internal energy (per unit area) of the domain wall. u is the effective spin drift velocity and is proportional to the applied current density J,

$$u = \frac{Pg\mu_B}{2eM_s}J,$$

where P is the spin polarisation, μ_B is the Bohr magneton, and e is the electron charge.

The nonadiabatic term is particularly important for wall propagation, as it plays the same role as an applied magnetic field. As a result its relative strength, compared with the adiabatic term, determines the qualitative behaviour of the current-driven dynamics, particularly with respect to whether any intrinsic threshold current exists for wall motion (Tatara 2004, Thiaville 2005). However, the physical origin of this non-adiabatic term re-

mains a subject of debate. In one line of inquiry, different authors have sought to associate β with the viscous damping coefficient α, since both parameters describe dissipative processes (Duine 2007). Barnes and Maekawa suggested that β and α should be equal because of Galilean invariance (Barnes 2005), while Kohno *et al.* (2006), Duine *et al.* (Duine 2007), and Piéchon and Thiaville (Piéchon 2007) have found that β and α are not equal in general. In a different picture, Tatara and Kohno associate β with ballistic domain wall resistance (Tatara 2004), which is independent of α and depends only on the transport properties of the system. Much of the difficulty in reaching a consensus is therefore related to the complexity in defining the β-term theoretically and in measuring it experimentally.

To gain deeper insight into this issue, we sought to understand how realistic experimental conditions, such as finite temperatures and material defects, play a role in how β-term is determined. With Gen Tatara at the Tokyo Metropolitan University and Yann Le Maho, a PhD student I co-supervised, we examined how spin waves can contribute to the current-driven motion of a domain wall. Another aspect involves domain wall depinning under currents, where I developed a transition rate theory to describe how the effective energy barrier is modified by the spin torque terms. Elements of this theory were used to interpret the experimental data of Capucine Burrowes, a PhD student in out group. This work also served to explain depinning phenomena in more general terms, where I collaborated with Jean-Philippe Tétienne (PhD), Thomas Hingant (PhD), and Vincent Jacques of the *Laboratoire Aimé Cotton* (CNRS/ENS Cachan/Univ. Paris-Sud), who conducted experiments using nitrogen-vacancy nano-magnetometry to image domain wall hopping in ultrathin films. In the following, I describe this theoretical work in some detail and highlight some of the key experimental results involved.

5.2. Spin wave contributions to current-driven domain wall motion

With Yann Le Maho and Gen Tatara, we were motivated by the hypothesis that the interaction between the domain wall and spin waves produces a term similar to the nonadiabatic term, but in the presence of *only* the adiabatic component of spin transfer. The role of spin waves on field-driven domain wall dynamics has been examined by a number of authors in the past (Winter 1961, Janak 1964, Bouzidi 1990, Helman 1991), but their role on current-driven wall dynamics had not been studied in much detail theoretically when our work on this topic started. While most theories on the β-term have focused on the transport properties of the conduction electrons, few studies have considered the motion of the nonequilibrium magnetisation by taking into account the fluctuations. Nevertheless, the interplay between spin waves and the domain wall should be important for at least two reasons. Firstly, thermal spin waves account for a decrease in the magnetisation which can be important if the system temperature approaches the Curie temperature. This is certainly the case in dilute magnetic semiconductors. Secondly, the spin waves act as a thermal bath with which energy can be exchanged with the domain wall. Indeed, the importance of spin waves as a channel for energy

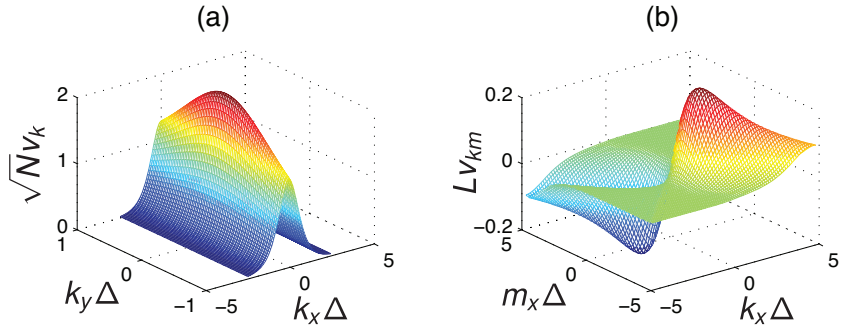

Fig. 5.1 Coefficients of the interaction potentials v_k and v_{km} as a function of wave vector. N is the total number of spins and L is the length of the wire considered. After Figure 3 of Le Maho (2009).

dissipation in magnetic system has long been recognised. In the context of the ferromagnetic resonance, for example, two-, three- and four-magnon processes have been shown to be crucial for explaining resonance line widths of ferromagnetic insulators (Sparks 1964). In the context of domain wall motion, Bouzidi and Suhl have showed that power is diverted from the domain wall motion through the amplification of some thermal spin waves (Bouzidi 1990).

The role of spin waves on current-driven domain wall motion is accounted for by extending the approach used by Bouzidi and Suhl (1990), which associates some basic ideas form the theory of solitons (Rajaraman 1982) with spin wave theory (Winter 1961, Braun 1994, White 2007). The coupling between the domain wall and the thermal bath of the spin waves, which originates in the kinetic part (Berry phase) of the spin Lagrangian (Shibata 2005, Thompson 2008), has a number of consequences on the current-induced domain wall motion. By expanding about the static solution of the Bloch wall profile (θ_0, ϕ_0), we computed the spectrum of excitations in the fluctuations $(\delta\theta, \delta\phi)$ and derived the effective domain wall/spin wave Lagrangian in the presence of adiabatic spin torques,

$$L = S\sum_{\mathbf{k}} \frac{1}{4}\theta_{\mathbf{k}}\dot{\phi}_{-\mathbf{k}} + S(u-\dot{q})\left[-\frac{p}{S} + \sum_{\mathbf{k}} \frac{k_x}{2} c^*_{\mathbf{k}} c_{\mathbf{k}}\right] - \frac{p^2}{2m} - \sum_{\mathbf{k}} \hbar\Omega_{\mathbf{k}} c^*_{\mathbf{k}} c_{\mathbf{k}} - V, \tag{5.2}$$

where $(\theta_{\mathbf{k}}, \phi_{\mathbf{k}})$ are the amplitudes of the spin wave eigenfunctions, which when diagonalised with a Bogoliubov transformation can be expressed in terms of the amplitude $c_{\mathbf{k}}$ and a frequency $\Omega_{\mathbf{k}}$. p is the conjugate momentum to q, m is the domain wall mass, S is the spin, and V is the interaction potential between the spin waves and the domain wall,

$$V = S(u-\dot{q})\left[\sum_{\mathbf{k}} v_{\mathbf{k}} \frac{p}{S}\phi_{\mathbf{k}} - \sum_{\mathbf{km}} v_{\mathbf{km}}\theta_{\mathbf{k}}\phi_{\mathbf{m}}\right] \tag{5.3}$$

where $v_{\mathbf{k}}$ and $v_{\mathbf{k,m}}$ are scattering coefficients. A numerical evaluation of these coefficients is shown in Fig. 5.1. These results show that scattering with the domain wall is most efficient for long-wavelength spin waves, where the am-

plitudes are markedly reduced for $|k_x| \gtrsim 1/\Delta$ for the coefficient v_k. The domain wall motion also mediates coupling between spin wave modes, where an enhancement in the scattering can be seen for $k_x \sim -m_x \sim 1/\Delta$ for the coefficient v_{km}.

One of the key findings of this study relates to the dissipation function that can be derived from the scattering potential in (5.3). It describes to a new dissipation channel, whereby magnons can be absorbed or emitted as the domain wall propagates. In contrast to Gilbert damping, which drives the domain wall velocity $\dot{q}$ to zero, this dissipation channel relaxes the domain wall dynamics towards the solution $\dot{q} = u$, where the domain wall velocity and the conduction electron spin current are identical and Galilean invariance is restored. This dissipation process is somewhat analogous to Landau-damping in plasmas (Landau 1946). Interestingly, Galilean invariance is restored under current-driven torques when the adiabatic and nonadiabatic spin torque terms have the same magnitude, namely $\beta = \alpha$. In our theory, this invariance is restored because the dissipation channel, in this case the magnons, also "flows" with the effective drift velocity u through the Doppler effect (Vlaminck 2008). This suggests that any dissipation channel that drifts at the same velocity as the spin current u should lead to a similar dissipation channel, for which we can write symbolically as $\alpha_{\text{drift}} = \beta_{\text{drift}}$. In the context of the analogy to Landau damping, the charged particles of the plasma resemble the domain wall spins here and the field phase velocity is analogous to the spin-current velocity u.

5.3. Transition rate theory for current-induced depinning

Besides steady-state motion, the spin torques terms also affect how domain walls depin from pinning sites under thermal activation. At the outset of this work, one of the key issues involved whether the nonadiabatic term can simply be assimilated as an effective field in the energy barrier. Moreover, it was unclear whether the domain wall width influences the magnitude of the nonadiabatic term, since it might be expected that the degree of nonadiabaticity be related to how quickly conduction electron spins can track the local magnetisation as they traverse the domain wall. In the context of the ANR project ISTRADE, we sought to address these issues by examining how domain wall depinning is affected by spin torques in two different material systems. We studied current-driven domain wall dynamics in two different pseudo spin-valve systems based either on CoNi multilayers (Burrowes 2008) or FePt alloy thin films (Attané 2006, Mihai 2009), which possess large magnetocrystalline anisotropies that lead to narrow domain walls (Δ = 10 nm in CoNi and 1 nm in FePt). In these materials, the uniaxial anisotropy is perpendicular to the film plane, which results in simple Bloch wall structures.

Thermal activation over a single energy barrier is described by an Arrhenius law, whereby the probability of escape over the barrier E_b is exponential and characterised by a time constant $\tau = \tau_0 \exp(E_b/k_B T)$, with an attempt fre-

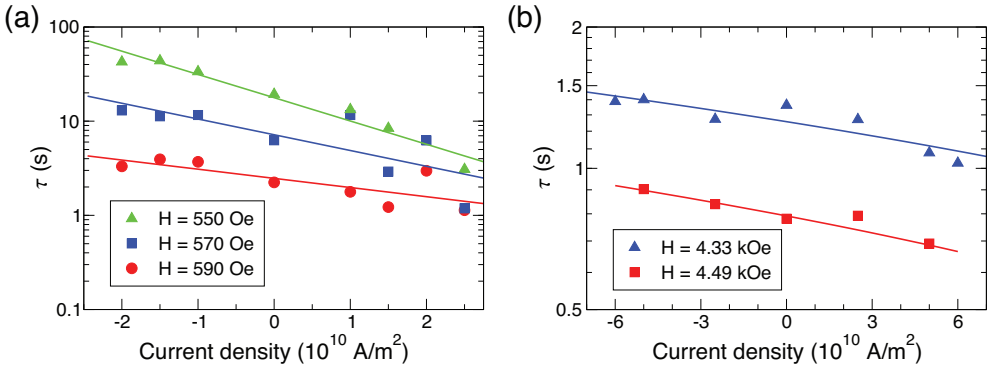

Fig. 5.2 Current dependence of the Arrhenius rate. (a,b), Characteristic time τ as a function of the applied dc current density for different magnetic field values for CoNi (a) and FePt (b). The symbols represent experimental data and the solid lines represent a linear fit on a log scale. After Figure 4 of Burrowes (2010).

quency τ_0^{-1} (Attané 2006, Kim 2009). This characteristic time was determined experimentally by measuring the distribution of times required to depin a domain wall from a defect under the action of sub-threshold currents. In CoNi, artificial notches were used as pinning sites in lithographically-defined magnetic wires, while intrinsic defects were studied in FePt (Burrowes 2010).

Fig. 5.2 shows the variation of the Arrhenius time τ as a function of low current densities, under different applied fields, for the CoNi and FePt systems. In both cases, we observe a clear linear current dependence for $\ln\tau$, implying a linear reduction in the barrier height, E_b. We can therefore suppose that the current-dependent energy barrier has the form $E_b = E_{b,0} - \sigma I$, where the efficiency parameter σ is proportional to the nonadiabatic parameter β. The linear variation of the $\ln\tau$ as a function of current has also been confirmed in micromagnetics simulations in which we considered wall depinning from a single defect. By taking into account the measured Joule heating in our fits of the experimental data, values of $\beta_{\mathrm{CoNi}} = 0.022\pm0.002$ and $\beta_{\mathrm{FePt}} = 0.06\pm0.03$ were obtained using the following theory. We note that these values are similar to known values of the Gilbert damping constant, $\alpha_{\mathrm{CoNi}} = 0.032\pm0.006$ and $\alpha_{\mathrm{FePt}} \sim 0.1$.

We extended the one-dimensional domain wall model to obtain a physical picture for the current-dependence of the energy barrier. The starting point are the stochastic versions of the one-dimensional model (5.1) with spin transfer torques,

$$\dot{\varphi} + \alpha\frac{\dot{q}}{\Delta} = \gamma_0 H_a - \left(\frac{\gamma}{2M_s}\right)\frac{\partial U_{\mathrm{pin}}}{\partial q} + \frac{\beta u}{\Delta} + f_q(t), \tag{5.4a}$$

$$\frac{\dot{q}}{\Delta} - \alpha\dot{\varphi} = \frac{1}{2}\gamma_0 H_\perp \sin 2\varphi + \left(\frac{\gamma}{2M_s\Delta}\right)\frac{\partial U_{\mathrm{pin}}}{\partial \varphi} + \frac{u}{\Delta} + f_\varphi(t), \tag{5.4b}$$

where we have written explicitly the contributions from the applied field, H_a,

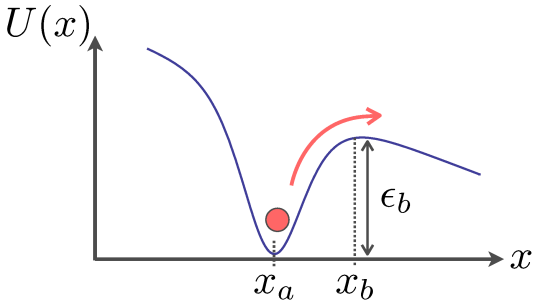

Fig. 5.3 Escape of a particle over an energy barrier by thermal activation. $U(x)$ describes the energy landscape and ε_b is the energy barrier.

and transverse anisotropy, $H_\perp$, to the conservative forces acting on the wall coordinates. U_{pin} represents the pinning potential due to defects. Eq. (5.4a) shows explicitly the correspondence between the applied and the nonadiabatic spin torque term β (at least for the dynamics). As for the oscillator model discussed in Chapter 2, f_q and f_φ are Gaussian white noise terms that represent random forces, which have zero mean $\langle f(t)\rangle = 0$ and satisfy the usual two-time correlation function, $\langle f_i(t) f_j(t')\rangle = 2D\delta_{ij}\delta(t-t')$, with D being a diffusion constant. We seek the solution of the corresponding Fokker-Planck equation for the probability distribution function $P(q,\varphi)$, rather than solving the Langevin equations (5.4) directly. This distribution function is useful because it allows transition rates due to thermal activation to be calculated using Kramer's approach. Consider the analogy with the thermally-activated escape of a particle from the well illustrated in Fig. 5.3. The particle is described by its position x and its velocity v. The transition rate of particles out of the potential well located at x_a can be estimated by (Hänggi 1990),

$$\frac{1}{\tau} = \frac{j_b}{n_a}, \tag{5.5}$$

where n_a represents the particle population in the well,

$$n_a = \int_{\text{well}} dx \int_{-\infty}^{\infty} dv\, P(x,v), \tag{5.6}$$

and j_b represents the particle current at summit of the potential barrier,

$$j_b = \int_{-\infty}^{\infty} dv\, J_x(x_b, v). \tag{5.7}$$

Here, J_x is the probability current density,

$$J_x = D_x P - \frac{\partial}{\partial x_j} D_{x,j} P, \tag{5.8}$$

which can be expressed in terms of the drift and diffusion terms, parametrised by D_x and $D_{x,j}$, respectively (Kim 2009). The probability density in (5.6)-(5.8) is precisely the solution to the (equivalent) Fokker-Planck problem.

By recognising that the wall velocity is proportional to φ at low velocities, we can use the solution to the Fokker-Planck problem for (5.4) as the suitable probability density for the transition rate theory outlined above (Kim 2009).

We find that thermally activated depinning of a domain wall over a single energy barrier is indeed given by an Arrhenius law,

$$\frac{1}{\tau} = \frac{1}{\tau_0} \exp\left[-\frac{E_b(u)}{k_B T}\right], \tag{5.9}$$

but with a current-dependent effective energy barrier,

$$E_b(u) = E_{b,0} - \left(\frac{2M_s V_d}{\gamma \Delta}\right) \beta u + \frac{1}{2m_w} \left(\frac{2M_s S_c}{\gamma \Delta}\right)^2 \left(\frac{1}{\omega_a^2} + \frac{1}{\omega_b^2}\right) (\beta u)^2. \tag{5.10}$$

Here, V_d is the defect volume, m_w is the domain wall mass, S_c is the cross-sectional area of the magnetic wire, and $\omega_{a,b}$ represent the curvature of the energy landscape at the bottom of the potential well (x_a) and at the summit of the energy barrier (x_b), respectively. While a linear current dependence of the energy barrier is found, which is consistent with the experimental data shown in Fig. 5.2, the nonadiabatic term also results in a quadratic current dependence, where details of the energy landscape play a role. However, we find numerically that the quadratic term is small compared with the linear term, which should dominate the thermal activation process in realistic systems.

5.4. Transition rate theory for domain wall hopping

The theory on domain wall depinning discussed in the previous section is based on the one-dimensional model that assumes the domain wall can be assimilated to a rigid particle. While electrical measurements, through the extraordinary Hall effect or magnetoresistance, can give some idea of the validity of this approximation, it is difficult to study any possible changes in the wall structure during the depinning process. One experimental technique that can provide deep insight into this problem is scanning nitrogen-vacancy (NV) centre microscopy, which exploits the single spin of the NV defect as an atomic-scale magnetic field sensor (Rondin 2014). The defect is created artificially in a diamond nanocrystal, which is placed on the tip of an atomic-force microscope. By illuminating the defect with a laser and a microwave field, the transitions between different spin states of the NV defect are induced, whereby the Zeeman shifts and spin-dependent photoluminescence intensity of the NV defect allow local magnetic fields (projected along the quantisation axis of the spin) to be precisely measured.

In 2013, I began a collaboration with the research group of Vincent Jacques at the *Laboratoire Aimé Cotton* (CNRS/ENS Cachan/Univ. Paris-Sud) to study domain wall processes in ultrathin ferromagnetic films. A 1.5-μm-wide Ta/CoFeB(1 nm)/ MgO wire that exhibits perpendicular magnetic anisotropy was studied (Tetienne 2014). For an ideal magnetic sample, the domain wall should be straight and perpendicular to the wire axis to minimise the wall energy. However, the presence of structural or fabrication defects locally modifies the energy landscape, creating pinning sites for the wall. To occupy a local energy minimum, the wall can become distorted across the width of the wire. Indeed, while repeating magnetic field measurements above the magnet-

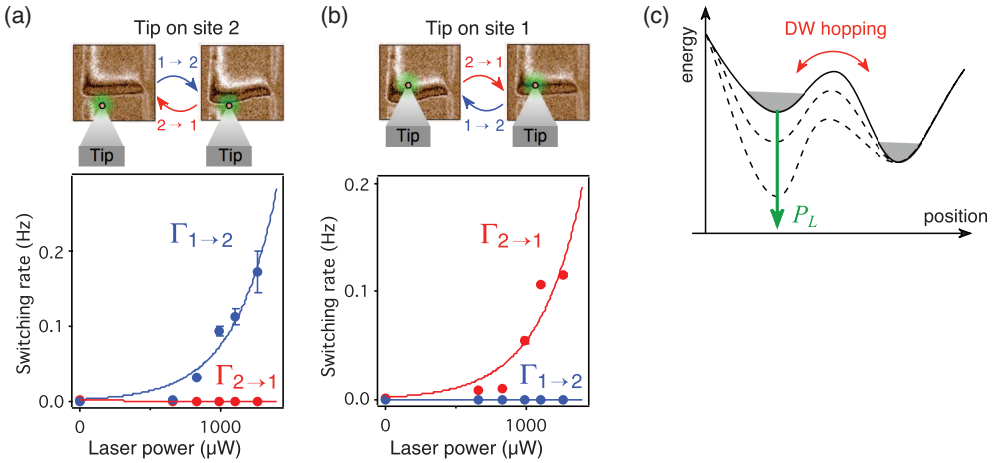

Fig. 5.4 Laser control of domain wall hopping. Hopping rates as a function of the laser power, measured with the tip placed above site 2 (a) or site 1 (b). Solid lines correspond to the theoretical model. (c) Schematic energy diagram: The laser locally reduces the domain wall energy by causing local heating, thereby stabilising the wall at the illuminated site. After Figure 3 of Tetienne (2014).

ic wire, discrete jumps of the domain wall between two pinning sites were observed. The position profiles of the domain wall at each pinning site reveal a spatial separation ranging from 50±30 nm (near the right-hand edge of the wire) to 200±30 nm (left-hand edge). The hopping of the DW between the two pinning sites, driven by thermal fluctuations, is known as the *Barkhausen effect* (Zapperi 1998).

A key experimental result is shown in Fig. 5.4. Time-resolved measurements of the magnetometer signal were made while the microscope was positioned above each of the pinning sites. The telegraph signals measured indicate that the domain wall hops stochastically between the two sites. Interestingly, the transition rate between the two sites depend strongly on the laser power P_L used to excite the NV centre, which indicates that local heating affects the energy landscape seen by the domain wall. When the microscope tip is placed above site 2, the transition rate from site 1 to site 2 increases exponentially with P_L while the back-hopping rate remains negligible [Fig. 5.4(a)]. The opposite occurs when the tip is placed above site 1 [Fig. 5.4(b)]. This suggests that the laser, through heating of the sample, acts to pin the domain wall at the site above which the microscope tip is located by lowering the potential minimum, as shown schematically in Fig. 5.4(c).

To provide a better understanding of the experimental data and a firm basis for the process illustrated in Fig. 5.4(c), I extended the stochastic theory presented in the previous section to take into account a double-well system and laser-induced heating, which alters the pinning energy landscape. A number of experimental features were taken into account. First, the spatially resolved domain wall profiles were used to determine the effective q in the one-dimensional model. The profiles at the two pinning sites are shown in Fig. 5.5(a), where the points are experimental data and the solid lines represent an inter-

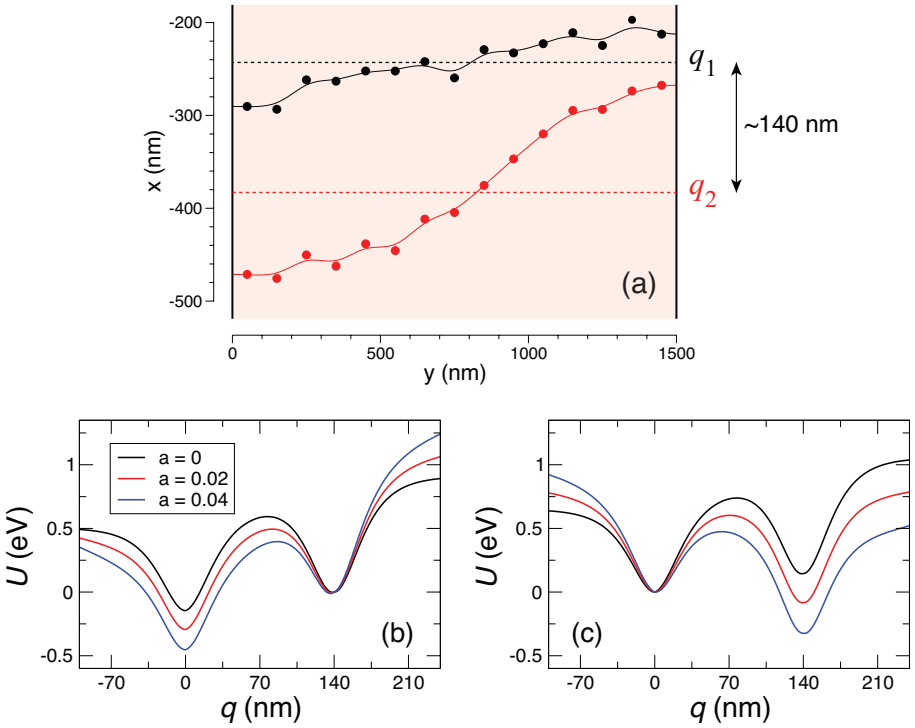

Fig. 5.5 (a) Variation in the domain wall centre across the width of the nanowire at Site 1 and Site 2. The dots correspond to experimental measurements and the solid curves represent a spline interpolation. The hopping distance computed using the centre-of-mass of the wall is approximately 140 nm. (b,c) Energy landscape under laser-induced heating, for the cases where the laser is focused on Site 1 (b) and Site 2 (c). The laser power is proportional to the parameter *a*, which correspond to experimental values. After the Supplementary Material to Tetienne (2014).

polation function. From these profiles, we can define the effective positions of the two pinning sites in the reduced model, which are denoted by q_1 and q_2. Second, we note that the length of the domain wall changes between the two sites, which also leads to a difference in the domain wall energy. This is accounted for by an additional term in the energy landscape. Third, we incorporate the laser-induced heating by using the measured heating rates and linking these to the temperature dependence of the magnetisation, which is then included into the effective potential as a variation in the local pinning field. By assuming a point-defect model, we combined these features to obtain the laser-induced double well potentials in Fig. 5.5(b) and 5.5(c). We note that the schematic picture in Fig. 5.4(c) is justified, where the laser focus at a particular pinning site results in a deeper potential minimum at that site, while the minimum at the other site is only weakly affected.

Based on the potentials, we computed the transition rates $\Gamma_{1\to2}$ and $\Gamma_{2\to1}$ between them using Kramer's approach, as discussed in the previous section, to obtain the curves shown in Fig. 5.4(a) and Fig. 5.4(b). The only fitting parameters are the pinning fields, where experimental values were used, and the attempt frequency, where estimates were based on the wall resonance frequency. Overall, the agreement between theory and experiment is very good,

which lends strong support to the idea of laser-induced pinning of domain walls in such ultrathin ferromagnetic films.

Related Publications

Spin-wave contributions to current-driven domain-wall dynamics
Y. Le Maho, J.-V. Kim, and G. Tatara
Physical Review B **79**, 174404 (2009).

Influence of magnetic viscosity on domain wall dynamics under spin-polarized currents
J.-V. Kim and C. Burrowes
Physical Review B **80**, 214424 (2009).

Non-adiabatic spin-torques in narrow magnetic domain walls
C. Burrowes, A. P. Mihai, D. Ravelosona, J.-V. Kim, C. Chappert, L. Vila, A. Marty, Y. Samson, F. Garcia-Sanchez, L. D. Buda-Prejbeanu, I. Tudosa, E. E. Fullerton, and J.-P. Attané
Nature Physics **6**, 17 (2010).

Nanoscale imaging and control of domain-wall hopping with a nitrogen-vacancy center microscope
J.-P. Tetienne, T. Hingant, J.-V. Kim, L. Herrera Diez, J.-P. Adam, K. Garcia, J.-F. Roch, S. Rohart, A. Thiaville, D. Ravelosona, and V. Jacques
Science **334**, 1366 (2014).

6. Skyrmion dynamics in ultrathin films

6.1. Background

Throughout the preceding chapters, I have presented different facets of the dynamics of magnetic solitons such as domain walls and vortices. These represent particular solutions to nonlinear differential equations and possess a nontrivial topology, which governs their behaviour. Over the past few years, focus has turned to another kind of magnetic soliton — the magnetic skyrmion (Bogdanov 1989, Bogdanov 1999, Rößler 2006). Like vortices, skyrmions represent whirls of magnetisation with a distinct core and possess a topological charge. Unlike vortices, however, skyrmions are not extended but represent true particle-like objects, much like domain walls. In a perpendicularly magnetised ultrathin thin film, for example, skyrmions are bubble-like configurations of reversed magnetisation, where boundary conditions pose no constraint on their numbers (unlike vortices). An example of Bloch and Néel skyrmions are given in Fig. 6.1. The topological charge Q of a skyrmion is given by (Braun 2012)

$$Q = \frac{1}{4\pi}\int d^2\mathbf{r}\ \mathbf{m}\cdot\left(\frac{\partial\mathbf{m}}{\partial x}\times\frac{\partial\mathbf{m}}{\partial y}\right) = \pm 1 \qquad (6.1)$$

where it is assumed that x and y span the film plane. Note that this is twice the value for a vortex, which is a meron.

Skyrmions are stabilised by chiral interactions of the Dzyaloshinskii-Moriya form (Dzyaloshinsky 1958, Moriya 1960, Moriya 1960b). One of the first experimental observations of such objects involves neutron scattering on MnSi, a B20 material that exhibits skyrmion lattices over a range of applied magnetic fields and temperatures (Muhlbauer 2009, Pappas 2009). Other experiments followed shortly afterwards with Lorentz microscopy measurements on $Fe_{0.5}Co_{0.5}Si$ (Yu 2010) and Cu_2OSeO_3 (Seki 2012), which provided real-space imaging of skyrmion lattices. Subsequent experiments showed that such lattices can be displaced under very low current densities (Jonietz 2010), which provided a strong impetus for many research efforts in the field. Skyrmions and skyrmion lattices have also been seen in monolayer ferromagnets (Heinze 2011), where the Dzyaloshinskii-Moriya interaction is induced by the strong spin-orbit coupling of an adjacent buffer layer or substrate, as discussed in Chapter 4. The observation in 2013 of the writing and deleting of individual skyrmions in a PdFe bilayer on Ir(111) gave a second impetus to this field (Romming 2013). Since, the prospects of introducing

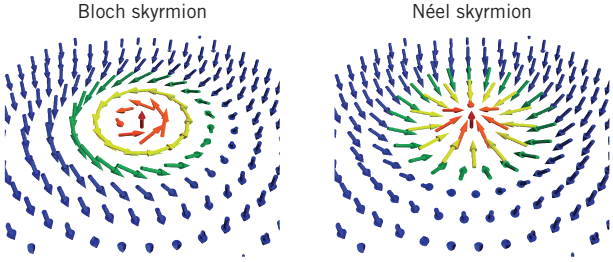

Fig. 6.1 Spin configurations of Bloch and Néel skyrmions in ultrathin films.

skyrmions into real spintronics devices have been greatly improved with several observations of room temperature skyrmions in sputtered ultrathin film ferromagnets, such as Pt/Co/Ir (Moreau-Luchaire 2016), Pt/Co/MgO (Boulle 2016), Ta/CoFeB/TaOx (Jiang 2015), Pt/CoFe/MgO (Woo 2016), Pt/Co/Pd/Co/Pt (Pollard 2017), and symmetric Pt/Ni/Co/Ni bilayers (Hrabec 2016). Skyrmions have also been observed in multilayers with a large number of repeats, such as Fe/Gd (Lee 2016, Montoya 2017, Seaberg 2017), where dipolar effects are more important.

Such experimental work has been accompanied by a plethora of theoretical and simulation-based studies, which have examined many aspects of skyrmion dynamics such as scattering with notch defects (Sampaio 2013, Iwasaki 2013), scattering with spin waves (Schütte 2014, Schroeter 2015), and dynamical instabilities (Lin 2013) and modes (Zhou 2015), and potential applications of skyrmions such as racetrack memories (Sampaio 2013, Tomasello 2014), microwave detectors (Finocchio 2015), spin-torque nano-oscillators (Garcia-Sanchez 2016), and probabilistic computing (Pinna 2018). The potential of using skyrmions for information storage technologies was recognised shortly after their first observations (Kiselev 2011).

I initiated research on this topic at IEF in 2013 shortly before the publication of the seminal work by Sampaio *et al*. in 2013. This came about as a result of a number of fruitful discussions with André Thiaville, Stanislas Rohart, Vincent Cros, and Joao Sampaio. The focus of my work has been on the dynamic aspects, which follows naturally from the large body of work conducted on magnetic vortices as described in Chapter 3. In the following, I give an overview of the theoretical work I have undertaken on skyrmion dynamics, namely breathing modes in confined systems, spin-torque--driven oscillations with inhomogeneous polarisers, and the role of disorder in current-driven skyrmion motion, and more recent work on antiskyrmion dynamics These studies have been carried out with Felipe Garcia-Sanchez and Myoung-Woo Yoo, who were both postdoctoral researchers in our group, along with Ulrike Ritzmann (Uppsala) and Bertrand Dupé (Mainz).

6.2. Breathing modes in ultrathin film dots

One of the challenges faced by experimentalists studying skyrmion dynamics is their detection, given their nanoscale size. In this section, we describe a theoretical study of the microwave response of skyrmions in ultrathin film dots. In particular, focus is directed toward the breathing dynamics of the skyrmion, which is known to provide a distinct microwave response from experiments conduced on skyrmion crystals in helimagnetic insulators (Onose 2012) and multilayers (Montoya 2017b). Particular attention is given to how the breathing dynamics is affected by the confinement and to the interaction between the breathing mode and the geometrically-quantised spin wave eigenmodes of the dot. The dynamics is studied primarily with static and dynamic magnetic fields applied perpendicular to the film plane, where it is shown that the magnetic response in this geometry provides clear signa-

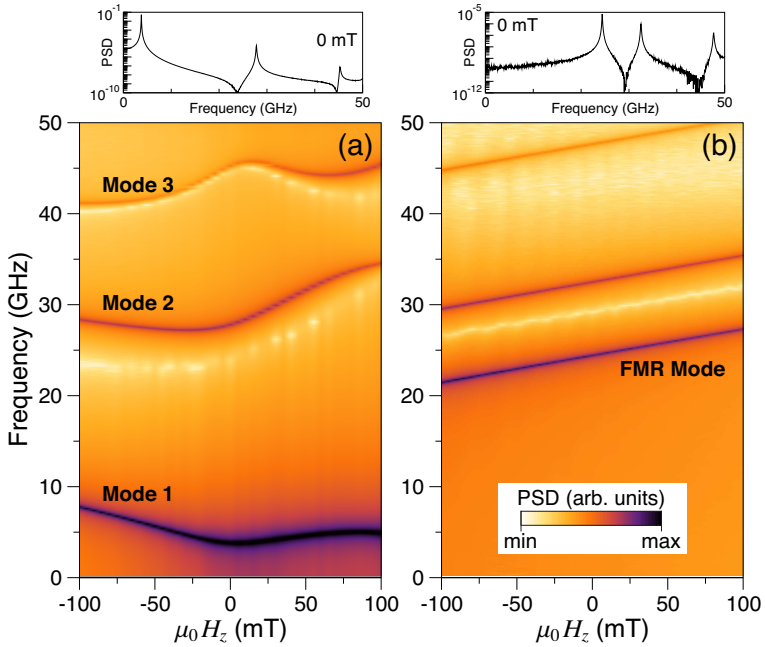

Fig. 6.2 Map of the power spectral density (PSD) of excitations as function of the applied static field H_z. (a) Single isolated skyrmion in ground state. (b) Nominally uniform ground state. FMR denotes the ferromagnetic resonance or uniform precession mode. The insets at the top show the corresponding PSD in zero static field. After Figure 3 of Kim (2014).

tures of the skyrmion excitation and therefore an alternative means of quantifying the DMI.

The static and dynamic states of the isolated skyrmion in a confined magnetic dot were studied using numerical micromagnetics simulations with a modified version of the MuMax2 code (Vansteenkiste 2011). The calculations performed involve the dynamic response of the perpendicular magnetisation to perpendicular ac fields h_z,

$$m_z(\omega) = \chi_{zz}(\omega) h_z(\omega).$$

In the absence of the DMI, the equilibrium ground state is uniformly magnetised along the easy z axis (perpendicular to the film plane), which means that the linear susceptibility χ_{zz} is vanishingly small. In the context of spin wave excitations, this corresponds to the parallel pumping geometry in which the lowest-order response involves nonlinear spin wave processes that appear above a finite threshold of the pumping field (Sparks 1964). However, the presence of the DMI in a finite-sized system necessarily leads to a non-uniform magnetic configuration. First, magnetisation tilts away from the easy axis at boundary edges as a result of nontrivial boundary conditions, leading to a state that can be described by pinned partial Néel domain walls at the edges, as discussed in Chapter 4. Second, a skyrmion involves large magnetisation tilts across its core, with variations between $m_z \pm 1$ that can extend over a sizeable fraction of the dots studied (Sampaio 2013, Rohart 2013). These tilts allow for coupling to the perpendicular ac field and lead to a finite response for χ_{zz} even for vanishingly small driving ac fields h_z. Moreover, the

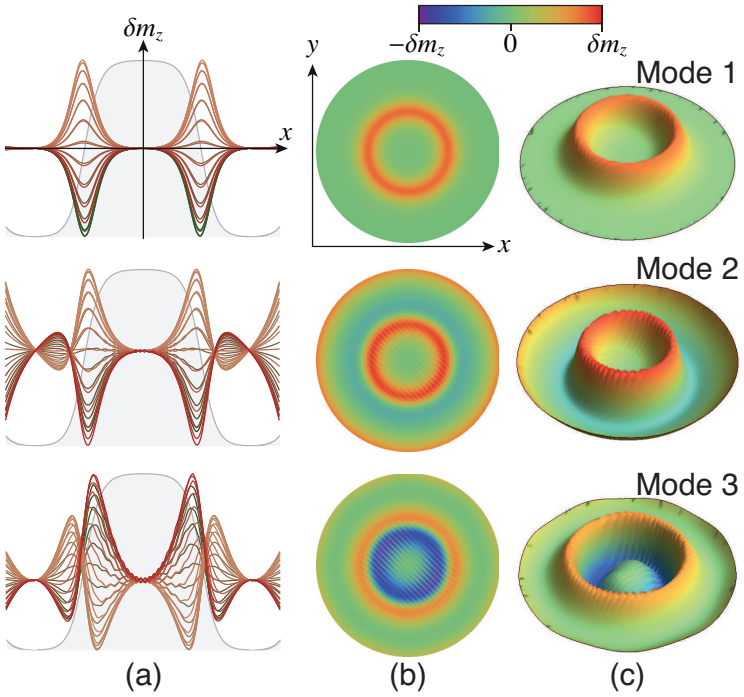

Fig. 6.3 Spatial profiles the fluctuation in the magnetisation component m_z of the skyrmion breathing modes for at zero field. (a) Spatial profile of the fluctuation across the dot, where each curve represents a different instant t over one period of oscillation with the static core profile given in grey. (b) A two-dimensional snapshot of the mode. (c) A three-dimensional snapshot of the mode. After Figure 4 of Kim (2014).

use of perpendicular ac fields minimises the complication involved with skyrmion gyration.

An example of the calculated power spectrum of excitations is shown in Fig. 6.2. For the ground state comprising a skyrmion at the dot centre [Fig. 6.2(a)], three distinct modes are observed in the frequency range considered, whose frequencies exhibit a nontrivial dependence on the applied magnetic field. To highlight the distinct features associated with the presence of the skyrmion, the power spectrum for a dot with no skyrmion is shown in Fig 6.2(b). The lowest order mode corresponds to the uniform precession or ferromagnetic resonance (FMR) mode. All three modes shown in Fig. 6.2(b) exhibit a linear static field dependence, which is expected for spin waves in this geometry. It is interesting to note that the lowest-order mode in the skyrmion case exhibits a much lower frequency than the FMR mode in the uniform case, while the second and third order modes have similar frequencies. The FMR mode is also absent when a skyrmion is present. Together, these features suggest that the appearance of a low-frequency excitation, such as the branch below 10 GHz in Fig. 6.2(a), is a strong signature of the presence of a confined skyrmion in a dot and a measure of the DMI.

Representative spatial profiles of the three confined skyrmion modes in Fig. 6.2(a) are presented in Fig. 6.3 for zero applied static field. From these images, mode 1 is deduced to be the breathing mode of the skyrmion, where the magnetisation fluctuation is localised to the core region of the skyrmion.

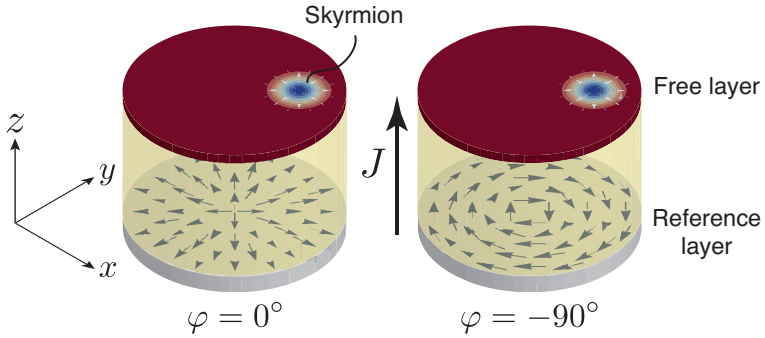

Fig. 6.4 Geometry and operating principle of a skyrmion-based spin-torque nano-oscillator. (a) Circular nanopillar with a gyrating skyrmion in the free layer and two possible vortex-like magnetic configurations in the reference layer. The current J flows perpendicular to the film plane along the z direction. After Figure 1 of Garcia-Sanchez (2016).

From the time dependence in Fig. 6.3(a), the breathing at opposite sides of the core is seen to be in phase, which indicates that the core shrinks and expands whilst preserving its radial symmetry with no discernible azimuthal component to the dynamics. Mode 2 corresponds to a hybridisation between the breathing mode and a radial spin wave mode of the circular dot. The amplitude of this excitation is largest around the core, but a significant component also appears at the dot edges. Mode 3 is a similar hybridised mode, with the key difference being the larger mode amplitude occurring within the core itself and one node in the mode profile appearing at the core boundary. Detection of such modes experimentally would give a strong indication of the presence of a skyrmion in ultrathin film dots.

6.3. Self-oscillations with inhomogeneous polarisers

Like magnetic vortices, the dynamics of skyrmions is inherently gyrotropic, which suggests that they might be useful for applications as spin-torque nano-oscillators. Previous work involving nanocontacts has shown that self-sustained gyration of skyrmions can be induced by the nonuniform current flow in that geometry (Zhang 2015). We explored using micromagnetics simulations and analytical modelling the conditions under which self-sustained oscillations of skyrmions driven by spin transfer torques are possible in confined geometries such as ultrathin film circular dots. Here, it is the boundary edges (Rohart 2013) that act as a suitable confining potential.

With Felipe Garcia-Sanchez, we considered a spin-torque nano-oscillator based on a circular nanopillar geometry as depicted in Fig. 6.4. Spin torques acting on the skyrmion in the free layer arise from a spin-polarised current flowing perpendicular to the film plane (CPP), where the spin polarisation takes the form of a vortex-like state in the reference layer. Bloch-like vortices ($\varphi = \pm 90°$) are micromagnetic ground states in ferromagnetic dots with certain aspect ratios (Guslienko 2008), while Néel-like vortices ($\varphi = 0°,180°$) can be stabilised in synthetic antiferromagnets (Phatak 2012, Wintz 2013). The basic idea is that the vortex-like polarisation structure will favour a continuously rotating skyrmion Hall angle, which, when combined with the con-

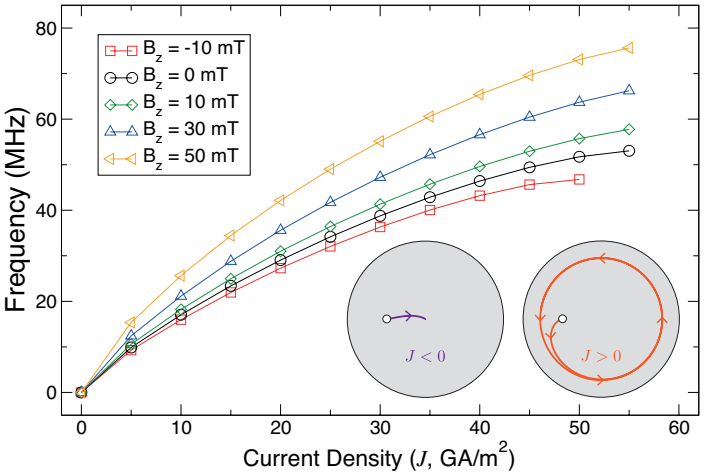

Fig. 6.5 Current dependence of the skyrmion gyration frequency for different perpendicular applied fields, B_z. An upper critical current density exists at which the skyrmion is expelled from the dot. The inset shows the transient trajectories of the skyrmion core for opposite current polarities. . After Figure 2 of Garcia-Sanchez (2016).

finement potential at the edges, will result in a steady state gyration of the skyrmion around the dot.

We studied this gyrotropic dynamics using analytical modelling and micromagnetics simulations. In Fig. 6.5 we show the current dependence of the skyrmion gyration frequency for a Néel-type vortex polariser. Several values of the perpendicular applied field are considered, which act to modify the size of the skyrmion core (Kiselev 2011). In the inset of the figure, the transient dynamics of the skyrmion core are shown, with an initial position off-centred. For negative current densities, the spin torques drive the skyrmion core with a clockwise gyration toward the dot centre, where it remains immobile indefinitely. This occurs because the resultant spin torque polarisation is oriented radially inwards toward the dot centre for negative currents, resulting in an inward spiralling motion of the skyrmion core in a clockwise direction. On the other hand, positive currents drive the core outwards from the dot centre toward the boundaries and reaches a steady state gyration in a counterclockwise sense, as expected from hand-waving arguments. Note there is no critical current for the onset of oscillations. However, an upper critical current is found between 50 and 60 GA/m^2 at which the skyrmion is expelled from the dot. This occurs because the confining potential due to the repulsion from the partial domain walls at the boundary (Rohart 2013) is no longer sufficiently strong to counteract the radial component of the spin-torque induced force on the skyrmion core that propels it outwards.

We also examined the effect of different vortex-like configurations for the polarisation vector, which can be characterised by the angle φ as shown in Fig. 6.6(a). The dependence of the gyration frequency on the polariser angle is shown in Fig. 6.6(b) for a fixed current density. The range of φ was chosen to favour steady state gyration, i.e., such that the spin torques drive skyrmion motion radially outward from the dot centre. We observe a large variation in

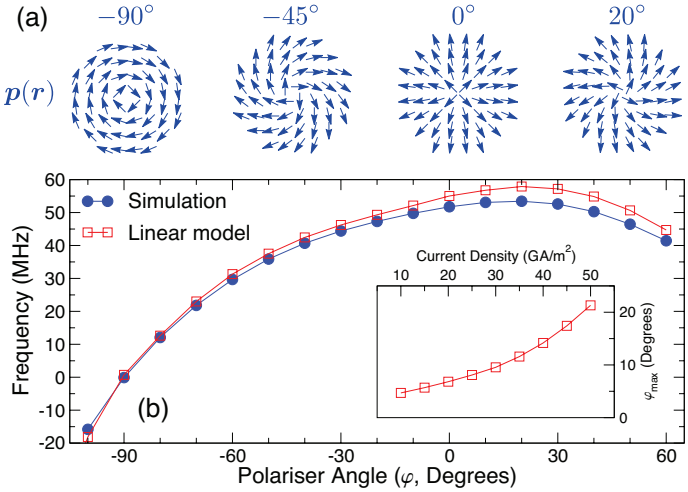

Fig. 6.6 Gyration frequency as a function of polariser angle. (a) Example of different vortex-like polariser configurations. (b) Dependence of the gyration frequency on the polariser angle for an applied current density of J = 50 GA/m² and zero applied field. The blue dots represent data computed from micromagnetics simulations, while the red squares represent the predicted frequency from the Thiele equation. The inset shows how the polariser angle at which the maximum gyration frequency occurs varies with the applied current density as computed from the linear model. After Figure 5 of Garcia-Sanchez (2016).

the gyration frequency, with a maximum attained at around $\varphi = 20°$ and a change in sign at around $\varphi = -90°$ for $J = 50$ GA/m². For the latter, the spin torques and the restoring force from the boundary edge drive the azimuthal motion of the skyrmion gyration in different directions but are equal in magnitude, which results in the skyrmion being driven to the dot boundary but with a vanishing frequency of gyration. For the former, on the other hand, the spin torques and the restoring force lead to motion in the same direction, which results in the maximum in the gyration frequency. Since the restoring force depends on how strongly the skyrmion is pushed against the boundary, the polariser angle at which the maximum gyration frequency occurs also depends on the applied current density. The predicted behaviour from the Thiele model is shown in the inset of Fig. 6.6(b), where linear motion along a straight edge is considered with a uniform polariser at different angles with respect to this edge (Garcia-Sanchez 2016). The negative frequencies correspond to a change in the sense of gyration of the skyrmion core, where the motion occurs in a clockwise direction (when viewed from above the film) rather than the counterclockwise sense for positive frequencies.

6.4. Current-driven motion in disordered films

For interface-driven DMI, most material systems investigated to date involve ultrathin ferromagnets with perpendicular magnetic anisotropy. These systems have also been studied extensively for magnetic domain wall dynamics (Metaxas 2007, Miron 2011, Ryu 2013, Emori 2013, Hrabec 2014, Torrejon 2014), where observations of strong pinning are common. In the context of skyrmion dynamics, it is natural to enquire whether the same disorder that leads to wall pinning can also have an influence on skyrmion propagation. Experimentally, it has been established that pinning can be strong (Han-

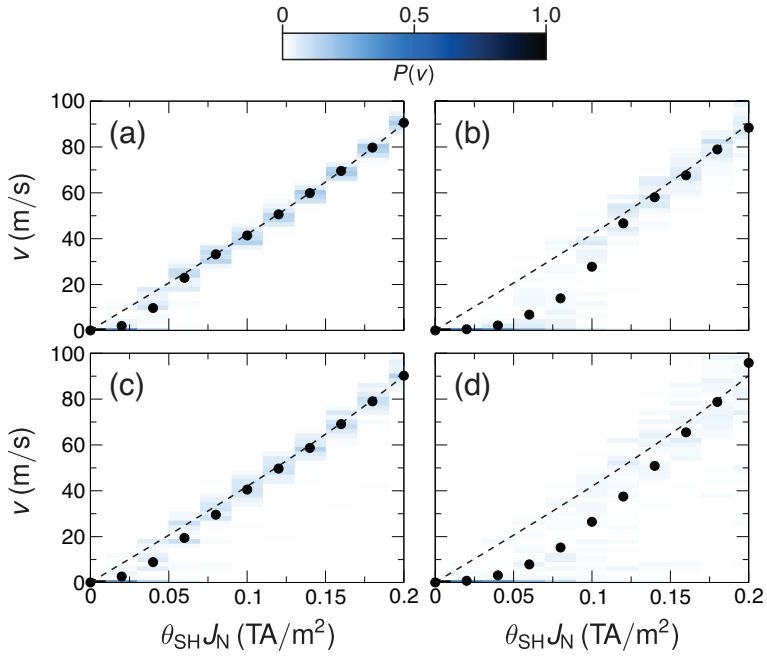

Fig. 6.7 Average skyrmion velocity as a function applied spin Hall current density for different disorder parameters: (a) 5% anisotropy fluctuations, 10 nm average grain size; (b) 10%, 10 nm; (c) 5%, 20 nm; (d) 10%, 20 nm. Points are simulation data and dashed lines correspond to the behaviour in the disorder-free system. The background of each plot is a probability density map of the velocity, with the legend given at the top of the figure. After Figure 2 of Kim (2017).

neken 2016). While the effects of boundary edges on skyrmion propagation have been studied (Sampaio 2013), studies of the role of random disorder to date have been limited to atomistic (Iwasaki 2013, Müller 2015) or particle-based models (Lin 2013b, Reichhardt 2015, Reichhardt 2016).

With Myoung-Woo Yoo, we examined the problem of pinning by using micromagnetics simulations to model more realistic disorder that is relevant to ultrathin films. Specifically, the disorder is modelled as a random grain structure in which the local anisotropy of each grain is drawn from a Gaussian distribution centred on a mean value consistent with experimental values. The grain structure is constructed using Voronoi tessellation and different average grain sizes are considered. An example of the defect-induced behaviour is presented in Fig. 6.7, where the average skyrmion velocity is shown as a function of current-induced spin Hall torques for different disorder parameters. We can identify a pinning regime at low current densities in which the average velocity is significantly below the value for the disorder-free case. This behaviour is mainly determined by events for which the skyrmion becomes pinned by the disorder within the 10-ns simulation window, either at the onset or after a certain duration during which a finite displacement takes place. We note that the exponential-like increase at low currents, followed by a smooth transition toward the disorder-free case, is typical of driven interface motion in disordered media (Chauve 2000), such as domain wall propagation in perpendicular anisotropy materials (Metaxas 2007). Our results therefore highlight the similarity with the depinning dynamics of domain walls and confirm that skyrmions are not im-

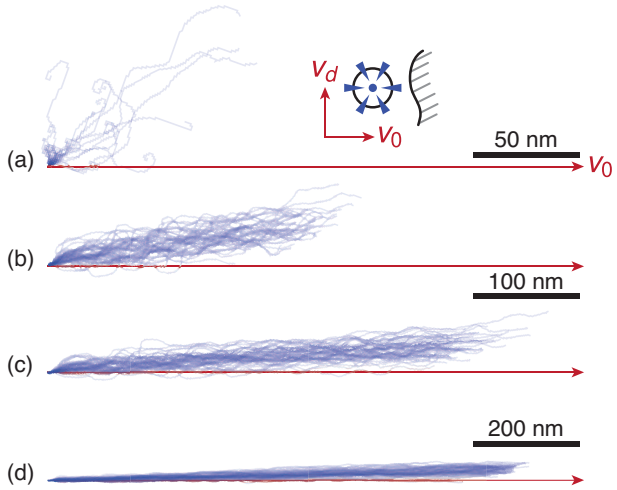

Fig. 6.8 Skyrmion trajectories with 5% of anisotropy fluctuations and 10 nm average grain size under different spin Hall torques: (a) 0.02 TA/m^2, (b) 0.06 TA/m^2, (c) 0.1 TA/m^2, and (d) 0.2 TA/m^2. The horizontal axis (v_0) indicates the propagation direction in the disorder-free case. The length scales are given in each sub-figure, where for (b) and (c) the scale bar of 100 nm applies. The inset in (a) illustrates the extrinsic skyrmion Hall motion along v_d due to a potential barrier.. After Figure 4 of Kim (2017).

pervious to defect-induced pinning for realistic disorder. We note that similar trends have been observed in recent experiments on current-driven skyrmion motion (Woo 2016, Hrabec 2017, Legrand 2017). We also performed simulations of current-driven motion under Zhang-Li torques and found similar trends (Kim 2017).

The disorder potential is also found to strongly influence the direction of the skyrmion propagation. In Fig. 6.8, the trajectories for 50 different realisations for a set of disorder parameters are shown for four values of spin-Hall torques. For the lowest current shown, we observe that most realisations lead to a pinned skyrmion close to its initial position, while only few cases of propagation over tens of nm are seen. We can also observe spirals in some of the trajectories, which possess the same handedness and results from the gyrotropic nature of the skyrmion motion. We note that the trajectories do not lead to an average displacement along the disorder-free direction v_0, but rather at an appreciable angle. This result can be understood in terms of the gyrotropic response of a skyrmion to a force; as the skyrmion is driven toward a boundary edge (in our case, a defect-induced potential barrier), the restoring force due to this edge drives the skyrmion along a direction perpendicular to this force. As such, each time the skyrmion encounters a potential barrier whilst propagating along the v_0 direction, it experiences a restoring force that results in an addition deflection along v_d, perpendicular to v_0. We therefore bring to light an *extrinsic* skyrmion Hall effect, which becomes less pronounced as the current is increased where the current-driven torques become sufficiently large to overcome the pinning potential.

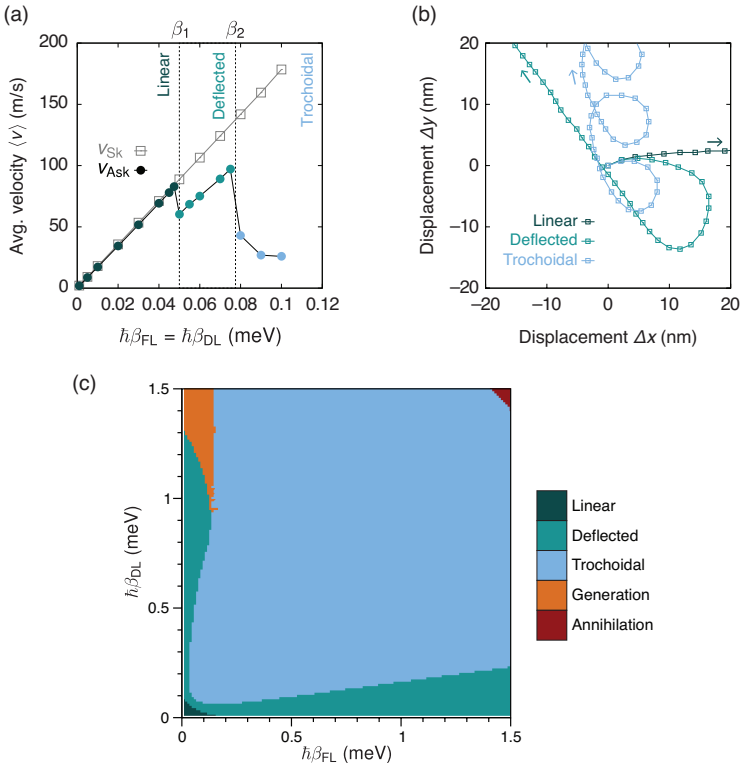

Fig. 6.9 Motion of antiskyrmions under current induced spin transfer torques. (a) Variation of the average velocity of skyrmions and antiskyrmions as a function of SOT, where field-like and damping-like torques are equal. Three propagation regimes are identified for antiskyrmions: rectilinear motion at low currents, deflected motion at intermediate currents, and trochoidal motion at high currents. (b) Example of antiskyrmion trajectories for linear (0.04 meV), deflected (0.06 meV) and trochoidal motion (0.09 meV). The arrows indicate the propagation direction. (c) Phase diagram for the antiskyrmion dynamics. After Fig. 2 of Ritzmann (2018).

6.5. Trochoidal motion and pair generation under spin-orbit torques

Recent attention in the field has turned toward antiskyrmions, which are the antiparticle counterparts of skyrmions. One means to stabilise antiskyrmions is with an anisotropic form of the DMI, which can appear at certain material interfaces (Camosi 2017, Hoffmann 2017) or in the bulk of Heusler alloys (Nayak 2017). Another involves frustrated exchange interactions, where next-nearest and next-next-nearest antiferromagnetic couplings can also stabilise antiskyrmion states (Dupé 2016, Rózsa 2017).

Antiskyrmions possess the opposite topological charge (6.1) to skyrmions. One way this manifests itself is in the gyrotropic response to applied forces, since the gyrovector in the Thiele equation (3.1) depends explicitly on the topological charge, $G = -QG_0\hat{\mathbf{z}}$. In most studies to date, however, the robustness of the symmetry between opposite topological charges has not been examined in detail. In particular, the roles of core deformation beyond inertial effects (Büttner 2015), the internal degrees of freedom, and the underlying symmetry of the magnetic interactions that stabilise the skyrmions remain an open question. To explore this in greater depth, I collaborated with Ulrike Ritzmann (Mainz/Uppsala), Bertrand Dupé (Mainz), and Stefan Heinze (Kiel) to study this question using atomistic spin dynamics simulations. A particular

feature of these simulations is that the parameters for the model Hamiltonian are determined from first-principles electronic structure calculations for the PdFe/Ir(111) system, where frustrated exchange interactions and the DMI are present. Moreover, it has previously been shown that both skyrmions and antiskyrmions are metastable states in this system (Dupé 2016), which allow direct comparisons on their dynamics to be made.

We considered the action of spin-orbit torques (SOT, parametrised by β), where both field-like (β_{FL}) and damping-like (β_{DL}) contributions were included (Ritzmann 2018). A comparison between the current skyrmion and antiskyrmion dynamics are shown in Fig. 6.9(a). While the skyrmion velocity increases linearly with the SOT, as expected from the Thiele equation, the behaviour is not monotonous for antiskyrmions. A linear regime is found at low currents up to a first threshold, β_1, where a discontinuity in the velocity curve can be seen. Above this threshold, the velocity continues to increase linearly as a function of β but with a different slope. A second threshold β_2 is found as the strength of the SOT is increased, where the velocity decreases with the applied current. The calculated trajectories for the antiskyrmion core are presented in Fig. 6.9(b). For linear motion, we observe that the spin configuration of the core is slightly deformed but remains close to its equilibrium static configuration. Above the first threshold β_1, the trajectory is linear at long times but exhibits a large transient phase in which the motion is curved. The rotation ceases when a new steady state regime is reached, which then allows for linear motion to proceed indefinitely (albeit with a different Hall angle with respect to the linear case $\beta < \beta_1$). More interestingly, the core undergoes trochoidal motion for $\beta > \beta_2$ which comprises an average displacement along a line that is accompanied by oscillations resulting in loops along the trajectory. The onset of these oscillations results in the sharp decrease in the average velocity shown in Fig. 6.9(a). It turns out that this dynamics is analogous to Walker breakdown in domain wall motion (Ritzmann 2018).

The phase diagram of the different behaviour is shown in Fig. 6.9(c) for different values and ratios of the field-like to damping-like torques. We used algorithms based on machine learning to classify the three types of trajectories (linear, deflected, and trochoidal), which exhibit a wide range of velocities and propagation directions. We note that the trochoidal motion occurs over a wide range of SOT parameters. For sufficiently large torques, we see that the antiskyrmion is annihilated. One unexpected feature is the region denoted 'generation', where skyrmion-antiskyrmion pairs are generated periodically as the antiskyrmion core undergoes trochoidal motion. An example of the generation process is shown in Fig 6.10. This regime is strongly nonlinear and represents a complete breakdown of the single-particle picture described by the Thiele equation. The pair is generated as follows: As the antiskyrmion undergoes its trochoidal trajectory, it is accompanied by a large deformation which represents an elongation of the core [i.e., at 3 ps in Fig. 6.10(a)], similar to the dynamics seen for gyrating magnetic vortices close to the core reversal transition (Van Waeyenberge 2006, Yamada 2007, Gaididei 2010).

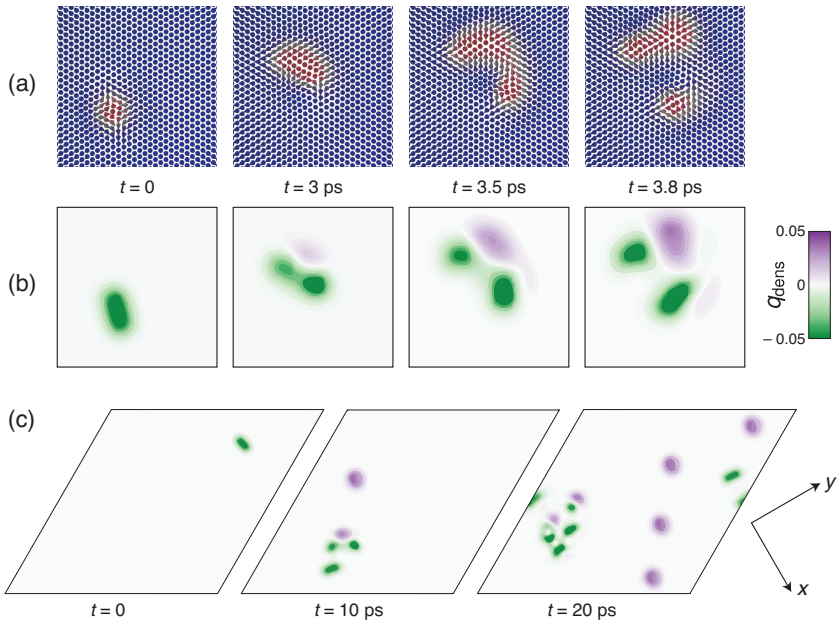

Fig. 6.10 Skyrmion-antiskyrmion pair generation from trochoidal antiskyrmion dynamics. (a) Snapshots of the trochoidal motion of a single antiskyrmion, where large deformations in the spin structure of the core leads to the nucleation of a skyrmion-antiskyrmion pair. (b) Topological charge density corresponding to the spin states in (a). (c) Snapshots in time of skyrmion-antiskyrmion pair generation, where pairs are nucleated and annihilated periodically. Antiskyrmions that survive become subsequent sources of pair generation. After Fig. 4 of Ritzmann (2018).

This elongation, which represents a skyrmion-antiskyrmion pair with a net charge of $Q = 0$, then separates from the core itself (3.5 to 3.8 ps). The corresponding topological charge density for these processes is shown in Fig. 6.10(b). Once nucleated, the pair itself separates since the SOTs lead to different motion for the skyrmion and antiskyrmion constituents. The skyrmion propagates away from the nucleation site by undergoing rectilinear motion, while the nucleated antiskyrmion executes trochoidal motion and becomes itself a new source of pair generation. This remarkable phenomenon leads to the generation of a gas of skyrmions and antiskyrmions [Fig. 6.10(c)]; the relative population of the two species varies in time as collisions between skyrmions and antiskyrmions lead to annihilation, while pair generation continues for antiskyrmions that survive. This process suggests that it is possible to generate an indefinite number of skyrmions and antiskyrmions from a *single* antiskyrmion 'seed'. Combined with the attractive interaction between cores made possible by the frustrated exchange, this dynamics can eventually lead to a skyrmion `crystallite' that condenses from the disordered gas phase (Ritzmann 2018).

Related Publications

Breathing modes of confined skyrmions in ultrathin magnetic dots
J.-V. Kim, F. Garcia-Sanchez, J. Sampaio, C. Moreau-Luchaire, V. Cros, and A. Fert
Physical Review B **90**, 064410 (2014).

A skyrmion-based spin-torque nano-oscillator
F. Garcia-Sanchez, J. Sampaio, N. Reyren, V. Cros, and J.-V. Kim
New Journal of Physics **18**, 075011 (2016).

Current-driven skyrmion dynamics in disordered films
J.-V. Kim and M.-Y. Woo
Applied Physics Letters **110**, 132404 (2017).

Current-driven skyrmion expulsion from magnetic nanostrips
M.-Y. Woo, V. Cros, and J.-V. Kim
Physical Review B **95**, 184423 (2017).

Trochoidal motion and pair generation in skyrmion and antiskyrmion dynamics under spin-orbit torques
U. Ritzmann, S. von Malottki, J.-V. Kim, S. Heinze, J. Sinova, and B. Dupé
Nature Electronics **1**, 451 (2018).

7. Perspectives

Information technologies are at a crucial juncture: the data deluge of the information age demands increasingly greater computing power, but important roadblocks remain to achieve this using conventional microelectronics. Many alternatives are being explored to meet this challenge. One broad approach involves replacing silicon with other materials that generate less heat, such as magnetic materials, where the inherent non-volatility of the ferromagnetic state is exploited. Another involves redesigning the architecture of processors altogether, such as quantum computing, which uses quantum effects to obtain exponential speedups of certain algorithms (Ladd 2010), neuromorphic computing, which aims to reproduce the cognitive processes of the human brain (Merolla 2014), and memcomputing, which combines memory and computation within a single element (Di Ventra 2015).

In this context, the research work I have outlined in the preceding chapters offers a number of avenues to explore how magnetic and spintronic devices could be useful to meet these challenges. I detail below some of these ideas, which range from the fundamental to the practical and encompass different aspects of condensed matter theory, materials science, and nonlinear dynamical systems.

7.1. Chaos-based information processing

One avenue toward nonconventional computing involves *chaos*. Chaotic systems are deterministic but their time evolution is characterised by an extreme sensitivity to initial conditions. For information processing applications, the central idea is that chaotic signals contain an *infinite amount* of information. To appreciate this, consider first the simpler periodic system that cycles at a constant frequency. Once the initial phase is determined, no additional information is gleaned by watching subsequent cycles because its future behaviour is completely predictable. On the other hand, a chaotic signal is aperiodic and completely unpredictable if the initial conditions are not known *precisely*. The infinite amount of information contained in the signal is therefore linked to the infinite precision in the knowledge of the initial conditions needed to accurately predict the evolution of the chaotic system.

How can such an abstract concept be put to good use? One established application is fast **random-number generation**. The common feature of random and chaotic signals is that they produce entropy. Due to the sensitivity to initial conditions, any intrinsic noise in the system can be greatly amplified by the transitions between unstable periodic orbits to give a large "random" character to the signal, i.e., by making the probability of any given event independent of its history, like a fair coin toss. By digitising such signals, a sequence of random binary digits can be generated. This chaos-based method for random number generation has been demonstrated at rates of Gbit/s using photonic devices (Uchida 2008, Virte 2012; Fig. 7.1), optical cavities

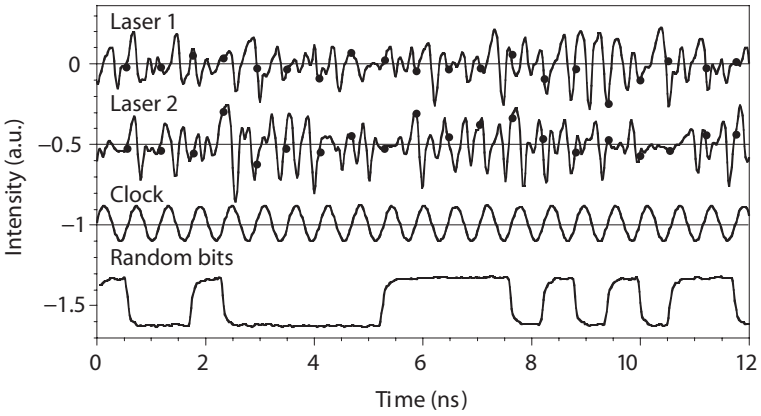

Fig. 7.1 Random number generation using chaos from a laser diode. After Figure 4 of Sciamanna (2015).

(Naruse 2014), and semiconductor superlattices (Li 2013). Random number generation is at the heart of many data encryption schemes and forms the basis of stochastic computing.

Another application is to improve the signal-to-noise ratio of communication channels by utilising the **symbolic dynamics** of a chaotic signal as a means of encoding information (Schweizer 2001, 2001b). The symbolic dynamics involves representing particular patterns in a time series as "words", which can be useful for encoding information (Bollt 2003). The dynamical system defines a specific "grammar" that dictates which sequences of words are naturally allowed, but specific sequences can be chosen by applying small perturbations to "target" certain orbits. This method of using chaos for communication has been demonstrated with electronic circuits (Hayes 1994) and chemical systems (Bollt 1997).

Finally, certain neuromorphic computing schemes, such as **reservoir computing**, rely on dynamical systems at the *edge* of chaos. An important application of reservoir computing is the classification of complex inputs, such as pattern or voice recognition – tasks deemed to be computationally hard. A recent example of interest is a temporal-based version, where a single nonlinear device is exploited with delayed feedback (Appeltant 2011). The idea is to recreate the functionality of a reservoir by mapping the network of nodes onto a sequence of time-delayed signals acting on the device and utilising its complex transient response. A recent implementation of this time-delay architecture using photonic devices has demonstrated classification of up to *1 million words per second* (Larger 2017).

Through the recently funded ANR project "CHIPMuNCS" (2018-2021), I will coordinate a consortium to investigate how such applications could be implemented using the chaotic state of the nanocontact vortex oscillator, as described in Chapter 3. We will use advanced materials (such as Heusler alloys) and improved device geometries to increase the magnetoresistance signal so that chaotic time series can be measured and exploited for possible information processing tasks. Recent experimental data of time-resolved elec-

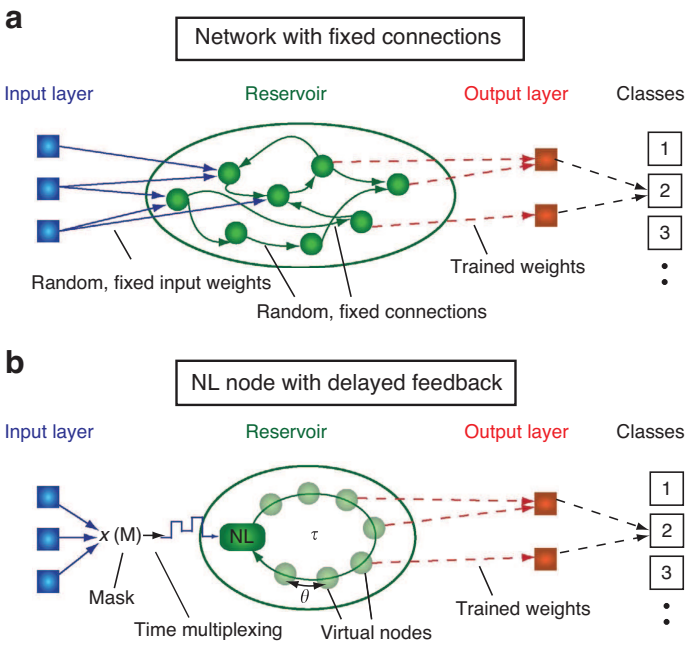

Fig. 7.2 Reservoir computing schemes. (a) Inputs are fed into the reservoir, a dynamical system comprising a network of interconnected nodes, where the outputs represent a nonlinear transformation of the inputs. Training is performed on the outputs to perform classification. (b) Time-delay architecture in which nodes of the reservoir are reconstructed as a temporal feedback sequence with a single nonlinear node. After Figure 1 of Appeltant (2015).

trical measurements show that aperiodic patterns can indeed be identified. From a scientific point of view, these studies will get to the heart of the nature of chaos in such systems, including the role of thermal noise and materials parameters on vortex core reversal. Along these lines, it will also be of interest to examine how periodic core reversal can be modulated by external signals and where similar parametric excitations are possible (Bortolotti 2013). We hope that the work will also stimulate new ways of thinking about chaotic behaviour in other spintronic devices, such as spin-torque nano-oscillators and domain wall racetracks.

7.2. Time-delay phenomena in micromagnetics

The time-delay architecture discussed above in the context of reservoir computing leads us to consider a more fundamental question for dynamical states in micromagnetics: what is the role of delayed feedback in general?

Time-delayed feedback is a well-established way to control the dynamical properties of a system and also a common method of generating chaos. Mathematically, chaos can only occur in a dynamical system if the dimensions of its phase space are greater than two. The inclusion of delayed feedback increases this dimension and allows chaotic dynamics to occur. An archetypical example is the Mackey-Glass oscillator (Mackey 1977), which is a first-order nonlinear differential-delay equation used to model physiological systems. Indeed, the implementation of a reservoir computer based on a single nonlinear device (discussed above) represents a form of the Mackey-Glass

system (Appeltant 2011). Delayed feedback is also a general feature of neural networks.

Remarkably, despite the ubiquity of delayed feedback in engineering and in the natural world, its role in the magnetisation dynamics of spintronic devices has largely been ignored to date. It is a feature that would be relatively straightforward to implement in real devices, since measured changes in the giant or tunnel magnetoresistance of a device could be re-injected as an additional AC component in the drive current. The same applies for more advanced geometries, involving multiferroic or piezoelectric materials, for example, where the feedback could be applied through electric fields or strains. Recent theoretical and experimental studies have shown that such delayed self-injection can be used to improve the spectral linewidth and modify the critical current of vortex oscillators in the nanopillar geometry (Khalsa 2015, Tsunegi 2016), while another has focused on how delayed feedback can improve the sensitivity of spin-torque nano-oscillators to external signals (Tiberkevich 2014). However, the role of delayed feedback for generating chaos or inducing complex transient states remains largely unexplored in spintronics.

With Jérôme Williame, a PhD student I'm supervising, and in collaboration with Damien Rontani at *CentraleSupelec* in Metz, we have begun to study how delayed feedback can lead to more complex transient dynamics and chaotic states. For a macrospin oscillator, we have shown that transitions between in-plane precession and out-of-plane precession, mediated by spin-transfer torques, can lead to modulated phases and chaotic dynamics for certain delays and feedback amplitudes (Williame 2017). We are currently implementing methods to include feedback signals in the micromagnetics code MuMax, which will allow for other geometries to be studied. Preliminary results also indicate that the Mackey-Glass oscillator, used as the prototype node in the time-delay architecture for reservoir computing (Appeltant 2011), can be realised with a domain wall racetrack with a suitable readout scheme.

7.3. Stochastic processes in chiral spin systems

The promise of exploiting skyrmions for information technologies has led to intense efforts in materials design that aim to optimise the Dzyaloshinskii-Moriya interaction in ultrathin ferromagnetic films. Besides stabilising chiral spin textures such as skyrmions, we showed in Chapter 4 that the DMI also leads to nonreciprocal propagation of spin waves. Given that thermal spin waves are naturally present at finite temperatures and also provide a measure of damping processes (through the fluctuation-dissipation theorem), it is natural to enquire how stochastic processes in general are influenced by the DMI. Some hints of strong asymmetries have been seen in the nucleation of domain walls in Pt/Co-based systems (Pizzini 2015).

In collaboration with Louise Desplat (PhD student), Dieter Suess, and Robert Stamps, we have begun to quantify lifetimes of chiral textures such as skyrmions by using Langer's theory for the decay of metastable states (Langer

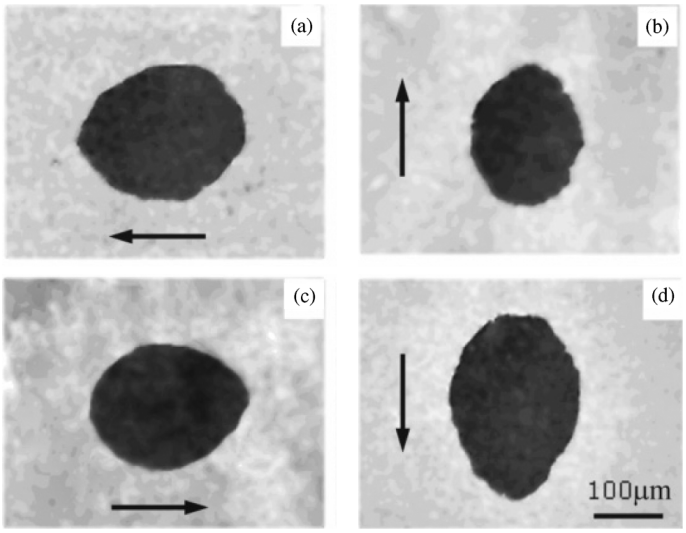

Fig. 7.3 Kerr microscopy images of asymmetric growth of nucleated domains in Pt/Co (0.6 nm)/Pt films under in-plane applied fields (orientations given by arrows). After Figure 3 of Kabanov (2010).

1969, Fiedler 2012). While energy barriers are relatively straightforward to compute using geodesic nudged elastic band methods (Rohart 2016), the overall lifetime τ also requires the Arrhenius prefactor τ_0 (Section 5.3) to be quantified. Detailed knowledge of lifetimes is also important for understanding thermal stability of skyrmions for information storage applications. Preliminary work suggests that internal eigenmodes of the skyrmion play an important role in determining the lifetimes (Desplat 2018). It would be of interest to examine similar questions for other metastable skyrmion states, such as the antiskyrmion.

Besides thermally-activated depinning in wires, domain walls can undergo creep motion in continuous films, which is characterised by a power law in the energy barrier E_b of the corresponding Arrhenius relation for the wall velocity (Jeudy 2016),

$$v = v_0 \exp\left(-\frac{E_b}{k_B T}\right), \tag{7.1a}$$

$$E_b = k_B T_d \left[\left(\frac{H_d}{H}\right)^{\mu} - 1\right], \tag{7.1b}$$

where H_d is a depinning field, T_d is a characteristic disorder temperature (energy), and the critical exponent $\mu = 1/4$ in two-dimensional systems. The creep motion comprises depinning events involving avalanches, which is a critical phenomenon that is general to driven (n-1)-dimensional elastic interfaces in n-dimensional disordered systems. In the presence of DMI, numerous experimental studies have shown that asymmetries develop in the growth of reversed domains under creep motion when magnetic fields are applied in the film plane (Kabanov 2010, Je 2013, Hrabec 2014, Vanatka 2015, Soucaille 2016; Fig. 7.3).

While there is a consensus on DMI being the underlying mechanism of such asymmetric growth, how it enters Eq. (7.1) exactly remains an open question. Given that experiments are often performed at room temperature, we can rule out emergent chirality effects seen in quantum antiferromagnets (Braun 2005). An initial attempt based on a field-dependent wall energy (or elasticity), which competes with the DMI that favours a Néel profile, gives a qualitative explanation but misrepresents the Zeeman energy and does not account for changes in the domain states. Our work on skyrmion motion in disordered films also suggests that DMI might affect the depinning field and disorder temperature. While there is no general theory for the velocity prefactor v_0, our work on skyrmion lifetimes suggests that domain wall eigenmodes might be important, which would also bring into play questions concerning nonreciprocal propagation and how this might influence dissipation processes. It will be interesting to explore how numerical simulation of domain wall creep can address such issues. Creep dynamics has been studied by simulation for in-plane walls (Laurson 2011, Leliaert 2016).

This last point brings us back to the initial discussion in this section, namely how dissipation processes may be different in chiral systems. Indeed, chiral damping has been proposed to explain certain experimental features (Jue 2015), although at this stage the jury is still out on this case. As I showed phenomenologically (Kim 2015), there are cogent reasons to believe that chiral damping should appear in ultrathin ferromagnetic films with DMI, but it remains unclear what the general form should take. The nonreciprocal spin wave propagation discussed in Section 4.1 suggest that thermal magnons might transport away spin-angular momentum in one direction, which in turn could affect the damped dynamics of spin textures such as domain walls and skyrmions. While such questions touch upon issues at a fundamental level, they will remain relevant for future information technologies as long as magnetic solitons in ultrathin films play a central role.

References

Appeltant, L, M C Soriano, G Van der Sande, J Danckaert, S Massar, J Dambre, B Schrauwen, C R Mirasso, and I Fischer, 2011, "Information Processing Using a Single Dynamical Node as Complex System," Nat. Commun. **2**, 468.

Attané, J, D Ravelosona, A Marty, Y Samson, and C Chappert, 2006, "Thermally Activated Depinning of a Narrow Domain Wall From a Single Defect," Phys. Rev. Lett. **96**, 147204.

Barnes, S, and S Maekawa, 2005, "Current-Spin Coupling for Ferromagnetic Domain Walls in Fine Wires," Phys. Rev. Lett. **95**, 107204.

Bayer, C, H Schultheiss, B Hillebrands, and R L Stamps, 2005, "Phase Shift of Spin Waves Traveling Through a 180° Bloch-Domain Wall," IEEE Trans. Magn. **41**, 3094.

Belmeguenai, M, J-P Adam, Y Roussigné, S Eimer, T Devolder, J-V Kim, S M Cherif, A Stashkevich, and A Thiaville, 2015, "Interfacial Dzyaloshinskii-Moriya Interaction in Perpendicularly Magnetized Pt/Co/AlOx Ultrathin Films Measured by Brillouin Light Spectroscopy," Phys. Rev. B **91**, 180405.

Berger, L, 1984, "Exchange Interaction Between Ferromagnetic Domain Wall and Electric Current in Very Thin Metallic Films," J. Appl. Phys. **55**, 1954.

Berger, L, 1992, "Motion of a Magnetic Domain Wall Traversed by Fast-Rising Current Pulses," J. Appl. Phys. **71**, 2721.

Berger, L, 1996, "Emission of Spin Waves by a Magnetic Multilayer Traversed by a Current," Phys. Rev. B **54**, 9353.

Bertotti, G, C Serpico, I Mayergoyz, A Magni, M D'Aquino, and R Bonin, 2005, "Magnetization Switching and Microwave Oscillations in Nanomagnets Driven by Spin-Polarized Currents," Phys. Rev. Lett. **94**, 127206.

Bianchini, L, S Cornelissen, J-V Kim, T Devolder, W Van Roy, L Lagae, and C Chappert, 2010, "Direct Experimental Measurement of Phase-Amplitude Coupling in Spin Torque Oscillators," Appl. Phys. Lett. **97**, 032502.

Bloch, F, 1930, "Zur Theorie Des Ferromagnetismus," Z. Phys. A **61**, 206.

Bogdanov, A N, and D A Yablonskii, 1989, "Thermodynamically Stable 'Vortices' in Magnetically Ordered Crystals. the Mixed State of Magnets," JETP **68**, 101.

Bogdanov, A, and A Hubert, 1994, "Thermodynamically Stable Magnetic Vortex States in Magnetic Crystals," J. Magn. Magn. Mater. **138**, 255.

Bogoliubov, N N, 1947, "On the theory of superfluidity," J. Phys. (USSR) **11**, 23.

Bollt, E M, and M Dolnik, 1997, "Encoding Information in Chemical Chaos by Controlling Symbolic Dynamics," Phys. Rev. E **55**, 6404.

Bollt, E M, 2003, "Review of Chaos Communication by Feedback Control of Symbolic Dynamics," IJBC **13**, 269.

Bonin, R, M D'Aquino, G Bertotti, C Serpico, and I D Mayergoyz, 2012, "Analysis of Magnetization Instability Patterns in Spin-Transfer Nano-Oscillators," Eur. Phys. J. B **85**, 47.

Bortolotti, P, E Grimaldi, A Dussaux, J Grollier, V Cros, C Serpico, K Yakushiji, et al., 2013, "Parametric Excitation of Magnetic Vortex Gyrations in Spin-Torque Nano-Oscillators," Phys. Rev. B **88**, 174417.

Boulle, O, J Vogel, H Yang, S Pizzini, D de Souza Chaves, A Locatelli, T Onur Mentes, et al., 2016, "Room-Temperature Chiral Magnetic Skyrmions in Ultrathin Magnetic Nanostructures," Nat. Nanotechnol. **11**, 449.

Bouzehouane, K, S Fusil, M Bibes, J Carrey, T Blon, M Le Dû, P Seneor, V Cros, and L Vila, 2003, "Nanolithography Based on Real-Time Electrically Controlled Indentation with an Atomic Force Microscope for Nanocontact Elaboration," Nano Lett. **3**, 1599.

Bouzidi, D, and H Suhl, 1990, "Motion of a Bloch Domain Wall," Phys. Rev. Lett. **65**, 2587.

Braganca, P M, B A Gurney, B A Wilson, J A Katine, S Maat, and J R Childress, 2010, "Nanoscale Magnetic Field Detection Using a Spin Torque Oscillator," Nanotechnology **21**, 235202.

Braun, H-B, 1994, "Fluctuations and Instabilities of Ferromagnetic Domain-Wall Pairs in an External Magnetic Field," Phys. Rev. B **50**, 16485.

Braun, H-B, and D Loss, 1996, "Berry's Phase and Quantum Dynamics of Ferromagnetic Solitons," Phys. Rev. B **53**, 3237.

Braun, H-B, J Kulda, B Roessli, D Visser, K W Krämer, H-U Güdel, and P Böni, 2005, "Emergence of Soliton Chirality in a Quantum Antiferromagnet," Nat. Phys. **1**, 159.

Braun, H-B, 2012, "Topological Effects in Nanomagnetism: From Superparamagnetism to Chiral Quantum Solitons," Adv. Phys. **61**, 1.

Burrowes, C, D Ravelosona, C Chappert, S Mangin, Eric E Fullerton, J A Katine, and B D Terris, 2008, "Role of Pinning in Current Driven Domain Wall Motion in Wires with Perpendicular Anisotropy," Appl. Phys. Lett. **93**, 172513.

Burrowes, C, A P Mihai, D Ravelosona, J-V Kim, C Chappert, L Vila, A Marty, et al., 2010, "Non-Adiabatic Spin-Torques in Narrow Magnetic Domain Walls," Nat. Phys. **6**, 17.

Büttner, F, C Moutafis, M Schneider, B Krüger, C M Günther, J Geilhufe, C v Korff Schmising, et al., 2015, "Dynamics and Inertia of Skyrmionic Spin Structures," Nat. Phys. **11**, 225.

Camley, R E, and A A Maradudin, 1983, "Phonon Focusing at Surfaces," Phys. Rev. B **27**, 1959.

Camosi, L, S Rohart, O Fruchart, S Pizzini, M Belmeguenai, Y Roussigné, A Stashkevich, et al., 2017, "Anisotropic Dzyaloshinskii-Moriya Interaction in Ultrathin Epitaxial Au/Co/W(110)," Phys. Rev. B **95**, 214422.

Chauve, P, T Giamarchi, and P Le Doussal, 2000, "Creep and Depinning in Disordered Media," Phys. Rev. B **62**, 6241.

Cho, J, N-H Kim, S Lee, R Lavrijsen, A Solignac, Y Yin, D-S Han, *et al.*, 2015, "Thickness Dependence of the Interfacial Dzyaloshinskii–Moriya Interaction in Inversion Symmetry Broken Systems," Nat. Commun. **6**, 7635.

Consolo, G, B Azzerboni, G Gerhart, G Melkov, V Tiberkevich, and A Slavin, 2007, "Excitation of Self-Localized Spin-Wave Bullets by Spin-Polarized Current in in-Plane Magnetized Magnetic Nanocontacts: a Micromagnetic Study," Phys. Rev. B **76**, 144410.

Consolo, G, G Gubbiotti, L Giovannini, and R Zivieri, 2011, "Lagrangian Formulation of the Linear Autonomous Magnetization Dynamics in Spin-Torque Auto-Oscillators," App. Math. Comp. **217**, 8204.

Cortés-Ortuño, D, and P Landeros, 2013, "Influence of the Dzyaloshinskii–Moriya Interaction on the Spin-Wave Spectra of Thin Films," J. Phys.: Condens. Matter **25**, 156001.

Costa, A, R Muniz, S Lounis, A Klautau, and D L Mills, 2010, "Spin-Orbit Coupling and Spin Waves in Ultrathin Ferromagnets: the Spin-Wave Rashba Effect," Phys. Rev. B **82**, 014428.

Csaba, G, M Pufall, D E Nikonov, G I Bourianoff, A Horvath, T Roska, and W Porod, 2012, "Spin Torque Oscillator Modes for Applications in Associative Memories," 13th International Workshop on Cellular Nanoscale Networks and Their Applications (CNNA).

Demidov, V E, S O Demokritov, K Rott, P Krzysteczko, and G Reiss, 2007, "Self-Focusing of Spin Waves in Permalloy Microstripes," Appl. Phys. Lett. **91**, 252504.

Demidov, V E, S O Demokritov, D Birt, B O'Gorman, M Tsoi, and X Li, 2009, "Radiation of Spin Waves From the Open End of a Microscopic Magnetic-Film Waveguide," Phys. Rev. B **80**, 014429.

Desplat, L, D Suess, J-V Kim, and R L Stamps, 2018, "Thermal stability of metastable magnetic skyrmions: Entropic narrowing and significance of internal eigenmodes," Phys. Rev. B **98**, 134407.

Di, K, V L Zhang, H S Lim, S C Ng, M H Kuok, J Yu, J Yoon, X Qiu, and H Yang, 2015, "Direct Observation of the Dzyaloshinskii-Moriya Interaction in a Pt/Co/Ni Film," Phys. Rev. Lett. **114**, 047201.

Di, K, V Li Zhang, H S Lim, S C Ng, M H Kuok, X Qiu, and H Yang, 2015b, "Asymmetric Spin-Wave Dispersion Due to Dzyaloshinskii-Moriya Interaction in an Ultrathin Pt/CoFeB Film," Appl. Phys. Lett. **106**, 052403.

Di Ventra, M, and Y V Pershin, 2015, "Just Add Memory," Sci. Am. **312**, 56.

Duine, R, A Núñez, J Sinova, and A Macdonald, 2007, "Functional Keldysh Theory of Spin Torques," Phys. Rev. B **75**, 214420.

Dupé, B, C N Kruse, T Dornheim, and S Heinze, 2016, "How to Reveal Metastable Skyrmionic Spin Structures by Spin- Polarized Scanning Tunneling Microscopy," New J. Phys. **18**, 055015.

Dussaux, A, B Georges, J Grollier, V Cros, A V Khvalkovskiy, A Fukushima, M Konoto, et al., 2010, "Large Microwave Generation From Current-Driven Magnetic Vortex Oscillators in Magnetic Tunnel Junctions," Nat. Commun. **1**, 8.

Dyakonov, M I and V I Perel, 1971, "Possibility of Orienting Electron Spins with Current," JETP Lett. **13**, 467.

Dzyaloshinsky, I, 1958, "A Thermodynamic Theory of 'Weak' Ferromagnetism of Antiferromagnetics," J. Phys. Chem. Solids **4**, 241.

Emori, S, U Bauer, S-M Ahn, E Martinez, and G S D Beach, 2013, "Current-Driven Dynamics of Chiral Ferromagnetic Domain Walls," Nat. Mater. **12**, 611.

Fiedler, G, J Fidler, J Lee, T Schrefl, R L Stamps, H-B Braun, and D Suess, 2012, "Direct Calculation of the Attempt Frequency of Magnetic Structures Using the Finite Element Method," J. Appl. Phys. **111**, 093917.

Finocchio, G, M Ricci, R Tomasello, A Giordano, M Lanuzza, V Puliafito, P Burrascano, B Azzerboni, and M Carpentieri, 2015, "Skyrmion Based Microwave Detectors and Harvesting," Appl. Phys. Lett. **107**, 262401.

Freitas, P P, and L Berger, 1985, "Observation of *s–d* Exchange Force Between Domain Walls and Electric Current in Very Thin Permalloy Films," J. Appl. Phys. **57**, 1266.

Gaididei, Y, V P Kravchuk, and D D Sheka, 2010, "Magnetic Vortex Dynamics Induced by an Electrical Current," Int. J. Quantum Chem. **110**, 83.

Garcia-Sanchez, F, P Borys, A Vansteenkiste, J-V Kim, and R L Stamps, 2014, "Nonreciprocal Spin-Wave Channeling Along Textures Driven by the Dzyaloshinskii-Moriya Interaction," Phys. Rev. B **89**, 224408.

Garcia-Sanchez, F, P Borys, R Soucaille, J-P Adam, RoRbert L Stamps, and J-V Kim, 2015, "Narrow Magnonic Waveguides Based on Domain Walls," Phys. Rev. Lett **114**, 247206.

Garcia-Sanchez, F, J Sampaio, N Reyren, V Cros, and J-V Kim, 2016, "A Skyrmion-Based Spin-Torque Nano-Oscillator," New J. Phys. **18**, 075011.

Gilbert, T L, 2004, "A Phenomenological Theory of Damping in Ferromagnetic Materials," IEEE Trans. Magn. **40**, 3443.

Grimaldi, E, A Dussaux, P Bortolotti, J Grollier, G Pillet, A Fukushima, H Kubota, K Yakushiji, S Yuasa, and V Cros, 2014, "Response to Noise of a Vortex Based Spin Transfer Nano-Oscillator," Phys. Rev. B **89**, 104404.

Guslienko, K Yu, 2008, "Magnetic Vortex State Stability, Reversal and Dynamics in Restricted Geometries," J. Nanosci. Nanotechnol. **8**, 2745.

Hänggi, P, P Talkner, and M Borkovec, 1990, "Reaction-Rate Theory: Fifty Years After Kramers," Rev. Mod. Phys. **62**, 251.

Hanneken, C, A Kubetzka, K von Bergmann, and R Wiesendanger, 2016, "Pinning and Movement of Individual Nanoscale Magnetic Skyrmions via Defects," New J. Phys. **18**, 055009.

Hayes, S, C Grebogi, E Ott, and A Mark, 1994, "Experimental Control of Chaos for Communication," Phys. Rev. Lett. **73**, 1781.

Heinze, S, K von Bergmann, M Menzel, J Brede, A Kubetzka, R Wiesendanger, G Bihlmayer, and S Blügel, 2011, "Spontaneous Atomic-Scale Magnetic Skyrmion Lattice in Two Dimensions," Nat. Phys. **7**, 713.

Helman, J S, H-B Braun, J S Broz, and W Baltensperger, 1991, "General Solution of the Landau-Lifshitz-Gilbert Equations Linearized Around a Bloch Wall," Phys. Rev. B **43**, 5908.

Hertel, R, W Wulfhekel, and J Kirschner, 2004, "Domain-Wall Induced Phase Shifts in Spin Waves," Phys. Rev. Lett. **93**, 257202.

Hinzke, D, and U Nowak, 2011, "Domain Wall Motion by the Magnonic Spin Seebeck Effect," Phys. Rev. Lett. **107**, 027205.

Hirsch, J E, 1999, "Spin Hall Effect," Phys. Rev. Lett. **83**, 1834.

Hoffmann, M, B Zimmermann, G P Müller, D Schürhoff, N S Kiselev, C Melcher, and S Blügel, 2017, "Antiskyrmions Stabilized at Interfaces by Anisotropic Dzyaloshinskii-Moriya Interactions," Nat. Commun. **8**, 308.

Holstein, T, and H Primakoff, 1940, "Field Dependence of the Intrinsic Domain Magnetization of a Ferromagnet," Phys. Rev. **58**, 1098.

Houssameddine, D, U Ebels, B Delaët, B Rodmacq, I Firastrau, F Ponthenier, M Brunet, et al., 2007, "Spin-Torque Oscillator Using a Perpendicular Polarizer and a Planar Free Layer," Nat. Mater. **6**, 447.

Houssameddine, D, U Ebels, B Dieny, K Garello, J-P Michel, B Delaet, B Viala, M-C Cyrille, J Katine, and D Mauri, 2009, "Temporal Coherence of MgO Based Magnetic Tunnel Junction Spin Torque Oscillators," Phys. Rev. Lett. **102**, 257202.

Hrabec, A, N A Porter, A Wells, M J Benitez, G Burnell, S McVitie, D McGrouther, T A Moore, and C H Marrows, 2014, "Measuring and Tailoring the Dzyaloshinskii-Moriya Interaction in Perpendicularly Magnetized Thin Films," Phys. Rev. B **90**, 020402.

Hrabec, A, J Sampaio, M Belmeguenai, I Gross, R Weil, S M Cherif, A Stashkevich, et al., 2017, "Current-Induced Skyrmion Generation and Dynamics in Symmetric Bilayers," Nat. Commun. **8**, 15765.

Iwasaki, J, M Mochizuki, and N Nagaosa, 2013, "Current-Induced Skyrmion Dynamics in Constricted Geometries," Nat. Nanotechnol. **8**, 742.

Janak, J, 1964, "Quantum Theory of Domain-Wall Motion," Phys. Rev. **134**, A411.

Je, S-G, D-H Kim, S-C Yoo, B-C Min, K-J Lee, and S-B Choe, 2013, "Asymmetric Magnetic Domain-Wall Motion by the Dzyaloshinskii-Moriya Interaction," Phys. Rev. B **88**, 214401.

Jeudy, V, A Mougin, S Bustingorry, W Savero Torres, J Gorchon, A B Kolton, A Lemaître, and J-P Jamet, 2016, "Universal Pinning Energy Barrier for Driven Domain Walls in Thin Ferromagnetic Films," Phys. Rev. Lett. **117**, 057201.

Jiang, W, P Upadhyaya, W Zhang, G Yu, M B Jungfleisch, F Y Fradin, J E Pearson, et al., 2015, "Blowing Magnetic Skyrmion Bubbles," Science **349**, 283.

Jonietz, F, S Muhlbauer, C Pfleiderer, A Neubauer, W Munzer, A Bauer, T Adams, et al., 2010, "Spin Transfer Torques in MnSi at Ultralow Current Densities," Science **330**, 1648.

Jue, E, C K Safeer, M Drouard, A Lopez, P Balint, L Buda-Prejbeanu, O Boulle, et al., 2015, "Chiral Damping of Magnetic Domain Walls," Nat. Mater. **15**, 272.

Kabanov, Y P, Y L Iunin, V. I. Nikitenko, A. J. Shapiro, R D Shull, L Y Zhu, and C L Chien, 2010, "In-Plane Field Effects on the Dynamics of Domain Walls in Ultrathin Co Films with Perpendicular Anisotropy," IEEE Trans. Magn. **46**, 2220.

Khalsa, G, M D Stiles, and J Grollier, 2015, "Critical Current and Linewidth Reduction in Spin-Torque Nano-Oscillators by Delayed Self-Injection," Appl. Phys. Lett. **106**, 242402.

Kikuchi, T, T Koretsune, R Arita, and G Tatara, 2016, "Dzyaloshinskii-Moriya Interaction as a Consequence of a Doppler Shift Due to Spin-Orbit-Induced Intrinsic Spin Current," Phys. Rev. Lett. **116**, 247201.

Kim, J-V, and R L Stamps, 2005, "Hysteresis From Antiferromagnet Domain-Wall Processes in Exchange-Biased Systems: Magnetic Defects and Thermal Effects," Phys. Rev. B **71**, 094405.

Kim, J-V, 2006, "Stochastic Theory of Spin-Transfer Oscillator Linewidths," Phys. Rev. B **73**, 174412.

Kim, J-V, V Tiberkevich, and A Slavin, 2008, "Generation Linewidth of an Auto-Oscillator with a Nonlinear Frequency Shift: Spin-Torque Nano-Oscillator," Phys. Rev. Lett. **100**, 017207.

Kim, J-V, Q Mistral, C Chappert, V Tiberkevich, and A Slavin, 2008b, "Line Shape Distortion in a Nonlinear Auto-Oscillator Near Generation Threshold: Application to Spin-Torque Nano-Oscillators," Phys. Rev. Lett. **100**, 167201.

Kim, J-V, and C Burrowes, 2009, "Influence of Magnetic Viscosity on Domain Wall Dynamics Under Spin-Polarized Currents," Phys. Rev. B **80**, 214424.

Kim, J-V, F Garcia-Sanchez, J Sampaio, C Moreau-Luchaire, V Cros, and A Fert, 2014, "Breathing Modes of Confined Skyrmions in Ultrathin Magnetic Dots," Phys. Rev. B **90**, 064410.

Kim, J-V, 2015, "Role of Nonlinear Anisotropic Damping in the Magnetization Dynamics of Topological Solitons," Phys. Rev. B **92**, 014418.

Kim, J-V, R L Stamps, and R E Camley, 2016, "Spin Wave Power Flow and Caustics in Ultrathin Ferromagnets with the Dzyaloshinskii-Moriya Interaction," Phys. Rev. Lett. **117**, 197204.

Kim, J-V, and M-W Yoo, 2017, "Current-Driven Skyrmion Dynamics in Disordered Films," Appl. Phys. Lett. **110**, 132404.

Kiselev, N S, A N Bogdanov, R Schäfer, and U K Rößler, 2011, "Chiral Skyrmions in Thin Magnetic Films: New Objects for Magnetic Storage Technologies?," J. Phys. D: Appl. Phys. **44**, 392001.

Kiselev, S I, J C Sankey, I N Krivorotov, N C Emley, R J Schoelkopf, R A Buhrman, and D C Ralph, 2003, "Microwave Oscillations of a Nanomagnet Driven by a Spin-Polarized Current," Nature **425**, 380–383.

Kiselev, S, J Sankey, I N Krivorotov, N Emley, M Rinkoski, C Perez, R Buhrman, and D Ralph, 2004, "Current-Induced Nanomagnet Dynamics for Magnetic Fields Perpendicular to the Sample Plane," Phys. Rev. Lett. **93**, 036601.

Kohno, H, G Tatara, and J Shibata, 2006, "Microscopic Calculation of Spin Torques in Disordered Ferromagnets," J. Phys. Soc. Jpn. **75**, 113706.

Kubo, R., 1962, "A Stochastic Theory of Line-Shape and Relaxation," in *Fluctuation, Relaxation and Resonance in Magnetic Systems*, edited by D Ter Haar (Oliver & Boyd, Edinburgh), pp. 23–68.

Ladd, T D, F Jelezko, R Laflamme, Y Nakamura, C Monroe, and J L O'Brien, 2010, "Quantum Computers," Nature **464**, 45.

Landau, L, 1946, "On the vibration of the electronic plasma," J. Phys. USSR **10**, 26.

Langer, J, 1969, "Statistical Theory of the Decay of Metastable States," Ann. Phys. (NY) **54**, 258.

Larger, L, A Baylón-Fuentes, R Martinenghi, V S Udaltsov, Y K Chembo, and M Jacquot, 2017, "High-Speed Photonic Reservoir Computing Using a Time-Delay-Based Architecture: Million Words Per Second Classification," Phys. Rev. X **7**, 011015.

Laurson, L, C Serpico, G Durin, and S Zapperi, 2011, "Thermally Activated Domain Wall Dynamics in a Disordered Magnetic Nanostrip," J. Appl. Phys. **109**, 07D345.

Le Maho, Y, J-V Kim, and G Tatara, 2009, "Spin-Wave Contributions to Current-Induced Domain Wall Dynamics," Phys. Rev. B **79**, 174404.

Lee, J C T, J J Chess, S A Montoya, X. Shi, N Tamura, S K Mishra, P Fischer, et al., 2016, "Synthesizing Skyrmion Bound Pairs in Fe-Gd Thin Films," Appl. Phys. Lett. **109**, 022402.

Legrand, W, D Maccariello, N Reyren, K Garcia, C Moutafis, C Moreau-Luchaire, S Collin, K Bouzehouane, V Cros, and A Fert, 2017, "Room-Temperature Current-Induced Generation and Motion of Sub-100 Nm Skyrmions," Nano Lett. **17**, 2703.

Leliaert, J, B Van de Wiele, A Vansteenkiste, L Laurson, G Durin, Luc Dupré, and B Van Waeyenberge, 2016, "Creep Turns Linear in Narrow Ferromagnetic Nanostrips," Sci. Rep. **6**, 20472.

Li, W, I Reidler, Y Aviad, Y Huang, H Song, Y Zhang, N Rosenbluh, and I Kanter, 2013, "Fast Physical Random-Number Generation Based on Room-Temperature Chaotic Oscillations in Weakly Coupled Superlattices," Phys. Rev. Lett. **111**, 044102.

Lin, S-Z, C Reichhardt, C D Batista, and A Saxena, 2013, "Driven Skyrmions and Dynamical Transitions in Chiral Magnets," Phys. Rev. Lett. **110**, 207202.

Lin, S-Z, C Reichhardt, C D Batista, and A Saxena, 2013b, "Particle Model for Skyrmions in Metallic Chiral Magnets: Dynamics, Pinning, and Creep," Phys. Rev. B **87**, 214419.

Locatelli, N, V V Naletov, J Grollier, G De Loubens, V Cros, C Deranlot, C Ulysse, G Faini, O Klein, and A Fert, 2011, "Dynamics of Two Coupled Vortices in a Spin Valve Nanopillar Excited by Spin Transfer Torque," Appl. Phys. Lett. **98**, 062501.

Macià, F, A D Kent, and F C Hoppensteadt, 2011, "Spin-Wave Interference Patterns Created by Spin-Torque Nano-Oscillators for Memory and Computation," Nanotechnology **22**, 095301.

Mackey, M C, and L Glass, 1977, "Oscillation and Chaos in Physiological Control Systems.," Science **197**, 287–289.

Madami, M, S Bonetti, G Consolo, S Tacchi, G Carlotti, G Gubbiotti, F B Mancoff, M A Yar, and J Åkerman, 2011, "Direct Observation of a Propagating Spin Wave Induced by Spin-Transfer Torque," Nat. Nanotechnol. **6**, 635.

Malozemoff, A P, and J C Slonczewski, 1979, Magnetic Domain Walls in Bubble Materials (Academic Press, New York).

Manfrini, M, T Devolder, J-V Kim, P Crozat, N Zerounian, C Chappert, W Van Roy, L Lagae, G Hrkac, and T Schrefl, 2009, "Agility of Vortex-Based Nanocontact Spin Torque Oscillators," Appl. Phys. Lett. **95**, 192507.

Manfrini, M, T Devolder, J-V Kim, P Crozat, C Chappert, W Van Roy, and L Lagae, 2011, "Frequency Shift Keying in Vortex-Based Spin Torque Oscillators," J. Appl. Phys. **109**, 083940.

Manfrini, M, J-V Kim, S Petit-Watelot, W Van Roy, L Lagae, C Chappert, and T Devolder, 2014, "Propagation of Magnetic Vortices Using Nanocontacts as Tunable Attractors," Nat. Nanotechnol. **9**, 121.

Mauri, D, H C Siegmann, P S Bagus, and E Kay, 1987, "Simple Model for Thin Ferromagnetic Films Exchange Coupled to an Antiferromagnetic Substrate," J. Appl. Phys. **62**, 3047.

Merolla, P A, J V Arthur, R Alvarez-Icaza, A S Cassidy, J Sawada, F Akopyan, B L Jackson, et al., 2014, "A Million Spiking-Neuron Integrated Circuit with a Scalable Communication Network and Interface," Science **345**, 668.

Metaxas, P, J-P Jamet, A Mougin, M Cormier, J Ferré, V Baltz, B Rodmacq, B Dieny, and R L Stamps, 2007, "Creep and Flow Regimes of Magnetic Domain-Wall Motion in Ultrathin Pt/Co/Pt Films with Perpendicular Anisotropy," Phys. Rev. Lett. **99**, 217208.

Metlov, K L, and K Y Guslienko, 2002, "Stability of Magnetic Vortex in Soft Magnetic Nano-Sized Circular Cylinder," J. Magn. Magn. Mater. **242-245**, 1015.

Mihai, A P, J P Attané, L Vila, C Beigné, J C Pillet, and A Marty, 2009, "Magnetization Reversal Dominated by Domain Wall Pinning in FePt Based Spin Valves," Appl. Phys. Lett. **94**, 122509.

Mikhaĭlov, A V, and A I Yaremchuk, 1984, "Forced Motion of a Domain Wall in the Field of a Spin Wave," JETP Lett. **39**, 354.

Miron, I M, T Moore, H Szambolics, L D Buda-Prejbeanu, S Auffret, B Rodmacq, S Pizzini, et al., 2011, "Fast Current-Induced Domain-Wall Motion Controlled by the Rashba Effect," Nat. Mater. **10**, 419.

Mistral, Q, J-V Kim, T Devolder, P Crozat, C Chappert, J A Katine, M J Carey, and K Ito, 2006, "Current-Driven Microwave Oscillations in Current Perpendicular-to-Plane Spin-Valve Nanopillars," Appl. Phys. Lett. **88**, 192507.

Mistral, Q, M Van Kampen, G Hrkac, J-V Kim, T Devolder, P Crozat, C Chappert, L Lagae, and T Schrefl, 2008, "Current-Driven Vortex Oscillations in Metallic Nanocontacts," Phys. Rev. Lett. **100**, 257201.

Mohseni, S M, S R Sani, J Persson, T N A Nguyen, S Chung, Y Pogoryelov, P K Muduli, *et al.*, 2013, "Spin Torque-Generated Magnetic Droplet Solitons," Science **339**, 1295.

Montoya, S A, S Couture, J J Chess, J C T Lee, N Kent, D Henze, S. K. Sinha, et al., 2017, "Tailoring Magnetic Energies to Form Dipole Skyrmions and Skyrmion Lattices," Phys. Rev. B **95**, 024415.

Montoya, S A, S Couture, J J Chess, J C T Lee, N Kent, M-Y Im, S D Kevan, et al., 2017b, "Resonant Properties of Dipole Skyrmions in Amorphous Fe/Gd Multilayers," Phys. Rev. B **95**, 224405.

Moon, J-H, S-M Seo, K-J Lee, K-W Kim, J Ryu, H-W Lee, R D McMichael, and M D Stiles, 2013, "Spin-Wave Propagation in the Presence of Interfacial Dzyaloshinskii-Moriya Interaction," Phys. Rev. B **88**, 184404.

Moreau-Luchaire, C, C Moutafis, N Reyren, J Sampaio, C A F Vaz, N Van Horne, K Bouzehouane, et al., 2016, "Additive Interfacial Chiral Interaction in Multilayers for Stabilization of Small Individual Skyrmions at Room Temperature," Nat. Nanotechnol. **11**, 444.

Moriya, T, 1960, "New Mechanism of Anisotropic Superexchange Interaction," Phys. Rev. Lett. **4**, 228.

Moriya, T, 1960b, "Anisotropic Superexchange Interaction and Weak Ferromagnetism," Phys. Rev. **120**, 91.

Muhlbauer, S, B Binz, F Jonietz, C Pfleiderer, A Rosch, A Neubauer, R Georgii, and P Boni, 2009, "Skyrmion Lattice in a Chiral Magnet," Science **323**, 915.

Müller, J, and A Rosch, 2015, "Capturing of a Magnetic Skyrmion with a Hole," Phys. Rev. B **91**, 054410.

Naruse, M, S-J Kim, M Aono, H Hori, and M Ohtsu, 2014, "Chaotic Oscillation and Random-Number Generation Based on Nanoscale Optical-Energy Transfer," Sci. Rep. **4**, 6039.

Nayak, A K, V Kumar, T Ma, P Werner, E Pippel, R Sahoo, F Damay, U K Rößler, C Felser, and S S P Parkin, 2017, "Magnetic Antiskyrmions Above Room Temperature in Tetragonal Heusler Materials," Nature **548**, 561.

Nembach, H T, J M Shaw, M Weiler, E Jue, and T J Silva, 2015, "Linear Relation Between Heisenberg Exchange and Interfacial Dzyaloshinskii–Moriya Interaction in Metal Films," Nat. Phys. **11**, 825.

Nobis, T, E M Kaidashev, A Rahm, M Lorenz, and M Grundmann, 2004, "Whispering Gallery Modes in Nanosized Dielectric Resonators with Hexagonal Cross Section," Phys. Rev. Lett. **93**, 103903.

Onose, Y, Y Okamura, S Seki, S Ishiwata, and Y Tokura, 2012, "Observation of Magnetic Excitations of Skyrmion Crystal in a Helimagnetic Insulator Cu_2OSeO_3," Phys. Rev. Lett. **109**, 037603.

Pappas, C, E Lelièvre-Berna, P Falus, P Bentley, E Moskvin, S Grigoriev, P Fouquet, and B Farago, 2009, "Chiral Paramagnetic Skyrmion-Like Phase in MnSi," Phys. Rev. Lett. **102**, 197202.

Parkin, S S P, M Hayashi, and L Thomas, 2008, "Magnetic Domain-Wall Racetrack Memory," Science **320**, 190.

Petit-Watelot, S, J-V Kim, A Ruotolo, R M Otxoa, K Bouzehouane, J Grollier, A Vansteenkiste, B Van de Wiele, V Cros, and T Devolder, 2012, "Commensurability and Chaos in Magnetic Vortex Oscillations," Nat. Phys. **8**, 682.

Petit-Watelot, S, R M Otxoa, and M Manfrini, 2012b, "Electrical Properties of Magnetic Nanocontact Devices Computed Using Finite-Element Simulations," Appl. Phys. Lett. **100**, 083507.

Phatak, C, A Petford-Long, and O Heinonen, 2012, "Direct Observation of Unconventional Topological Spin Structure in Coupled Magnetic Discs," Phys. Rev. Lett. **108**, 067205.

Piéchon, F, and A Thiaville, 2007, "Spin Transfer Torque in Continuous Textures: Semiclassical Boltzmann Approach," Phys. Rev. B **75**, 174414.

Pinna, D, F Abreu Araujo, J-V Kim, V Cros, D Querlioz, P Bessière, J Droulez, and J Grollier, 2018, "Skyrmion Gas Manipulation for Probabilistic Computing," Phys. Rev. Appl. **9**, 064018.

Pizzini, S, J Vogel, S Rohart, L D Buda-Prejbeanu, E Jué, O Boulle, I M Miron, et al., 2014, "Chirality-Induced Asymmetric Magnetic Nucleation in Pt/Co/AlO_x Ultrathin Microstructures," Phys. Rev. Lett. **113**, 047203.

Pollard, S D, J A Garlow, J Yu, Z Wang, Y Zhu, and H Yang, 2017, "Observation of Stable Néel Skyrmions in Cobalt/Palladium Multilayers with Lorentz Transmission Electron Microscopy," Nat. Commun. **8**, 14761.

Pribiag, V S, I N Krivorotov, G D Fuchs, P M Braganca, O Ozatay, J C Sankey, D C Ralph, and R A Buhrman, 2007, "Magnetic Vortex Oscillator Driven by D.C. Spin-Polarized Current," Nat. Phys. **3**, 498.

Pufall, M, W Rippard, M Schneider, and S Russek, 2007, "Low-Field Current-Hysteretic Oscillations in Spin-Transfer Nanocontacts," Phys. Rev. B **75**, 140404.

Quinsat, M, D Gusakova, J F Sierra, J P Michel, D Houssameddine, B Delaet, M-C Cyrille, et al., 2010, "Amplitude and Phase Noise of Magnetic Tunnel Junction Oscillators," Appl. Phys. Lett. **97**, 182507.

Rajaraman, R, 1982, Solitons and Instantons (North Holland).

Rayleigh, Lord, 1888, "CXII. The problem of the whispering gallery," Philosophical Magazine **20**, 1001.

Reichhardt, C, D Ray, and C J Olson Reichhardt, 2015, "Collective Transport Properties of Driven Skyrmions with Random Disorder," Phys. Rev. Lett. **114**, 217202.

Reichhardt, C, and C J Olson Reichhardt, 2016, "Noise Fluctuations and Drive Dependence of the Skyrmion Hall Effect in Disordered Systems," New J. Phys. **18**, 095005.

Rezende, S, F De Aguiar, and A Azevedo, 2005, "Spin-Wave Theory for the Dynamics Induced by Direct Currents in Magnetic Multilayers," Phys. Rev. Lett. **94**, 037202.

Ritzmann, U, S von Malottki, J-V Kim, S Heinze, J Sinova, and B Dupé, 2018, "Trochoidal motion and pair generation in skyrmion and antiskyrmion dynamics under spin-orbit torques," arXiv:1803.00534 [cond-mat.mes-hall].

Rippard, W H, M R Pufall, and T J Silva, 2003, "Quantitative Studies of Spin-Momentum-Transfer-Induced Excitations in Co/Cu Multilayer Films Using Point-Contact Spectroscopy," Appl. Phys. Lett. **82**, 1260.

Rippard, W, M Pufall, S Kaka, T Silva, and S Russek, 2004, "Current-Driven Microwave Dynamics in Magnetic Point Contacts as a Function of Applied Field Angle," Phys. Rev. B **70**, 100406.

Rippard, W, M Pufall, S Kaka, S Russek, and T Silva, 2004b, "Direct-Current Induced Dynamics in Co90Fe10/Ni80Fe20 Point Contacts," Phys. Rev. Lett. **92**, 027201.

Risken, H, 1989, The Fokker-Planck Equation (Springer-Verlag, Berlin), 2nd ed.

Rohart, S, and A Thiaville, 2013, "Skyrmion Confinement in Ultrathin Film Nanostructures in the Presence of Dzyaloshinskii-Moriya Interaction," Phys. Rev. B **88**, 184422.

Rohart, S, J Miltat, and A Thiaville, 2016, "Path to Collapse for an Isolated Néel Skyrmion," Phys. Rev. B **93**, 214412.

Romming, N, C Hanneken, M Menzel, J E Bickel, B Wolter, K Von Bergmann, A Kubetzka, and R. Wiesendanger, 2013, "Writing and Deleting Single Magnetic Skyrmions," Science **341**, 636.

Rondin, L, J P Tetienne, T Hingant, J F Roch, P Maletinsky, and V Jacques, 2014, "Magnetometry with Nitrogen-Vacancy Defects in Diamond," Rep. Prog. Phys. **77**, 056503.

Rößler, U K, A N Bogdanov, and C Pfleiderer, 2006, "Spontaneous Skyrmion Ground States in Magnetic Metals," Nature **442**, 797.

Rózsa, L, K Palotás, A Deák, E Simon, R Yanes, L Udvardi, L Szunyogh, and U Nowak, 2017, "Formation and Stability of Metastable Skyrmionic Spin Structures with Various Topologies in an Ultrathin Film," Phys. Rev. B **95**, 094423.

Ruiz-Calaforra, A, A Purbawati, T Brächer, J Hem, C Murapaka, E Jiménez, D Mauri, et al., 2017, "Frequency Shift Keying by Current Modulation in a MTJ-Based STNO with High Data Rate," Appl. Phys. Lett. **111**, 082401.

Ruotolo, A, V Cros, B Georges, A Dussaux, J Grollier, C Deranlot, R Guillemet, K Bouzehouane, S Fusil, and A Fert, 2009, "Phase-Locking of Magnetic Vortices Mediated by Antivortices," Nat. Nanotechnol. **4**, 528.

Ryu, K-S, L Thomas, S-H Yang, and S S P Parkin, 2013, "Chiral Spin Torque at Magnetic Domain Walls," Nat. Nanotechnol. **8**, 527.

Sampaio, J, V Cros, S Rohart, A Thiaville, and Albert Fert, 2013, "Nucleation, Stability and Current-Induced Motion of Isolated Magnetic Skyrmions in Nanostructures," Nat. Nanotechnol. **8**, 839.

Sankey, J, I N Krivorotov, S Kiselev, P Braganca, N Emley, R Buhrman, and D Ralph, 2005, "Mechanisms Limiting the Coherence Time of Spontaneous Magnetic Oscillations Driven by dc Spin-Polarized Currents," Phys. Rev. B **72**, 224427.

Schneider, T, A A Serga, A V Chumak, C W Sandweg, S Trudel, S Wolff, M P Kostylev, V S Tiberkevich, A N Slavin, and B Hillebrands, 2010, "Nondiffractive Subwavelength Wave Beams in a Medium with Externally Controlled Anisotropy," Phys. Rev. Lett. **104**, 197203.

Schroeter, S, and M Garst, 2015, "Scattering of High-Energy Magnons Off a Magnetic Skyrmion," Low Temp. Phys. **41**, 817.

Schryer, N L, and L R Walker, 1974, "The Motion of 180° Domain Walls in Uniform Dc Magnetic Fields," J. Appl. Phys. **45**, 5406.

Schütte, C, and M Garst, 2014, "Magnon-Skyrmion Scattering in Chiral Magnets," Phys. Rev. B **90**, 094423.

Schweizer, J, and T Schimming, 2001, "Symbolic Dynamics for Processing Chaotic Signals. I. Noise Reduction of Chaotic Sequences," IEEE Trans. Circuits Syst. I **48**, 1269.

Schweizer, J, and T Schimming, 2001b, "Symbolic Dynamics for Processing Chaotic Signal. II. Communication and Coding," IEEE Trans. Circuits Syst. I **48**, 1283.

Sciamanna, M, and K A Shore, 2015, "Physics and Applications of Laser Diode Chaos," Nat. Photon. **9**, 151.

Seaberg, M H, B Holladay, J C T Lee, M Sikorski, A H Reid, S A Montoya, G L Dakovski, et al., 2017, "Nanosecond X-Ray Photon Correlation Spectroscopy on Magnetic Skyrmions," Phys. Rev. Lett. **119**, 067403.

Sebastian, T, T Brächer, P Pirro, A A Serga, B Hillebrands, T Kubota, H Naganuma, M Oogane, and Y Ando, 2013, "Nonlinear Emission of Spin-Wave Caustics From an Edge Mode of a Microstructured $Co_2Mn_{0.6}Fe_{0.4}Si$ Waveguide," Phys. Rev. Lett. **110**, 067201.

Seki, S, X Z Yu, S Ishiwata, and Y Tokura, 2012, "Observation of Skyrmions in a Multiferroic Material," Science **336**, 198.

Shibata, J, G Tatara, and H Kohno, 2005, "Effect of Spin Current on Uniform Ferromagnetism: Domain Nucleation," Phys. Rev. Lett. **94**, 076601.

Sierra, J F, M Quinsat, F Garcia-Sanchez, U Ebels, I. Joumard, A. S. Jenkins, B Diény, M-C Cyrille, A Zeltser, and J A Katine, 2012, "Influence of Thermal Fluctuations on the Emission Linewidth in MgO-Based Spin Transfer Oscillators," Appl. Phys. Lett. **101**, 062407.

Slavin, A, and V Tiberkevich, 2005, "Spin Wave Mode Excited by Spin-Polarized Current in a Magnetic Nanocontact Is a Standing Self-Localized Wave Bullet," Phys. Rev. Lett. **95**, 237201.

Slavin, A N, and P Kabos, 2005b, "Approximate Theory of Microwave Generation in a Current-Driven Magnetic Nanocontact Magnetized in an Arbitrary Direction," IEEE Trans. Magn. **41**, 1264.

Slonczewski, J. C., 1996, "Current-Driven Excitation of Magnetic Multilayers," J. Magn. Magn. Mater. **159**, L1.

Slonczewski, J. C., 1999, "Excitation of Spin Waves by an Electric Current," J. Magn. Magn. Mater. **195**, L261.

Soucaille, R, M Belmeguenai, J Torrejon, J-V Kim, T Devolder, Y Roussigné, S-M Chérif, A A Stashkevich, M Hayashi, and J-P Adam, 2016, "Probing the Dzyaloshinskii-Moriya Interaction in CoFeB Ultrathin Films Using Domain Wall Creep and Brillouin Light Spectroscopy," Phys. Rev. B **94**, 104431.

Sparks, M, 1964, Ferromagnetic-Relaxation Theory (McGraw-Hill, New York).

Strogatz, S H, 1994, Nonlinear Dynamics and Chaos (Perseus Books, Reading, MA).

Suess, D, T Schrefl, S Fähler, M Kirschner, G Hrkac, F Dorfbauer, and J Fidler, 2005, "Exchange Spring Media for Perpendicular Recording," Appl. Phys. Lett. **87**, 012504.

Tatara, G, and H Kohno, 2004, "Theory of Current-Driven Domain Wall Motion: Spin Transfer Versus Momentum Transfer," Phys. Rev. Lett. **92**, 086601.

Taylor, B, H J Maris, and C Elbaum, 1969, "Phonon Focusing in Solids," Phys. Rev. Lett. **23**, 416.

Tetienne, J P, T Hingant, J-V Kim, L H Diez, J-P Adam, K Garcia, J F Roch, et al., 2014, "Nanoscale Imaging and Control of Domain-Wall Hopping with a Nitrogen-Vacancy Center Microscope," Science **344**, 1366.

Thiaville, A, Y Nakatani, J Miltat, and Y Suzuki, 2005, "Micromagnetic Understanding of Current-Driven Domain Wall Motion in Patterned Nanowires," Europhys. Lett. **69**, 990.

Thompson, L R, and P C E Stamp, 2008, "Effective Magnus Force on a Magnetic Vortex," Quantum Magnetism, 175.

Tiberkevich, V, A Slavin, and J-V Kim, 2008, "Temperature Dependence of Nonlinear Auto-Oscillator Linewidths: Application to Spin-Torque Nano-Oscillators," Phys. Rev. B **78**, 092401.

Tiberkevich, V S, R S Khymyn, H X Tang, and A N Slavin, 2014, "Sensitivity to External Signals and Synchronization Properties of a Non-Isochronous Auto-Oscillator with Delayed Feedback," Sci. Rep. **4**, 3873.

Tomasello, R, E Martinez, R Zivieri, L Torres, M Carpentieri, and G Finocchio, 2014, "A Strategy for the Design of Skyrmion Racetrack Memories," Sci. Rep. **4**, 6784.

Torrejon, J, J Kim, J Sinha, S Mitani, M Hayashi, M Yamanouchi, and H Ohno, 2014, "Interface Control of the Magnetic Chirality in CoFeB/MgO Heterostructures with Heavy-Metal Underlayers," Nat. Commun. **5**, 4655.

Tserkovnyak, Y, A Brataas, and G E W Bauer, 2002, "Enhanced Gilbert Damping in Thin Ferromagnetic Films," Phys. Rev. Lett. **88**, 117601.

Tsoi, M, A Jansen, J Bass, W-C Chiang, M Seck, V Tsoi, and P Wyder, 1998, "Excitation of a Magnetic Multilayer by an Electric Current," Phys. Rev. Lett. **80**, 4281.

Tsoi, M, V Tsoi, J Bass, A Jansen, and P Wyder, 2002, "Current-Driven Resonances in Magnetic Multilayers," Phys. Rev. Lett. **89**, 246803.

Tsunegi, S, E Grimaldi, R Lebrun, H Kubota, A S Jenkins, K Yakushiji, A Fukushima, et al., 2016, "Self-Injection Locking of a Vortex Spin Torque Oscillator by Delayed Feedback," Sci. Rep. **6**, 26849.

Tsunegi, S, K Yakushiji, A Fukushima, S Yuasa, and H Kubota, 2016b, "Microwave Emission Power Exceeding 10 μW in Spin Torque Vortex Oscillator," Appl. Phys. Lett. **109**, 252402.

Tveten, E G, A Qaiumzadeh, and A Brataas, 2014, "Antiferromagnetic Domain Wall Motion Induced by Spin Waves," Phys. Rev. Lett. **112**, 147204.

Uchida, A, K Amano, M Inoue, K Hirano, S Naito, H Someya, I Oowada, et al., 2008, "Fast Physical Random Bit Generation with Chaotic Semiconductor Lasers," Nat. Photon. **2**, 728.

Udvardi, L, and L Szunyogh, 2009, "Chiral Asymmetry of the Spin-Wave Spectra in Ultrathin Magnetic Films," Phys. Rev. Lett. **102**, 207204.

Urazhdin, S, V Tiberkevich, and A Slavin, 2010, "Parametric Excitation of a Magnetic Nanocontact by a Microwave Field," Phys. Rev. Lett. **105**, 237204.

Vanatka, M, J C Rojas Sánchez, J Vogel, M Bonfim, M Belmeguenai, Y Roussigné, A Stashkevich, A Thiaville, and S Pizzini, 2015, "Velocity Asymmetry of Dzyaloshinskii Domain Walls in the Creep and Flow Regimes," J. Phys.: Condens. Matter **24**, 326002.

Vansteenkiste, A, and B Van de Wiele, 2011, "MuMax a New High-Performance Micromagnetic Simulation Tool," J. Magn. Magn. Mater. **323**, 2585.

Vansteenkiste, A, J Leliaert, M Dvornik, M Helsen, F Garcia-Sanchez, and B Van Waeyenberge, 2014, "The Design and Verification of MuMax3," AIP Adv. **4**, 107133.

Van Waeyenberge, B, A Puzic, H Stoll, K W Chou, T Tyliszczak, R Hertel, M Fähnle, et al., 2006, "Magnetic Vortex Core Reversal by Excitation with Short Bursts of an Alternating Field," Nature **444**, 461.

Veerakumar, V, and R E Camley, 2006, "Magnon Focusing in Thin Ferromagnetic Films," Phys. Rev. B **74**, 214401.

Villard, P, U Ebels, D Houssameddine, J Katine, D Mauri, B Delaet, P Vincent, et al., 2010, "A GHz Spintronic-Based RF Oscillator," IEEE J. Solid-State Circuits **45**, 214.

Virte, M, E Mercier, H Thienpont, K Panajotov, and M Sciamanna, 2014, "Physical Random Bit Generation From Chaotic Solitary Laser Diode," Opt. Express **22**, 17271.

Vlaminck, V, and M Bailleul, 2008, "Current-Induced Spin-Wave Doppler Shift," Science **322**, 410.

Vodenicarevic, D, N Locatelli, J Grollier, and D Querlioz, 2016, "Synchronization Detection in Networks of Coupled Oscillators for Pattern Recognition", **arXiv:1607.01983** [cs.ET].

White, R M, 2007, Quantum Theory of Magnetism (Springer-Verlag, Berlin), 3rd ed.

Williame, J, A Difini Accioly, and J V Kim, 2017, "Chaotic dynamics in a macrospin spin-torque nano-oscillator with time-delayed feedback," **arXiv:1709.04310** [cond-mat.mes-hall].

Winter, J M, 1961, "Bloch Wall Excitation. Application to Nuclear Resonance in a Bloch Wall," Phys. Rev. **124**, 452.

Wintz, S, C Bunce, A Neudert, M Körner, T Strache, M Buhl, A Erbe, et al., 2013, "Topology and Origin of Effective Spin Meron Pairs in Ferromagnetic Multilayer Elements," Phys. Rev. Lett. **110**, 177201.

Woo, S, K Litzius, B Krüger, M-Y Im, L Caretta, K Richter, M Mann, et al., 2016, "Observation of Room-Temperature Magnetic Skyrmions and Their Current-Driven Dynamics in Ultrathin Metallic Ferromagnets," Nat. Mater. **15**, 501.

Yamada, K, S Kasai, Y Nakatani, K Kobayashi, H Kohno, A Thiaville, and T Ono, 2007, "Electrical Switching of the Vortex Core in a Magnetic Disk," Nat. Mater. **6**, 270.

Yu, X Z, Y Onose, N Kanazawa, J-H Park, J H Han, Y Matsui, N Nagaosa, and Y Tokura, 2010, "Real-Space Observation of a Two-Dimensional Skyrmion Crystal," Nature **465**, 901.

Zakeri, K, Y Zhang, J Prokop, T-H Chuang, N Sakr, W X Tang, and J Kirschner, 2010, "Asymmetric Spin-Wave Dispersion on Fe(110): Direct Evidence of the Dzyaloshinskii-Moriya Interaction," Phys. Rev. Lett. **104**, 137203.

Zapperi, S, P Cizeau, G Durin, and H Stanley, 1998, "Dynamics of a Ferromagnetic Domain Wall: Avalanches, Depinning Transition, and the Barkhausen Effect," Phys. Rev. B **58**, 6353.

Zhang, S, J Wang, Q Zheng, Q Zhu, X Liu, S Chen, C Jin, Q Liu, C Jia, and D Xue, 2015, "Current-Induced Magnetic Skyrmions Oscillator," New J. Phys. **17**, 023061.

Zhang, S, and Z Li, 2004, "Roles of Nonequilibrium Conduction Electrons on the Magnetization Dynamics of Ferromagnets," Phys. Rev. Lett. **93**, 127204.

Zhou, Y, E Iacocca, A A Awad, R K Dumas, F C Zhang, H B Braun, and J Åkerman, 2015, "Dynamically Stabilized Magnetic Skyrmions," Nat. Commun. **6**, 8193.

Zvezdin, A K, and A F Popkov, 1984, "Propagation of Spin Waves in a Moving Domain Wall," JETP Lett. **39**, 419.

List of Publications

Book Chapters

1. *Spin-torque oscillators*
   J.-V. Kim, in volume 63 of *Solid State Physics*, R. E. Stamps & R. E. Camley, eds. (Academic Press, 2012), pp. 217–294.
2. *Spin Waves on Spin Structures: Topology, Localization, and Nonreciprocity*
   R. L. Stamps, J.-V. Kim, F. Garcia-Sanchez, P. Borys, G. Gubbiotti, Y. Li & R. E. Camley, in *Spin Wave Confinement II: Propagating Wave*s, S. O. Demokritov, ed. (Pan Stanford Publishing, 2017), pp. 219-260.

Regular articles in International Peer-Reviewed Journals

3. *Angular dependence and interfacial roughness in exchange-biased ferromagnetic/antiferromagnetic bilayers*
   J.-V. Kim, R. L. Stamps, B. V. McGrath & R. E. Camley
   Physical Review B **61**, 8888 (2000).
4. *Roughness-induced instability in stripe domain patterns*
   J.-V. Kim, M. Demand, M. Hehn, K. Ounadjela & R. L. Stamps
   Physical Review B **62**, 6467 (2000).
5. *Defect-modified exchange bias*
   J.-V. Kim & R.L. Stamps
   Applied Physics Letters **79**, 2785 (2001).
6. *Exchange bias of polycrystalline antiferromagnets with perfectly compensated interface*
   D. Suess, M. Kirschner, T. Schrefl, J. Fidler, R. L. Stamps & J.-V. Kim
   Physical Review B **67**, 054419 (2003).
7. *Phase diagrams and energy barriers of exchange biased bilayers with additional anisotropies in the ferromagnet*
   T. Mewes, H. Nembach, J. Fassbender, B. Hillebrands, J.-V. Kim & R. L. Stamps
   Physical Review B **67**, 104422 (2003).
8. *Spin wave contributions to the high-frequency magnetic response of thin films obtained with inductive methods*
   G. Counil, J.-V. Kim, T. Devolder, C. Chappert, K. Shigeto & Y. Otani
   Journal of Applied Physics **95**, 5646 (2004).
9. *Precession-dominated switching of synthetic antiferromagnets*
   J.-V. Kim, T. Devolder, C. Chappert, C. Maufront & R. Fournel
   Applied Physics Letters **85**, 4094 (2004).
10. *Hysteresis from antiferromagnet domain-wall processes in exchange-biased systems: Magnetic defects and thermal effects*
    J.-V. Kim & R. L. Stamps
    Physical Review B **71**, 094405 (2005).
11. *Magnetic anisotropy of epitaxial MgO/Fe/MgO films studied by network analyzer ferromagnetic resonance*
    G. Counil, J.-V. Kim, T. Devolder, P. Crozat, C. Chappert & A. Cebollada
    Journal of Applied Physics **98**, 023901 (2005).
12. *Magnetization switching by spin torque using subnanosecond current pulses assisted by hard axis magnetic fields*
    T. Devolder, P. Crozat, J.-V. Kim, C. Chappert, K. Ito, M. J. Carey & J. A. Katine
    Applied Physics Letters **88**, 152502 (2006).
13. *Current-driven microwave oscillations in current perpendicular-to-plane spin-valve nanopillars*
    Q. Mistral, J.-V. Kim, T. Devolder, P. Crozat, C. Chappert, J. A. Katine, M. J. Carey & K. Ito
    Applied Physics Letters **88**, 192507 (2006).

14. *Stochastic theory of spin-transfer oscillator linewidths*
J.-V. Kim
Physical Review B **73**, 174412 (2006).

15. *Study of the dynamic magnetic properties of soft CoFeB films*
C. Bilzer, T. Devolder, J.-V. Kim, G. Counil, C. Chappert, S. Cardoso & P. P. Freitas
Journal of Applied Physics **100**, 053903 (2006).

16. *Microwave power generated by a spin-torque oscillator in the presence of noise*
V. Tiberkevich, A. Slavin & J.-V. Kim
Applied Physics Letters **91**, 192506 (2007).

17. *Generation Linewidth of an Auto-Oscillator with a Nonlinear Frequency Shift: Spin-Torque Nano-Oscillator*
J.-V. Kim, V. S. Tiberkevich & A. N. Slavin
Physical Review Letters **100**, 017207 (2008).

18. *Single-shot time-resolved measurements of nanosecond-scale spin-transfer induced switching: Stochastic versus deterministic aspects*
T. Devolder, J. Hayakawa, K. Ito, H. Takahashi, S. Ikeda, P. Crozat, N. Zerounian, J.-V. Kim, C. Chappert & H. Ohno
Physical Review Letters **100**, 057206 (2008).

19. *Line Shape Distortion in a Nonlinear Auto-Oscillator Near Generation Threshold: Application to Spin-Torque Nano-Oscillators*
J.-V. Kim, Q. Mistral, C. Chappert, V. S. Tiberkevich & A. N. Slavin
Physical Review Letters **100**, 167201 (2008).

20. *Current-driven vortex oscillations in metallic nanocontacts*
Q. Mistral, M. van Kampen, G. Hrkac, J.-V. Kim, T. Devolder, P. Crozat, C. Chappert, L. Lagae, & T. Schrefl
Physical Review Letters **100**, 257201 (2008).

21. *Temperature dependence of nonlinear auto-oscillator linewidths: Application to spin-torque nano-oscillators*
V. S. Tiberkevich, A. N. Slavin & J.-V. Kim
Physical Review B **78**, 092401 (2008).

22. *Spin-wave contributions to current-driven domain-wall dynamics*
Y. Le Maho, J.-V. Kim & G. Tatara
Physical Review B **79**, 174404 (2009).

23. *Time-resolved zero field vortex oscillations in point contacts*
T. Devolder, J.-V. Kim, P. Crozat, C. Chappert, M. Manfrini, M. van Kampen, W. Van Roy, L. Lagae, G. Hrkac & T. Schrefl
Applied Physics Letters **95**, 012507 (2009).

24. *Direct measurement of current-induced fieldlike torque in magnetic tunnel junctions*
T. Devolder, J.-V. Kim, C. Chappert, J. Hayakawa, K. Ito, H. Takahashi, S. Ikeda & H. Ohno
Journal of Applied Physics **105**, 113924 (2009).

25. *Auto-oscillation threshold and line narrowing in MgO-based spin-torque oscillators*
S. Cornelissen, L. Bianchini , G. Hrkac, M. Op de Beeck, L. Lagae, J.-V. Kim, T. Devolder, P. Crozat, C. Chappert & T. Schrefl
Europhysics Letters **87**, 57001 (2009).

26. *Dynamics of the exchange field supplied by MnIr layers studied by network analyzer ferromagnetic resonance*
C. Bilzer, T. Devolder, J.-V. Kim, C. Chappert, M. Ruehrig & L. Baer
Journal of Applied Physics **106**, 063918 (2009).

27. *Agility of vortex-based nanocontact spin torque oscillators*
M. Manfrini, T. Devolder, J.-V. Kim, P. Crozat, N. Zerounian, C. Chappert, W. Van Roy, L. Lagae, G. Hrkac & T. Schrefl
Applied Physics Letters **95**, 192507 (2009).

28. *Auto-oscillation and narrow spectral lines in spin-torque oscillators based on MgO magnetic tunnel junctions*
T. Devolder, L. Bianchini, J.-V. Kim, P. Crozat, C. Chappert, S. Cornelissen, M. Op de

Beeck & L. Lagae,
Journal of Applied Physics **106**, 103921 (2009).

29. *Current-driven vortex oscillations in metallic nanocontacts: Zero-field oscillations and training effects*
M. van Kampen, L. Lagae, G. Hrkac, T. Schrefl, J.-V. Kim, T. Devolder & C. Chappert
Journal of Physics D: Applied Physics **46**, 245001 (2009).
30. *Influence of magnetic viscosity on domain wall dynamics under spin-polarized currents*
J.-V. Kim & C. Burrowes
Physical Review B **80**, 214424 (2009).
31. *Non-adiabatic spin-torques in narrow magnetic domain walls*
C. Burrowes, A. P. Mihai, D. Ravelosona, J.-V. Kim, C. Chappert, L. Vila, A. Marty, Y. Samson, F. Garcia-Sanchez, L. D. Buda-Prejbeanu, I. Tudosa, E. E. Fullerton & J.-P. Attané
Nature Physics **6**, 17 (2010).
32. *Quantized spin wave modes in magnetic tunnel junction nanopillars*
A. Helmer, S. Cornelissen, T. Devolder, J.-V. Kim, W. van Roy, L. Lagae & C. Chappert
Physical Review B **81**, 094416 (2010).
33. *Free layer versus synthetic ferrimagnet layer auto-oscillations in nanopillars processed from MgO-based magnetic tunnel junction*s
S. Cornelissen, L. Bianchini, T. Devolder, J.-V. Kim, W. Van Roy, L. Lagae & C. Chappert
Physical Review B **81**, 144408 (2010).
34. *Influence of oscillation modes on the line width of rf emissions in MgO based nanopillars*
G. Hrkac, A. Goncharov, J. Dean, T. Schrefl, J.-V. Kim, T. Devolder, C. Chappert, S. Cornelissen, W. Van Roy & L. Lagae
Journal of Applied Physics **108**, 023917 (2010).
35. *Direct experimental measurement of phase-amplitude coupling in spin torque oscillators*
L. Bianchini, S. Cornelissen, J.-V. Kim, T. Devolder, W. Van Roy, L. Lagae & C. Chappert
Applied Physics Letters **97**, 032502 (2010).
36. *Vortex nucleation in spin-torque nanocontact oscillators*
T. Devolder, J.-V. Kim, M. Manfrini, W. Van Roy, L. Lagae & C. Chappert
Applied Physics Letters **97**, 072512 (2010).
37. *Spin-torque switching window, thermal stability, and material parameters of MgO tunnel junctions*
T. Devolder, L. Bianchini, K. Miura, K. Ito, J.-V. Kim, P. Crozat, V. Morin, A. Helmer, C. Chappert, S. Ikeda & H. Ohno
Applied Physics Letters **98**, 162502 (2011).
38. *Frequency shift keying in vortex-based spin torque oscillators*
M. Manfrini, T. Devolder, J.-V. Kim, W. Van Roy, P. Crozat, C. Chappert & L. Lagae
Journal of Applied Physics **109**, 083940 (2011).
39. *Configuration and temperature dependence of magnetic damping in spin valves*
X. Joyeux, T. Devolder, J.-V. Kim, Y. G. de la Torre, S. Eimer & C. Chappert
Journal of Applied Physics **110**, 063915 (2011).
40. *Fast magnetization switching in GaMnAs induced by electrical fields*
P. Balestriere, T. Devolder, J.-V. Kim, P. Lecoeur, J. Wunderlich, V. Novak, T. Jungwirth & C. Chappert
Applied Physics Letters **99**, 242505 (2011).
41. *Perpendicular-magnetic-anisotropy CoFeB racetrack memory*
Y. Zhang, W.-S. Zhao, D. Ravelosona, J.-O. Klein, J.-V. Kim & C. Chappert
Journal of Applied Physics **111**, 093925 (2012).
42. *Compact Modeling of Perpendicular-Anisotropy CoFeB/MgO Magnetic Tunnel Junctions*
Y. Zhang, W.-S. Zhao, Y. Lakys, J.-O. Klein, J.-V. Kim, D. Ravelosona & C. Chappert
IEEE Transactions on Electron Devices **59**, 819 (2012).
43. *Commensurability and chaos in magnetic vortex oscillations*
S. Petit-Watelot, J.-V. Kim, A. Ruotolo, R. M. Otxoa, K. Bouzehouane, J. Grollier, A. Vansteenkiste, B. Van de Wiele, V. Cros & T. Devolder
Nature Physics **8**, 682 (2012).

44. *Material parameters and thermal stability of synthetic ferrimagnet free layers in magnetic tunnel junction nanopillars*
D. Markó, T. Devolder, K. Miura, K. Ito, J.-V. Kim, C. Chappert, S. Ikeda & H. Ohno
Journal of Applied Physics **112**, 053922 (2012).

45. *Understanding nanoscale temperature gradients in magnetic nanocontacts*
S. Petit-Watelot, R. M. Otxoa, M. Manfrini, W. Van Roy, L. Lagae, J.-V. Kim & T. Devolder
Physical Review Letters **109**, 267205 (2012).

46. *Domain wall motion in nanopillar spin-valves with perpendicular anisotropy driven by spin-transfer torques*
J. Cucchiara, S. Le Gall, E. E. Fullerton, J.-V. Kim, D. Ravelosona, Y. Henry, J. A. Katine, A. D. Kent, D. Bedau, D. Gopman & S. Mangin
Physical Review B **86**, 214429 (2012).

47. *Strain-controlled magnetic domain wall propagation in hybrid piezoelectric/ferromagnetic structures*
N. Lei, T. Devolder, G. Agnus, P. Aubert, L. Daniel, J.-V. Kim, W.-S. Zhao, T. Trypiniotis, R. P. Cowburn, C. Chappert, D. Ravelosona & P. Lecoeur
Nature Communications **4**, 1378 (2013).

48. *Damping of CoxFe80-xB20 ultrathin films with perpendicular magnetic anisotropy*
T. Devolder, P.-H. Ducrot, J.-P. Adam, I. Barisic, N. Vernier, J.-V. Kim, B. Ockert & D. Ravelosona
Applied Physics Letters **102**, 022407 (2013).

49. *Low depinning fields in Ta-CoFeB-MgO ultrathin films with perpendicular magnetic anisotropy*
C. Burrowes, N. Vernier, J.-P. Adam, L. Herrera Diez, K. Garcia, I. Barisic, G. Agnus, S. Eimer, J.-V. Kim, T. Devolder, A. Lamperti, R. Mantovan, B. Ockert, E. E Fullerton & D. Ravelosona
Applied Physics Letters **103**, 182401 (2013).

50. *Propagation of magnetic vortices using nanocontacts as tunable attractors*
M. Manfrini, J.-V. Kim, S. Petit-Watelot, W. Van Roy, L. Lagae, C. Chappert & T. Devolder
Nature Nanotechnology **9**, 121 (2014).

51. *Nonreciprocal spin-wave channeling along textures driven by the Dzyaloshinskii-Moriya interaction*
F. Garcia-Sanchez, P. Borys, A. Vansteenkiste, J.-V. Kim & R. L. Stamps
Physical Review B **89**, 224408 (2014).

52. *Nanoscale imaging and control of domain-wall hopping with a nitrogen-vacancy center microscope*
J.-P. Tetienne, T. Hingant, J.-V. Kim, L. Herrera Diez, J.-P. Adam, K. Garcia, J.-F. Roch, S. Rohart, A. Thiaville, D. Ravelosona & V. Jacques
Science **334**, 1366 (2014).

53. *Breathing modes of confined skyrmions in ultrathin magnetic dots*
J.-V. Kim, F. Garcia-Sanchez, J. Sampaio, C. Moreau-Luchaire, V. Cros & A. Fert
Physical Review B **90**, 064410 (2014).

54. *Noise-Enhanced Synchronization of Stochastic Magnetic Oscillators*
N. Locatelli, A. Mizrahi, A. Accioly, R. Matsumoto, A. Fukushima, H. Kubota, S. Yuasa, V. Cros, L. G. Pereira, D. Querlioz, J.-V. Kim & J. Grollier
Physical Review Applied **2**, 034009 (2014).

55. *The nature of domain walls in ultrathin ferromagnets revealed by scanning nanomagnetometry*
J.-P. Tetienne, T. Hingant, L. J. Martinez, S. Rohart, A. Thiaville, L. Herrera Diez, K. Garcia, J.-P. Adam, J.-V. Kim, J.-F. Roch, I. M. Miron, G. Gaudin, L. Vila, B. Ocker, D. Ravelosona & V. Jacques
Nature Communications **6**, 6733 (2015).

56. *Interfacial Dzyaloshinskii-Moriya interaction in perpendicularly-magnetized Pt/Co/AlOx ultrathin films measured by Brillouin light spectroscopy*
M. Belmeguenai, J.-P. Adam, Y. Roussigné, S. Eimer, T. Devolder, J.-V. Kim, S. M. Cherif, A.

Stashkevich & A. Thiaville
Physical Review B **91**, 180405(R) (2015).

57. *Narrow Magnonic Waveguides Based on Domain Walls*
F. Garcia-Sanchez, P. Borys, R. Soucaille, J.-P. Adam, R. L. Stamps & J.-V. Kim
Physical Review Letters **114**, 247206 (2015).

58. *Current-driven asymmetric magnetization switching in perpendicularly magnetized CoFeB/MgO heterostructures*
J. Torrejon, F. Garcia-Sanchez, T. Taniguchi, J. Sinha, S. Mitani, J.-V. Kim & M. Hayashi
Physical Review B **91**, 214434 (2015).

59. *Dynamical influence of vortex-antivortex pairs in magnetic vortex oscillators*
R. M. Otxoa, S. Petit-Watelot, M. Manfrini, I. P. Radu, A. Thean, J.-V. Kim & T. Devolder
Journal of Magnetism and Magnetic Materials **394**, 292 (2015).

60. *Role of nonlinear anisotropic damping in the magnetization dynamics of topological solitons*
J.-V. Kim
Physical Review B **92**, 014418 (2015).

61. *Spin Wave Eigenmodes of Dzyaloshinskii Domain Walls*
P. Borys, F. Garcia-Sanchez, J.-V. Kim & R. L. Stamps
Advanced Electronic Materials **2**, 1500202 (2016).

62. *Time-resolved spin-torque switching in MgO-based perpendicularly magnetized tunnel junctions*
T. Devolder, J.-V. Kim, F. Garcia-Sanchez, J. Swerts, W. Kim, S. Couet, G. Kar & A. Furnemont
Physical Review B **93**, 024420 (2016).

63. *Spin wave amplification using the spin Hall effect in permalloy/platinum bilayers*
O. Gladii, M. Collet, K. Garcia-Hernandez, C. Cheng, S. Xavier, P. Bortolotti, V. Cros, Y. Henry, J.-V. Kim, A. Anane & M. Bailleul
Applied Physics Letters **108**, 202407 (2016).

64. *A skyrmion-based spin-torque nano-oscillator*
F. Garcia-Sanchez, J. Sampaio, N. Reyren, V. Cros & J.-V. Kim
New Journal of Physics **18**, 075011 (2016).

65. *Direct measurement of interfacial Dzyaloshinskii-Moriya interaction in X|CoFeB|MgO heterostructures with a scanning-NV magnetometer*
I. Gross, L. J. Martinez, J.-P. Tetienne, T. Hingant, J.-F. Roch, K. Garcia, R. Soucaille, J.-P. Adam, J.-V. Kim, S. Rohart, A. Thiaville, J. Torrejon, M. Hayashi & V. Jacques
Physical Review B **94**, 064413 (2016).

66. *Role of spin-transfer torques on synchronization and resonance phenomena in stochastic magnetic oscillators*
A. Accioly, N. Locatelli , A. Mizrahi , D. Querlioz , L. G. Pereira, J. Grollier & J.-V. Kim
Journal of Applied Physics **120**, 093902 (2016).

67. *Probing the Dzyaloshinskii-Moriya interaction in CoFeB ultrathin films using domain wall creep and Brillouin light spectroscopy*
R. Soucaille, M. Belmeguenai, J. Torrejon, J.-V. Kim, T. Devolder, Y. Roussigné, S.-M. Chérif, A. A. Stashkevich, M. Hayashi & J.-P. Adam
Physical Review B **94**, 104431 (2016).

68. *Spin Wave Power Flow and Caustics in Ultrathin Ferromagnets with the Dzyaloshinskii-Moriya Interaction*
J.-V. Kim, R. L. Stamps & R. E. Camley
Physical Review Letters **117**, 197204 (2016).

69. *Exchange stiffness in ultrathin perpendicularly magnetized CoFeB layers determined using the spectroscopy of electrically excited spin waves*
T. Devolder, J.-V. Kim, L. Nistor, R. Sousa, B. Rodmacq & B. Diény
Journal of Applied Physics **120**, 183902 (2016).

70. *Nanocontact based spin torque oscillators with two free layers*
R. Soucaille, J.-V. Kim, T. Devolder, S. Petit-Watelot, M. Manfrini, W. Van Roy & L. Lagae
Journal of Physics D: Applied Physics **50**, 085002 (2017).

71. *Spin transfer and spin-orbit torques in in-plane magnetized (Ga,Mn)As tracks*
L. Thevenard, B. Boutigny, N. Güsken, C. Ulysse, L. Becerra, S. Shihab, A. Lemaître, J.-V. Kim, V. Jeudy & C. Gourdon
Physical Review B **95**, 054422 (2017).

72. *Current-driven skyrmion dynamics in disordered films*
J.-V. Kim & M.-Y. Woo
Applied Physics Letters **110**, 132404 (2017).

73. *Current-driven skyrmion expulsion from magnetic nanostrips*
M.-Y. Woo, V. Cros & J.-V. Kim
Physical Review B **95**, 184423 (2017).

74. *Real-space imaging of non-collinear antiferromagnetic order with a single-spin magnetometer*
I. Gross, W. Akhtar, V. Garcia, L. J. Martínez, S. Chouaieb, K. Garcia, C. Carrétéro, A. Barthélémy, P. Appel, P. Maletinsky, J.-V. Kim, J. Y. Chauleau, N. Jaouen, M. Viret, M. Bibes, S. Fusil & V. Jacques
Nature **549**, 252-256 (2017).

75. *Material Developments and Domain Wall-Based Nanosecond-Scale Switching Process in Perpendicularly Magnetized STT-MRAM Cells*
T. Devolder, J.-V. Kim, J. Swerts, W. Kim, S. Couet, G. Kar, A. Furnemont & V. Nikitin
IEEE Transactions on Magnetics **54**, 3400109 (2018).

76. *Skyrmion Gas Manipulation for Probabilistic Computing*
D. Pinna, F. Abreu Araujo, J.-V. Kim, V. Cros, D. Querlioz, P. Bessière, J. Droulez & J. Grollier
Physical Review Applied **9**, 064018 (2018).

77. *Chaotic dynamics in a macrospin spin-torque nano-oscillator with time-delayed feedback*
J. Williame, A. Difini Accioly & J.-V Kim
arXiv:1709.04310 [cond-mat.mes-hall].

78. *Nonreciprocal flexural dynamics of Dzyaloshinskii domain walls*
R. Soucaille, F. Garcia-Sanchez, J.-V. Kim, T. Devolder & J.-P. Adam
Physical Review B **98**, 054426 (2018).

79. *Thermal stability of metastable magnetic skyrmions: Entropic narrowing and significance of internal eigenmodes*
L. Desplat, D. Suess, J.-V. Kim & R. L. Stamps
Physical Review B **98**, 134407 (2018).

80. *Trochoidal motion and pair generation in skyrmion and antiskyrmion dynamics under spin-orbit torques*
U. Ritzmann, S. von Malottki, J.-V. Kim, S. Heinze, J. Sinova & B. Dupé
Nature Electronics **1**, 451 (2018).

Conference proceedings in international peer-reviewed journals

81. *Magnetic properties of self-organized epitaxial cobalt structures*
M. Demand, M. Hehn, K. Ounadjela, J.-V. Kim, A.V. Vagov & R. L. Stamps
Journal of Applied Physics **85**, 5498 (1999).

82. *Magnetization Dynamics: A Study of the Ferromagnet/Antiferromagnet Interface and Exchange Biasing*
R. E. Camley, B. V. McGrath, R. J. Astalos, J.-V. Kim & R. L. Stamps
Journal of Vacuum Science and Technology A **17**, 1335 (1999).

83. *Exchange Bias: Interface Imperfections and Temperature Dependence*
J.-V. Kim, L. Wee, R. L. Stamps & R. Street
IEEE Transactions on Magnetics **35**, 2994 (1999).

84. *Temperature dependence of exchange biased thin films*
B. V. McGrath, R. E. Camley, Leonard Wee, J.-V. Kim & R.L. Stamps
Journal of Applied Physics **87**, 6430 (2000).

85. *Theory of long-wavelength spin waves in exchange biased bilayers*
J.-V. Kim & R. L. Stamps
Journal of Applied Physics **89**, 7651 (2001).

86. *Probing antiferromagnetic order with heat capacity in exchange-biased structures*
J.-V. Kim & R. E. Camley
Journal of Magnetism and Magnetic Materials **240**, 267 (2002).

87. *Micromagnetic Simulation of Antiferromagnetic/Ferromagnetic Structures*
D. Suess, T. Schrefl, W. Scholz, J.-V. Kim, R. L. Stamps & J. Fidler
IEEE Transactions on Magnetics **38**, 2397 (2002).

88. *Inductive measurement of the high frequency permeability of a Permalloy thin film*
G. Counil, J.-V. Kim, K. Shigeto, Y. Otani, T. Devolder, P. Crozat, H. Hurdequint & C. Chappert
Journal of Magnetism and Magnetic Materials **272-276**, 290 (2004).

89. *Magnetization dynamics of spin-valve structures with spin-pumping*
J.-V. Kim & C. Chappert
Journal of Magnetism and Magnetic Materials **286**, 56 (2005).

90. *Hysteresis from antiferromagnet domain-wall processes in exchange biased systems*
J.-V. Kim & R. L. Stamps
Journal of Magnetism and Magnetic Materials **286**, 233 (2005).

91. *Bit selection scheme and dipolar interactions in high density precessional MRAM*
T. Devolder, C. Maufront, J.-V. Kim, H. W. Schumacher, C. Chappert & R. Fournel
IEE Proc.-Sci. Meas. Technol. **152**, 196 (2005).

92. *Precession-dominated reversal of synthetic antiferromagnets and synthetic ferrimagnets*
C. Maufront, J.-V. Kim, T. Devolder, R. Fournel & C. Chappert
IEEE Transactions on Magnetics **41**, 2655 (2005).

93. *Temperature Dependences of the Resistivity and the Ferromagnetic Resonance Linewidth in Permalloy Thin Films*
G. Counil, T. Devolder, J.-V. Kim, P. Crozat, C. Chappert, S. Zoll & R. Fournel
IEEE Transactions on Magnetics **42**, 3323 (2006).

94. *Theory of Generation Linewidth in Spin-torque Nano-sized Auto-oscillators*
J.-V. Kim, Vasil Tiberkevich & Andrei N. Slavin
Journal of Magnetics (Korea) **12**, 53 (2007).

95. *Electrical time-domain observation of magnetization switching induced by spin transfer in magnetic nanostructures (invited)*
T. Devolder, J. Hayakawa, K. Ito, H. Takahashi, S. Ikeda, J. A. Katine, M. J. Carey, P. Crozat, J. V. Kim, C. Chappert & H. Ohno
Journal of Applied Physics **103**, 07A723 (2008).

96. *Effect of patterning on the saturation magnetization in MgO based nanopillars*
S. Cornelissen, L. Bianchini, A. Helmer, T. Devolder, J.-V. Kim, M. Op de Beeck, W. van Roy, L. Lagae & C. Chappert
Journal of Applied Physics **105**, 07B903 (2009).

97. *A compact model of domain wall propagation for logic and memory design*
W. S. Zhao, J. Duval, D. Ravelosona, J.-O. Klein, J.-V. Kim & C. Chappert
Journal of Applied Physics **109**, 07D501 (2011).

98. *Vortex Nucleation Phase in Spin Torque Oscillators Based on Nanocontacts*
T. Devolder, J.-V. Kim, S. Petit-Watelot, R. Otxoa, C. Chappert, M. Manfrini, W. van Roy & L. Lagae
IEEE Transactions on Magnetics **47**, 1595 (2011).

99. *Nanocontact size dependence of the properties of vortex-based spin torque oscillators*
R. Otxoa, M. Manfrini, T. Devolder, J.-V. Kim, W. Van Roy, L. Lagae & C. Chappert
Physica Status Solidi B **248**, 1615 (2011).

100. *A compact model of domain wall propagation for logic and memory design*
W.-S. Zhao, J. Duval, D. Ravelosona, J.-O. Klein, J.-V. Kim & C. Chappert
Journal of Applied Physics **109**, 07D501 (2011).

101. *Magnetic Vortex Core Oscillations in Multi Point Contact Spin Valve Stacks*
G. Hrkac, D. Hahn, L. Saharan, T. Schrefl, J.-V. Kim, T. Devolder & C. Chappert
IEEE Transactions on Magnetics **48**, 3811 (2012).

102. *Magnetic stochastic oscillators: Noise-induced synchronization to under-threshold excitation and comprehensive compact model*

A. Mizrahi, N. Locatelli, R. Matsumoto, A. Fukushima, H. Kubota, S. Yuasa, V. Cros, J.-V. Kim, J. Grollier & D. Querlioz
IEEE Transactions on Magnetics **51**, 1401404 (2015).

Conference proceedings without peer review

103. *Experimental study of current-driven vortex oscillations in magnetic nanocontacts*
T. Devolder, J.-V. Kim, M. Manfrini, G. Hrkac, P. Crozat, L. Lagae, T. Schrefl & C. Chappert
Proceedings of the SPIE **7398**, 739808 (2009).

104. *Measurement of nanosecond-scale spin-transfer torque magnetization switching*
K. Ito, K. Miura, J. Hayakawa, H. Takahashi, T. Devolder, P. Crozat, J.-V. Kim, C. Chappert, S. Ikeda & H. Ohno
Proceedings Of The 9th International Symposium On Foundations Of Quantum Mechanics In The Light Of New Technology, pp. 131-133 (2009).

105. *Voltage control of magnetism in ferromagnetic structures*
L. Herrera Diez, W. Lin, A. Bernand-Mantel, L. Ranno, D. Givord, L. Vila, P. Warin, A. Marty, N. Lei, T. Devolder, J.-V. Kim, N. Vernier, P. Lecoeur & D. Ravelosona
Proceedings of the SPIE **8461**, 84610Y (2012).

106. *Spin torque nanodevices for bio-inspired computing*
N. Locatelli, A. Mizrahi, A. Accioly, D. Querlioz, J.-V. Kim, V. Cros & J. Grollier
Proceedings Of The 14th International Workshop On Cellular Nanoscale Networks and their Applications (CNNA), 2014.

107. *Spintronic Devices as Key Elements for Energy-Efficient Neuroinspired Architectures*
N. Locatelli, A. F. Vincent, A. Mizrahi, J. S. Friedman, D. Vodenicarevic, J.-V. Kim, J.-O. Klein, W. Zhao, J. Grollier & D. Querlioz
Proceedings Of The Design, Automation & Test in Europe Conference (DATE), 2015.

Miscellaneous

108. *Metal Spintronics: Electronics free of charge* (News & Views)
C. Chappert & J.-V. Kim
Nature Physics **4**, 837 (2008).

109. *Solid-state physics: Siphoning spins* (News & Views)
J.-V. Kim
Nature **511**, 418 (2014).

Acknowledgements

People

IEF/C2N, Orsay
Jean-Paul Adam, **Laurence Bianchini**(†), Claus Bilzer, **Capucine Burrowes**(†), Claude Chappert, Guillaume Counil, Paul Crozat, Thibaut Devolder, **Artur Difini Accioly**(†,‡), Karin Garcia, **Felipe Garcia-Sanchez**(‡), **Yacine Halioua**(*), Annerose Helmer, **Yann Le Maho**(†), Na Lei, **Jérémy Létang**(*,†), Nicolas Locatelli, **Francesca Mineo**(*), **Quentin Mistral**(†), Alice Mizrahi, **Rubén Otxoa**(†), Damien Querlioz, Dafiné Ravelosona, Rémy Soucaille, **Jérôme Williame**(*,†), **Myoung-Woo Yoo**(‡)

Unité Mixte de Physique CNRS/Thales, Palaiseau
Madjid Anane, Manuel Bibes, Karim Bouzehouane, Vincent Cros, Vincent Garcia, Julie Grollier, **Daniele Pinna**(‡), Nicolas Reyren

Laboratoire de Physique des Solides, Orsay
Ales Hrabec, Vincent Jeudy, Stanislas Rohart, Joao Sampaio, André Thiaville

Institut Jean Lamour, Nancy
Sébastien Petit-Watelot(‡), Stéphane Mangin

Institut de Physique et de Chimie des Matériaux de Strasbourg
Matthieu Bailleul, Olga Gladii, Yves Henry

Laboratoire Aimé Cotton, Orsay | *Laboratoire Charles Coulomb*, Montpellier
Thomas Hingant, Vincent Jacques, Jean-Philippe Tétienne

Laboratoire Matériaux Optiques et Photonique, Metz
Damien Rontani, Marc Sciamanna

Institut des Nanosciences de Paris
Laura Thevenard

University of Glasgow, UK
Pablo Borys(†), **Louise Desplat**(†), Robert Stamps

University of Colorado at Colorado Springs, USA
Robert Camley

Oakland University, Michigan, USA
Andrei Slavin, Vasil Tiberkevich

IMEC, Leuven, Belgium
Sven Cornelissen, Liesbet Lagae, Mauricio Manfrini, Maarten van Kampen

University of Exeter, UK
Gino Hrkac

Technische Universität Wien, Austria
Dieter Suess

(*) Masters student supervised
(†) PhD (co-)supervised
(‡) Postdoc (co-)supervised

Universiteit Gent, Belgium
Jonathan Leliaert, Arne Vansteenkiste

RIKEN, Saitama, Japan
Gen Tatara

Johannes Gutenberg-Universität Mainz, Germany
Bertrand Dupé, Ulrike Ritzmann

National Institute for Materials Science, Tsukuba, Japan
Masamitsu Hayashi, Jacob Torrejon

University of Western Australia, Perth, Australia
Peter Metaxas

University of Leeds, UK
Chris Marrows, Kowsar Shahbazi

Christian-Albrechts-Universität zu Kiel, Germany
Stefan Heinze

New York University, USA
Andrew Kent

Funding

Agence Nationale de la Recherche (France)

ISTRADE (2008-2011), VOICE (2009-2012), NANOSWITI (2011-2015), MEMOS (2014-2018), ULTRASKY (2015-2017), SWANGATE (2017-2020), CHIPMUNCS (2018-2021), TOPSKY (2017-2021)

European Communities

FP6-NMP TUNAMOS (2005-2008), FP6-MOBILITY SPINSWITCH (2006-2010), FP7-PEOPLE SEMISPINNET (2008-2012), FP7-ICT MAGWIRE, H2020 FET-Open MAGICSKY, H2020 MSCA-IF CHAOSPIN (2018-2020)

Other

Partner University Fund (2011-2014), Deutscher Akademischer Austauchdienst (DAAD) (2017), University of Western Australia – Research Collaboration Award (2017-2018)